ELUCIDATING THE DISEASE RELEVANCE AND FUNCTION OF THE ALS/FTLD-ASSOCIATED PROTEIN C9ORF72

A Dissertation

Presented to the Faculty of the Graduate School

of Cornell University

In Partial Fulfillment of the Requirements for the Degree of

Doctor of Philosophy

by

Peter Mayo Sullivan

August 2017

ELUCIDATING THE DISEASE RELEVANCE AND FUNCTION OF THE ALS/FTLD-ASSOCIATED PROTEIN C9ORF72

Peter Mayo Sullivan, Ph. D.

Cornell University 2017

Intronic hexanucleotide repeat expansion in the C9orf72 gene is a leading cause of frontotemporal lobar degeneration (FTLD) with amyotrophic lateral sclerosis (ALS). Among several hypotheses, reduced expression of C9orf72 has been proposed as a possible disease mechanism. However, the function of C9orf72 remains unclear.

Here, I have presented data that begins to elucidate the function of C9orf72 at a cellular and organismal level. My data has found that C9orf72 binds SMCR8 and WDR41 to form a protein complex. Each component of this complex is important for the stability of the entire complex, as loss of any one of these three protein causes a decrease of other complex components. SMCR8 protein is almost completely lost in the C9orf72-/- mouse tissues, but has little change in the WDR41-/- mice, whereas C9orf72 levels are decreased by loss of either SMCR8 or WDR41. I have also shown that the C9orf72 complex interacts with the Ulk1-FIP200 complex, as well as the cytoskeletal component tubulin, and several Rab GTPases. Furthermore, I provide evidence that mTOR phosphorylation and localization is mis-regulated and that AKT phosphorylation is also altered in SMCR8-/- cells, leading to mis-regulated autophagy-lysosome functions. Finally, I have created knockout mice for C9orf72, SMCR8, and WDR41 using

CRISPR-Cas9 and preliminarily characterized the phenotypes that these mice exhibit. Altogether, my data support a role for the C9orf72-SMCR8-WDR41 complex in regulating the autophagy-lysosome pathway and maintaining proper immune regulation.

BIOGRAPHICAL SKETCH

Peter Sullivan grew up near Chicago, IL and first gained interest in biology during high school AP Biology. His interest in using analytical methods to understand the biology and chemistry of the world around him led to peruse a bachelor's degree at Lake Forest College. While at Lake Forest College, he participated in many student run organizations that helped to bring local researchers to give seminar at Lake Forest College and served on the board of the College's life science journal, *Eukaryon*. His first foray into bench science was as a Richter Apprentice Scholar in Dr. Shubhik DebBurman's lab studying Parkinson's disease. He continued studying neurodegeneration in Dr. Anthony West's lab at Rosalind Franklin University of Medicine and Science, where he completed an undergraduate senior thesis. Mr. Sullivan completed a Bachelor's of Arts in both Biology and Chemistry. He then choose to peruse a Ph.D. at Cornell University in the field of Biochemistry, Molecular and Cell Biology. He undertook his graduate studies in Dr. Fenghua Hu's lab studying the recently identified ALS/FTLD-associated gene C9orf72. As a graduate student, Mr. Sullivan was a member and president of the graduate student outreach group GEEKS, which was started in the Molecular Biology and Genetics department. Mr. Sullivan was also awarded the prestigious Henry and Samuel Mann Outstanding Graduate Award in the final year of his studies. He plans to continue his scientific training as a post-doc in Seattle, WA.

ACKNOWLEDGMENTS

I would like to express my gratitude towards my advisor Dr. Fenghua Hu for her guidance and mentorship that has helped me progress as a scientist over the past five years. Her continued support and feedback has improved my ability to identify important problems in our research, to focus on specific questions in context of a bigger picture, and to improve my organization and communication, all of which have been essential to my studies in her lab. Additionally, I would like to thank Dr. Yuxin Mao for his constructive criticism during our joint lab meetings.

I would also like to thank my academic committee members Dr. Scott Emr and Dr. Shu-Bing Qian. They have both provided encouragement alongside scientific discussions that have helped to improve my scientific work and restore excitement in my work when it begins to feels mundane. I would specially like to thank Dr. Emr for providing insightful career advice.

Beyond my committee, I was honored to interact with many wonderful mentors. Among them, I would specifically like to thank Dr. Volker Vogt for his mentorship while I was a teaching assistant for his course as well as his for his constructive feedback during each of my departmental seminars.

I am also grateful to Dr. Shubhik DebBurman and Dr. Tony West for their mentorship early in my scientific career and for propelling me forward to grad school, where they still provide valued advice and encouragement.

Finally, I would like to thank my fiancé, Nithya Kartha, who has encouraged and supported me through the many stresses of grad school and who reminds me to enjoy my life and take pride in my work.

TABLE OF CONTENTS

LIST OF FIGURES

LIST OF TABLES

LIST OF ABBREVIATIONS

AKT	Seine/Threonine-specific kinase
ANT2	Adenine nucleotide translocator 2
ATG13	Autophagy related Gene 13
ATG101	Autophagy related Gene 101
ALS	Amyotrophic Lateral Sclerosis
C9orf72	Chromosome 9 open reading frame 72
CIAO1	Cytosolic Iron-sulfur Assembly Component 1
CMA	Chaperone-Mediated Autophagy
Co-IP	Co-Immunoprecipitation
DENN	Differentially Expressed in Normal and Neoplastic
FAM96B	Family with sequence similarity 96 member B
FIP200	Focal adhesion Interacting Protein of 200kDa
FLCN	Folliculin
FTLD	Frontotemporal Lobar Degeneration
GAP	GTPase Activating Protein
GEF	Guanosine nucleotide Exchange Factor
GFP	Green Fluorescent Protein
GTPase	Guanosine TriPhosphatase
HEAT	Huntingtin, Elongation factor 3, protein phosphatase 2A, mTOR
HEK293T	Human Embryonic Kidney 293T
KO	Knock Out
MEF	Mouse Embryonic Fibroblast
MMS19	Methyl Methanesulfonate susceptibility protein 19
mTOR	mammalian Target of Rapamycin
N2a	Neuro 2A
NARFL	Nuclear prelamin A Recognition Factor-Like
PFA	Paraformaldehyde
PI3K	PhosphoInositide 3-Kinase
Rag	Ras-Related small GTP-binding protein
RANT	Repeat Associated Non-atg Translation
RNA	Ribonucleic Acid
SILAC	Stable Isotope Labeling of Amino acids in Cell culture
SMCR8	Smith-Magenis Chromosome Region candidate 8
TDP-43	TAR DNA-binding Protein of 43 kDa
TRiC	T-cplex protein-1 Ring Complex
ULK1	UNC51-Like Kinase 1
WDR41	WD-repeat protein 41
WT	Wild Type

CHAPTER 1

AUTOPHAGY-LYSOSOME DYSFUNCTION IN AMYOTROPHIC LATERAL SCLEROSIS AND FRONTOTEMPORAL LOBAR DEGENERATION

This work was submitted 12 February 2017 to be published by InTech and included in their forthcoming textbook *Lysosomes- associated diseases and methods to study its function*. ISBN 978-953-51-5281-1.

1.1 Introduction

Proper degradation machinery is necessary for neuronal survival, and disruption of lysosomal function is sufficient to cause neurodegeneration[1–4]. To recycle cellular material, cells use two major pathways: autophagy for organelles and long-lived proteins and the ubiquitin-proteasome system (UPS) for short-lived proteins[5,6]. Autophagy consists of three pathways that each ultimately delivers cellular contents to the lysosome for degradation. The pathways are chaperone-mediated autophagy (CMA), which uses HSC70 to recognize specific misfolded proteins; microautophagy, which directly invaginates material into the lysosome; and macroautophagy, which is responsible for the degradation of organelles, protein aggregates, and large protein complexes. Macroautophagy (hereafter referred to as autophagy) is the most common pathway. The autophagy pathways and molecular mechanisms have been recently reviewed elsewhere[7,8]. The presence of protein aggregates in most neurodegenerative diseases suggests common underlying problem in protein degradation systems. Here we summarize the connection between the autophagy-lysosome pathway and two neurodegenerative diseases Amyotrophic Lateral Sclerosis (ALS) and Frontal-Temporal Lobar Degeneration (FTLD)[9].

ALS is characterized by the loss of upper and lower motor neurons resulting in

progressive weakness and ultimately paralysis. Patients survive a median of 3-5 years from disease onset [10]. FTLD is characterized by the degeneration of neurons in the frontal cortex and anterior temporal lobes. This degeneration leads to changes in behavior and language impairment. The subtypes of FTLD can be distinguished by the prominent symptoms, which reflect the area affected by neuron loss[11,12]. The subtypes are behavioral variant frontotemporal dementia (bvFTD), semantic dementia (SD), and primary non-fluent aphasia (PNFA). bvFTD, the most common subtype, is characterized by changes in behavior such as disinhibition, loss of empathy, impaired social skills, and decline in personality. SD is characterized by impaired language comprehension, and PNFA disrupts speech production[9]. These subtypes often overlap and can additionally include Parkinson's disease like symptoms. Patients survive for a median of 7-11 years after diagnosis. There are no treatments for FTLD[9]. ALS and FTLD symptoms are often present in the same patient, an indication that these diseases have shared etiology[13,14]

Each disease is also subdivided by molecular pathology depending on the primary components of inclusion bodies: Tau, TDP-43, FUS, and ubiquitin in FTLD and SOD1, TDP-43 (with or without C9orf72 dipeptide repeats), and FUS in ALS[9,15]. In 2006, both ALS and FTLD were found to have neuronal inclusions composed largely of TDP-43, an RNA-binding protein, that are also ubiquitin and p62 positive, suggesting that these aggregates were tagged for degradation[16–18]. Additionally, genetic mutations have since been discovered that can lead to the development of both ALS and FTLD. Thus, these two diseases are linked by clinical concurrence, molecular pathology, and genetic overlap[13,14,19].

As many new genes have been identified for FTLD and ALS in the last decade, studies have revealed a common theme of these genes functioning in the lysosomal

network (Figure 1). Some mutations, such as *GRN*, *TMEM106B*, *CHMP2B* and *VCP* are associated with disrupted lysosomes and multivesicular bodies (MVB). Other mutations, such as in *p62/SQSTM1*, *OPTN*, *UBQLN2*, and *TBK1* directly disrupt selective autophagy and therefore prevent cargo from being degraded. Other mutations have a more complex relationship with autophagy and lysosome function, such as the RNA-binding proteins *TARDBP* and *FUS*. Here, we will discuss the genetic causes of ALS and FTLD in more detail with specific emphasis on lysosomal and autophagy impairment (Figure 1).

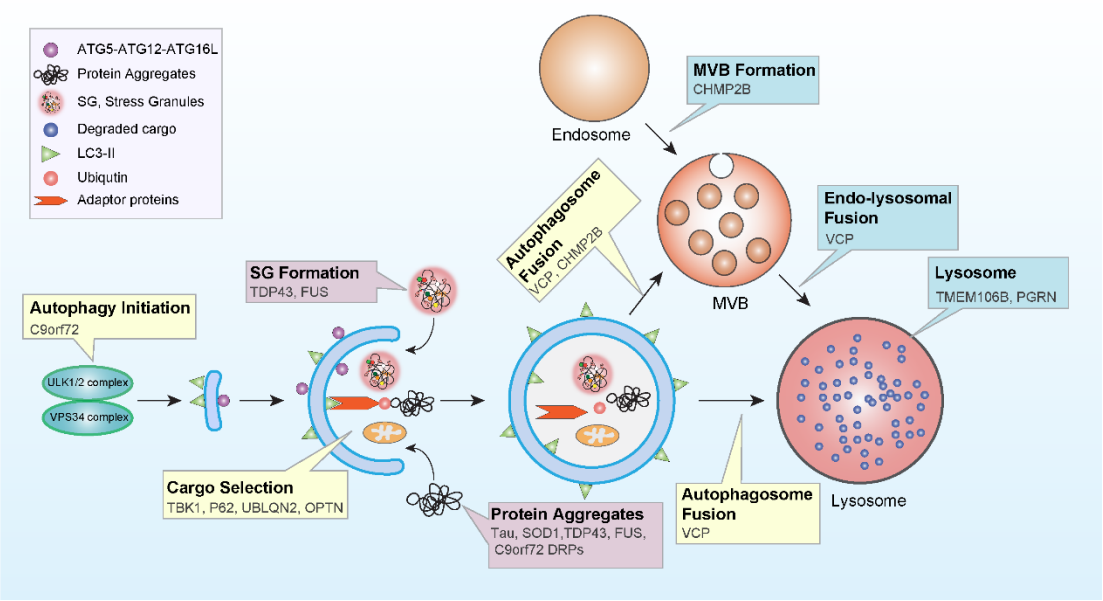

Figure 1-1: Functions of the ALS/FTLD genes in the autophagy-lysosome pathway. Many genes associated with ALS/FTLD play critical roles in the endosome-lysosomal pathway, regulate lysosomal functions or affect autophagy pathway directly or indirectly

1.2 Mutations affecting the endolysosome pathway: PGRN, TMEM106B, CHMP2B, and VCP

Progranulin (PGRN)

The most common cause of familial FTLD with ubiquitin positive aggregates is mutation of the *GRN* gene, which accounts for 10% of all FTLD cases and ~25% of familial FTLD (20,[21,22]. About 70 mutations in the *GRN* gene have been linked to FTLD, most of which have been shown or predicted to decrease PGRN protein level or disrupt secretion of PGRN[20,21,23,24]. While FTLD is caused by haploinsufficiency of PGRN, a more serve neurodegeneration is caused by homozygous loss of PGRN. This complete loss of PGRN results in neuronal ceroid lipofuscinosis (NCL), a type of lysosome storage disorder (LSD) characterized by the build-up of autofluorescent lipofuscin[25,26]. These findings suggest that loss of function mutations in the *GRN* gene causes neurodegenerative diseases in a dose-dependent manner and is important for lysosome function.

The function of PGRN is still under investigation: It is known to be a secreted glycoprotein comprised of 7.5 granulin repeats with pleiotropic roles, including protein homeostasis, inflammation, and neuronal survival and outgrowth [27]. Recently several lines of evidence suggest that it plays a vital role in lysosome function. First, *GRN* has been found to be regulated with other lysosomal genes[28]. Furthermore, *GRN* mRNA and PGRN protein levels are upregulated in response to lysosome or autophagy inhibition[29]. Finally, PGRN was found to be delivered to the lysosome[30,31]. PGRN reaches the lysosome through at two independent pathways. In one path, PGRN's extreme C-terminus binds the sorting receptor sortilin, which carries PGRN to the lysosome[30,32]. In the second pathway, PGRN binds prosaposin, and they are transported to the lysosome together by the cation-independent mannose-6-phosphate

receptor (CI-M6PR) and Low-Density Lipoprotein Receptor-Related Protein 1, LRP1 [31].

Mouse models of PGRN deficiency have consistently found increased levels of ubiquitin and p62, an adaptor for delivering cargo to the autophagosome[33], buildup of lipofuscin and its protein components saposin D and SCMAS, electron-dense storage granules, all of which suggest lysosome impairment[31,34–36]. Several models also found aggregation of TDP-43, similar to what is seen in FTLD patients[34,37,38]. Furthermore, PGRN-deficient mouse models also phenocopy FTLD symptoms such as decreased social interaction and mild learning/memory defects[35,38–40]. The presence of clear lysosomal problems in mouse models and in patients with complete loss of PGRN suggest that PGRN is necessary for lysosome function. FTLD- patients with GRN mutations also exhibit typical pathological features of NCL pathology[36], suggesting FTLD and NCL caused by PGRN mutations are pathologically linked and lysosomal dysfunction is one of underlying disease mechanisms for FTLD-GRN. However, how PGRN regulates lysosomal function remains to be investigated.

TMEM106B

Another gene associated with FTLD is *TMEM106B*, which is the only identified risk factor for FTLD with *GRN* mutations[41–44]. *TMEM106B* was also found to increase risk in patients with *C9orf72* hexanucleotide repeat expansions[45,46]. The *TMEM106B* SNP associated with FTLD increases the mRNA and protein levels of TMEM106B[36,44,47]. TMEM106B is a single pass type II transmembrane protein that localizes to the late endosome and lysosome[47–49]. Cellular studies on TMEM106B have pointed to roles in lysosome trafficking and lysosomal stress response[50,51]. Overexpression of TMEM106B in cells disrupts lysosome morphology and function[47,48]. Furthermore, when a transgenic TMEM106B mouse line was crossed with a PGRN deficient mouse, the lysosome abnormalities and lipofuscin accumulation

seen in PGRN deficient mouse were exacerbated[52]. The connection between TMEM106B's role at the lysosome and as a risk factor for FTLD with *GRN* mutations further highlights the importance of the lysosome pathway in FTLD etiology.

CHMP2B

The sole mutation identified to cause FTLD with ubiquitin positive, but Tau, TDP-43, and FUS negative inclusions, occurs in the gene *CHMP2B* [53,54]. *CHMP2B* has also been found to cause rare cases of ALS[55]. CHMP2B functions in the ESCRT-III complex, involved in MVB formation to deliver cargo from endocytic pathway to lysosomes[56,57]. The mutations identified create an early termination of the protein, resulting in an unregulated CHMP2B truncation that is unable to recruit VPS4 to recycle the ESCRT-III complex to new sites of MVB formation[58,59]. With ESCRT-III still engaged on the MVB, MVB-lysosome fusion cannot take place[54,60–62]. Furthermore, *CHMP2B* mutations impair autophagosome maturation, possibly through the disruption of amphisome formation between autophagosome and late endosomes [63–66]. Mouse models of *CHMP2B* mutations replicate both ALS and FTLD pathology, whereas *CHMP2B* knockout mice do not show neurodegenerative phenotypes, implicating a gain of function disease mechanism[67–70]. Similar to the PGRN deficiency mouse models, *CHMP2B* mutations cause protein inclusions and accumulation of autofluorescent aggregates in the frontal cortex, reminiscent of lysosome storage disorders[71]. Thus, FTLD-associated mutations in *CHMP2B* impair the endo-lysosomal pathway, which itself may cause additional defects in autophagy[66,69], providing additional evidence that disruption of the autophagy-lysosome pathway may drive ALS and FTLD.

VCP

Valosin-Containing Protein (VCP) has been implicated in several diseases

including FTLD [22,72–76], ALS [77], and Charcot Marie Tooth disease, a genetic peripheral nerve disorder [78]. VCP is an AAA^{+}-ATPase that delivers and unfolds ubiquitinated proteins, as well as ERAD (endoplasmic-reticulum-associated protein degradation) substrates, at the proteasome [79–83]. Furthermore, VCP binds to clathrin and EEA1 to regulate the size and selectivity of endosomes [83–85]. Pharmacological inactivation of VCP as well as VCP knockdown inhibits MVB formation and blocks autophagosome maturation, resulting in accumulated LC3-II, ubiquitin, and p62 levels along with cytoplasmic TDP-43 aggregation [86–88]. Disease-associated mutants of VCP present similar phenotypes in transgenic mouse models, whereas complete loss of VCP is embryonic lethal [86,89–91]. Finally, VCP mutants inhibit the autophagic turnover of stress granules, which may be relevant to the accumulation of TDP-43 positive aggregates found in patients with VCP mutations [76,92,93]. The precise mechanism that halts autophagosome maturation in VCP mutations remains unclear, though MVB dysfunction may play a role[66]. VCP's role in MVB formation and the observations of altered autophagic flux suggests that loss of VCP function may cause ALS, FTLD, and other related neurodegenerative diseases by impairing the lysosome-autophagy pathway.

1.3 Autophagy Adaptor proteins

Further evidence that ALS and FTLD are linked to autophagy and lysosome disruption comes from mutations that directly affect several autophagy adaptor proteins and their regulation. Genetic mutations in the adaptor proteins *p62/SQSTM1*, *UBQLN2*, and *OPTN* have been shown to contribute to rare cases of ALS[94–99] and FTLD[100,101].These adaptor proteins all contain an ubiquitin-associated (UBA) domain, which is able to bind poly-ubiquitin conjugated proteins that are tagged for

degradation by either the UPS or autophagy. The autophagy adaptors then associate with LC3 on the autophagosome to deliver the cargo for degradation through autophagy-lysosome pathway.

p62/SQSTM1

p62/SQSTM1 (p62) positive inclusions have been observed in patient tissue samples in both ALS and FTLD [18,102–104]. The association of p62 with inclusions suggests that the inclusion body has been targeted for degradation and the accumulation of such inclusions suggests that there may be defective mechanisms for protein turnover [33,105,106]. p62 bridges autophagy substrates to the autophagosome by interacting with ubiquitinated proteins via its UBA domain [107] and LC3 with its LC3-interacting region (LIR) [33,108,109].

p62 is activated by phosphorylation at Ser407 by ULK1, allowing further phosphorylation by Casein Kinase 2 or TANK-Binding Kinase 1 (TBK1), which increases p62's affinity for poly-ubiquitinated cargo[110–113]. p62 acts within the selective autophagy system by aggregating proteins and organelles together for the autophagosome to enclose[106,114]. These aggregated cargos are then subject to autophagy[115,116]. While p62 accumulation and association with protein aggregates broadly suggests a defect in autophagy, mutations in p62 directly link selective autophagy impairment to neurodegeneration.

The *p62* mutations identified in ALS and FTLD patients disrupt aggregate formation or decrease the amount of p62 protein produced, leading to loss of function[117–119]. Homozygous mutation of *p62* cause adolescence/childhood-onset neurodegeneration with a defect in mitochondrial depolarization response due to impaired autophagy[120]. Thus, a loss of normal p62 function in autophagy leads to neurodegeneration in a dose-dependent manner, with earlier onset correlating to lower levels of functional p62.

In addition to its role in autophagy, p62 also links ubiquitinated cargo to the proteasome through its UBA domain[106] and mediates the degradation of the protein via the UPS, indicating that p62 plays multiple roles in proteostasis[121].

Ubiquilin2

Another adaptor protein implicated in ALS and FTLD is Ubiquilin2 (UBQLN2)[95,122]. Similar to p62, UBQLN2 is able to recognize ubiquitinated proteins and bind them via its UBA domain[123]. The UBA domain is also required for UBQLN2 to associate with the autophagosome, though unlike p62 and OTPN, UBQLN2 does not directly recognize LC3[124,125].

Knockdown of UBQLN2 in culture reduced autophagosome formation and inhibited lysosomal degradation of mitochondria[124,125]. This loss of UBQLN2 also sensitizes cells to starvation-induced death in an autophagy-dependent manner[124]. Interestingly, UBQLN2 binds directly to TDP-43 holo-protein and C-terminal fragments and may regulate the levels of TDP-43 in the cell independent of ubiquitin[126]. Indeed, overexpression of UBQLN2 in culture can reduce aggregation of TDP-43[126].

Many of the disease-associated mutations map to the proline-rich domain in *UBQLN2*, which is important in mediating protein-protein interactions[95,127]. Furthermore, mutations in *UBQLN2* have a reduced binding to hnRNPA1, a RNA-binding protein implicated in ALS. Interestingly, ALS-associated mutations in hnRNPA1 also disrupt this binding[128], confirming that the interaction of autophagy adaptors with their intended cargos is important for neuronal survival.

UBQLN2 knockout in a rodent model showed no neuronal loss, implying that loss of function is not the disease mechanism or that other autophagy adaptors are able to compensate for its loss *in vivo*. Transgenic animals with the ALS/FTLD-associated *UBQLN2* mutations produce ubiquitin, p62, and UBLQN2 positive puncta accompanied

by neuronal loss, cognitive defects, and motor impairment[129–131]. Increased expression of the wildtype UBQLN2 also causes neurodegeneration in a rodent model[132]. Thus unlike mutations in *p62*, *UBQLN2* mutations appear to have a gain of function mechanism that impairs proper protein degradation by autophagy.

In addition to its function in the autophagy pathway, UBLQN2 binds to the proteasome through its ubiquitin-like (UBL) domain to deliver poly-ubiquitinated proteins and ERAD substrates to the proteasome for degradation[133]. A role of UBQLN2 in delivering protein aggregates to proteasome mediated degradation via HSP70 has been recently demonstrated[134]. UBQLN2 also function together with other ALS/FTLD-related proteins, such as regulating endosome constitution with OPTN[135] and delivering ERAD substrates to the proteasome with VCP[136].

Optineurin

Rare mutations in *OPTN* are also associated with both ALS [97,99] as well as FTLD[101]. These mutations are expected to decrease the level of OPTN protein, suggesting a loss of function resulting in disease[101]. In total, 1-4% of familial ALS cases are linked to mutations in OPTN[137]. OPTN, like p62 and UBQLN2, binds to poly-ubiquitin labeled proteins via a UBA domain[138]. OPTN also binds LC3 through a LIR to connect cargo to autophagosomes. Damaged mitochondria specifically recruit OPTN to induce mitophagy[139]. In support of a loss of function model for OPTN, depletion of OTPN in zebrafish causes motor defects[140].

OPTN also interacts with several other proteins associated with ALS. The E3 ubiquitin ligase HACE1 ubiquitinates OPTN to promote binding to p62 which forms a complex that enhances autophagic flux[141]. Similarly, phosphorylation of OPTN byTBK1 increases the interaction of OPTN and p62 to the same effect[138,142]. OPTN also binds directly to SOD1 aggregates independently of ubiquitination. Mutations in *OPTN* do not affect this interaction, but do impair autophagic clearance of SOD1 protein

aggregates through an unknown mechanism[138,140].

Mutation in *OPTN* had previously been linked to Primary Open-Angle Glaucoma (POAG) where these mutations were shown to decrease basal autophagy and inhibit autophagic flux upon autophagy induction[143]. Thus Mutations in *OPTN* have clear links to multiple neurodegenerative disease with consistent impairment in the autophagy pathway. How mutations in the same gene and similar cellular impairments can lead distinct clinical outcomes remains unclear.

TBK1

TBK1 has recently been associated with both ALS and FTLD[96,98,101,110,111,144–147]. TBK1 has functions in autophagy and in inflammation[148]. Regarding its function in autophagy, TBK1 phosphorylates p62 and OPTN to increase their binding to LC3 and ubiquitin, respectively[138,142]. Many of the discovered disease-associated mutations are expected to decrease TBK1 protein level, suggesting a loss of function model[96,101].

While TBK1 interacts with both p62 and OPTN, TBK1 and OPTN share several additional connections. Like OPTN, some mutations in TBK1 also cause glaucoma[149]. Furthermore, the mutation in OPTN that causes POAG enhances the binding of OPTN to TBK1, which may sequester TBK1 and prevent it from carrying out its normal function[142]. Finally, both TBK1 and OPTN are required specifically for mitophagy, with depletion of either component or expression of an ALS-associated mutant impairing mitophagy[150]. Taken together, mutations in *TBK1* cause decreased protein expression and prevent TBK1 from regulating p62 and OPTN in their autophagy roles, again supporting a role of autophagy in preventing ALS and FTLD.

1.4 Mutations in C9orf72

The most common known cause of both ALS and FTLD was discovered to be a hexanucleotide intronic repeat expansion in the gene *C9orf72*[151–153]. This repeat expansion is found in 18-25% of familial FTLD, 40% of familial ALS, and 4-8% of sporadic ALS and FTLD combined[154,155]. While patients with C9orf72 mutations display TDP-43 positive aggregates, they also have separate inclusions unique to this genetic mutation. These ubiquitin, p62, and occasionally UBQLN2 positive inclusions also contain dipeptide repeats generated from the repeat expansion[156–160]. Three molecular mechanisms of disease have been proposed: toxic gain of function of RNA repeats, gain of function of dipeptide repeats (DPR) produced by repeat-associated non-ATG translation, and haploinsufficiency of the C9orf72 protein.

RNA-repeats transcribed from the repeat expansion form nuclear foci and sequester many RNA-binding proteins, including several RNA-binding protein already implicated in ALS and FTLD[161–164]. In addition to disrupting RNA-binding proteins directly, the RNA foci disrupt nucleocytoplasmic transport[165,166]. Furthermore, nuclear TDP-43 is depleted in a fly model expressing C9orf72 repeats, which may allow TDP-43 to accumulate and aggregate in the cytosol[167]. This model is of interest because it connects to the RNA-binding proteins already associated with ALS and FTLD, such as TDP-43, which aggregates in both diseases. A second model suggests that five distinct DPRs are translated and can also alter nucleocytoplasmic transport to block TDP-43 import[168,169] as well as disrupt membrane-less, phase-separated organelles such as the nucleolus, nuclear pore, and stress granules[170].

Haploinsufficiency was also proposed as a disease mechanism[153,161,171–173]. Early C9orf72-depletion models in *c. elegans* and zebrafish showed motor dysfunction, supporting this model[174,175]. However, a neuronal specific C9orf72

knockout mouse showed no such phenotype[176]. Complete C9orf72 knockout mice also do not show much neurodegeneration, but instead exhibit severe immune problems similar to autoimmune disorders[177–182].

Interestingly, C9orf72 has been reported to play a role in autophagy and lysosome regulation. While many of the reports suggest that C9orf72 and its binding partners, SMCR8 and WDR41, play a role in regulating autophagy initiation or maturation, likely via the FIP200/ULK1 complex, the precise mechanism remains uncertain [180,183–187]. Other reports suggests that C9orf72 plays a role in mTOR and TFEB signaling[187,188], in stress granule assembly[189], or in actin dynamics[190].

1.5 RNA-binding proteins: TDP-43 and FUS

The RNA-binding proteins TDP-43 and FUS have been closely associated with ALS and FTLD. Pathogenic TDP-43 or FUS aggregates are present in both conditions, though mutations in these genes result primarily in ALS[191]. Both proteins travel between the nucleus and cytoplasm as they regulate gene splicing, mRNA stability and trafficking, and stress granule dynamics[192,193].

As both TDP-43 and FUS regulate the RNA from thousands of genes, many cellular problems could be anticipated. However, several lines of evidence have pointed out a role in regulating and challenging the autophagy pathway[194].

TDP-43

The identification of TDP-43 as the main component of protein aggregates in both ALS and FTLD spurred the awareness that ALS and FTLD had some underlying similarities[16,17]. Interestingly, mutations in *TARDBP*, the gene encoding TDP-43, lead overwhelmingly to ALS or ALS/FTLD, but not to FTLD alone[195,196]. While soluble TDP-43 can be cleared by chaperone-mediated autophagy through its

interaction with Hsc70[197], TDP-43 positive stress granules and aggregates are cleared by macroautophagy[198,199].

In addition being a substrate of autophagy, TDP-43 may play a direct role in regulating autophagy through its transcriptional regulation of *ATG7*[200]. As TDP-43 is sequestered in protein aggregates, it can no longer regulate *ATG7* transcription, impairing autophagy initiation and further promoting TDP-43 accumulation[199,200]. In a similar manner, TDP-43 also regulates the mRNA for *RPTOR* and *DCTN1*[198]. *RPTOR* encodes a component of the mTOR complex, and loss of *RPTOR* upregulates lysosome and autophagy biogenesis[198]. However, reduced *DCTN1* mRNA, which encodes Dynactin, a key component of autophagosome-lysosome fusion, leads to the accumulation of autophagosomes, preventing the turnover of aggregated TDP-43[198].

TDP-43 additionally plays an important role in stress granule dynamics and mutations in *TARDBP* have been shown to increase the stability of stress granules, possibly allowing them to become irreversible protein aggregates[199,201–204]. In support of this prolonged stress granule hypothesis, mutations in VCP decrease stress granule turnover by autophagy, leading to TDP-43 positive inclusion[92].

The interaction of TDP-43 with autophagy suggests a complex regulatory balance between the two under normal conditions. In disease states, a feedforward mechanism of TDP-43 sequestration into stress granules and aggregates followed by impaired autophagy could drive pathogenesis of ALS and FTLD[9,203].

FUS

Like *TARDBP*, mutations in *FUS* have been linked more closely to ALS, though protein aggregates positive for FUS appear in both ALS and FTLD[9]. FUS positive inclusions account for about 5-10% of FTLD cases[9] and 1% of ALS cases[15]. Several proposed mechanisms link FUS to disruption of the autophagy and lysosome pathway. First, the presence of FUS positive aggregates in both familial and sporadic cases of

ALS and FTLD suggest FUS may be particularly susceptible to aggregation. FUS is also involved in autoregulation, which could allow for a feed-forward cycle of increased FUS production followed by cytosolic accumulation and aggregation[199,205].

Additionally, mutations in *FUS* have been linked to altered stress granule dynamics[206,207]. FUS positive stress granules were found to be degraded by autophagy; however, stress granules containing mutant FUS were more stable and prevented stress granules disassembly[199]. As with TDP-43, stabilized stress granules may promote insoluble aggregate formation[203,208–210].This increases the burden on the autophagy pathway and may drive further cell damage. A recent study also found that ALS-associated mutant *FUS* was able to inhibit the early steps of autophasosome formation, leading to impaired autophagy flux[211]. Many of these studies found that enhancing autophagy, genetically or pharmaceutically, was able to reduce FUS-positive inclusions and prevent cellular toxicity[199,206,211]. While less well understood than TDP-43, the RNA-binding protein FUS seems to play a similar cellular role as TDP-43, including regulating the dynamics of stress granules. Besides increased burden on autophagy due to stabilized stress granules, FUS may also play a more direct role in autophagy impairment.

1.6 Microtubule-Associated Protein Tau

30% of familial FTLD cases are caused by mutations in *MAPT*, encoding the protein tau[212]. These cases are characterized by the presence of tau aggregates positive for ubiquitin and p62, suggesting impaired degradation of accumulated tau[121,213]. Generic disruption of autophagy cargo selection is sufficient to cause aggregation of pathogenic tau[214]. The tau protein is most well-known for its association with Alzheimer's disease, when it also forms aggregates and is accompanied

by neurodegeneration of the hippocampus[215]. How Alzheimer's disease and FTLD patients have overlapping cellular pathology but develop different clinical symptoms remains unclear.

Full length tau can be degraded by the UPS in an ubiquitin-dependent and independent manner[121,216,217], whereas misfolded or phosphorylated tau is sent to the autophagy pathway[218]. Generally, tau aggregation and toxicity correlates with autophagy activity, where enhanced autophagy rescues neurodegeneration and impairment exacerbates the symptoms[219–222]. Likewise, modulating TFEB to increase lysosome biogenesis prevents the accumulation of tau[223].

Tau is a microtubule binding protein that helps to stabilize axonal microtubules[224,225]. Small increases in unbound tau induces aggregation, suggesting that even mild impairment of the UPS or autophagy-lysosome pathway could lead to pathological tau accumulation[226,227]. In support of this idea, Niemann-Pick disease, another lysosome storage disorder, also develops tau aggregates[228,229]. These points show that tau is highly dependent on autophagy and lysosome function and disruption of this pathway may drive tau aggregation. Furthermore, since tau has a role in microtubule stability, disrupted cytoskeletal dynamics and trafficking have also been proposed as a disease mechanism. Since lysosomes, endosomes, MVB, and autophagosomes all move along microtubules, any disruptions would affect their ability to maintain proteostasis[230].

1.7 Discussion

ALS and FTLD are distinct clinical disorders that share overlapping symptoms, pathology and genetics. Many of the causative genetic mutations and risk factors result in disruption of the lysosome and autophagy pathway (Figure 1). Some disease-

associated mutants or alleles directly impact lysosomal function through yet unknown mechanisms, such as *PGRN* and *TMEM106B*, or through disruption of the late stages of the endo-lysosome pathway, as *VCP* and *CHMP2B* mutations are proposed to do. Beyond the lysosome, there are also many mutations in adaptor proteins that impair selective autophagy, including *p62/SQSTM1*, *OPTN*, and *UBQLN2*. The misregulation of these adaptors is sufficient to induce neurodegeneration, as seen with *TBK1* mutants. Finally, some mutations have a more intricate relationship to the autophagy and lysosome pathway that future research will have to address, including C9orf72 protein, repeat-associated RNA foci, and dipeptide repeats, as well as the microtubule binding protein Tau and the RNA-binding proteins TDP-43 and FUS.

Identifying the underlying cellular problems that lead to disease is an important step in being able to distinguish disorders and subtypes that may ultimately require distinct diagnosis and treatment. The genetic analysis of ALS and FTLD has improved our understanding of this disease spectrum and may inform us of the broad problems that underlie both familial and sporadic ALS and FTLD. The consistent impairment of cellular clearance pathways by ALS and FTLD-associated mutations points to a disease mechanism that is likely to be shared in undiscovered genetic causes, as well as environmental risk factors, that account for the cases of ALS and FTLD that have no known cause.

REFERENCES

1. Mizushima N, Hara T. Intracellular quality control by autophagy: How does autophagy prevent neurodegeneration? Autophagy. 2006;2(4):302–4.

2. Lee S, Sato Y, Nixon RA. Lysosomal proteolysis inhibition selectively disrupts axonal transport of degradative organelles and causes an Alzheimer's-like axonal dystrophy. J Neurosci. 2011;31(21):7817–30.

3. Komatsu, M., Waguri, S., Chiba, T., Murata, S., Iwata, J., Tanida, I., Ueno, T., Koike, M., Uchiyama, Y., Kominami, E., Tanaka K. Loss of autophagy in the central nervous system causes neurodegeneration in mice. Nature. 2006;441:880–4.

4. Nedelsky NB, Todd PK, Taylor JP. Autophagy and the ubiquitin-proteasome system: Collaborators in neuroprotection. Biochim Biophys Acta - Mol Basis Dis. 2008;1782(12):691–9.

5. Mizushima N. Autophagy : process and function. Genes Dev. 2007;21:2861–73.

6. Wong E, Cuervo AM. Integration of Clearance Mechanisms : The Proteasome and Autophagy. 2016;1–20.

7. Feng Y, Yao Z, Klionsky DJ. How to control self-digestion: Transcriptional, post-transcriptional, and post-translational regulation of autophagy. Vol. 25, Trends in Cell Biology. 2015. p. 354–63.

8. Carroll B, Hewitt G, Korolchuk VI. Autophagy and ageing: implications for age-related neurodegenerative diseases. Essays Biochem. 2013;55:119–31.

9. Gotzl JK, Lang CM, Haass C, Capell A. Impaired protein degradation in FTLD and related disorders. Ageing Res Rev. 2016;32:122–39.

10. Morgan S, Orrell RW. Pathogenesis of amyotrophic lateral sclerosis. Vol. 119, British Medical Bulletin. 2016. p. 87–97.

11. Ratnavalli E, Brayne C, Dawson K, Hodges JR. The prevalence of frontotemporal dementia. Neurology. 2002;58(11):1615–21.

12. Neary D, Snowden JS, Mann DM. Classification and description of frontotemporal dementias. Ann N Y Acad Sci. 2000;920(0):46–51.

13. Hardy J, Rogaeva E. Motor neuron disease and frontotemporal dementia: Sometimes related, sometimes not. Exp Neurol. 2014;262(PB):75–83.

14. Janssens J, Van Broeckhoven C. Pathological mechanisms underlying TDP-43

driven neurodegeneration in FTLD-ALS spectrum disorders. Hum Mol Genet. 2013;22(R1):77–87.

15. Guerrero EN, Wang H, Mitra J, Hegde PM, Stowell SE, Liachko NF, et al. TDP-43/FUS in motor neuron disease: Complexity and challenges. Prog Neurobiol. 2016;145–146:78–97.

16. Neumann M, Sampathu DM, Kwong LK, Truax AC, Micsenyi MC, Chou TT, et al. Ubiquitinated TDP-43 in frontotemporal lobar degeneration and amyotrophic lateral sclerosis. Science. 2006 Oct 6;314(5796):130–3.

17. Arai T, Hasegawa M, Akiyama H, Ikeda K, Nonaka T, Mori H, et al. TDP-43 is a component of ubiquitin-positive tau-negative inclusions in frontotemporal lobar degeneration and amyotrophic lateral sclerosis. Biochem Biophys Res Commun. 2006;351(3):602–11.

18. Tanji K, Zhang HX, Mori F, Kakita A, Takahashi H, Wakabayashi K. P62/sequestosome 1 binds to TDP-43 in brains with frontotemporal lobar degeneration with TDP-43 inclusions. J Neurosci Res. 2012;90(10):2034–42.

19. Ng ASL, Rademakers R, Miller BL. Frontotemporal dementia: A bridge between dementia and neuromuscular disease. Ann N Y Acad Sci. 2015;1338(1):71–93.

20. Baker M, Mackenzie IR, Pickering-Brown SM, Gass J, Rademakers R, Lindholm C, et al. Mutations in progranulin cause tau-negative frontotemporal dementia linked to chromosome 17. Nature. 2006;442(7105):916–9.

21. Cruts M, Gijselinck I, van der Zee J, Engelborghs S, Wils H, Pirici D, et al. Null mutations in progranulin cause ubiquitin-positive frontotemporal dementia linked to chromosome 17q21. Nature. 2006;442(August):920–4.

22. Sieben A, Van Langenhove T, Engelborghs S, Martin JJ, Boon P, Cras P, et al. The genetics and neuropathology of frontotemporal lobar degeneration. Acta Neuropathol. 2012;124(3):353–72.

23. Gass J, Cannon A, Mackenzie IR, Boeve B, Baker M, Adamson J, et al. Mutations in progranulin are a major cause of ubiquitin-positive frontotemporal lobar degeneration. Hum Mol Genet. 2006;15(20):2988–3001.

24. Shankaran SS, Capell A, Hruscha AT, Fellerer K, Neumann M, Schmid B, et al. Missense mutations in the progranulin gene linked to frontotemporal lobar degeneration with ubiquitin-immunoreactive inclusions reduce progranulin production and secretion. J Biol Chem. 2008;283(3):1744–53.

25. Smith KR, Damiano J, Franceschetti S, Carpenter S, Canafoglia L, Morbin M, et al. Strikingly different clinicopathological phenotypes determined by

progranulin-mutation dosage. Am J Hum Genet. 2012;90(6):1102–7.

26. Canafoglia L, Morbin M, Scaioli V, Pareyson D, D'Incerti L, Fugnanesi V, et al. Recurrent generalized seizures, visual loss, and palinopsia as phenotypic features of neuronal ceroid lipofuscinosis due to progranulin gene mutation. Epilepsia. 2014;55(6):56–9.

27. Kleinberger G, Capell A, Haass C, Van Broeckhoven C. Mechanisms of granulin deficiency: Lessons from cellular and animal models. Mol Neurobiol. 2013;47(1):337–60.

28. Belcastro V, Siciliano V, Gregoretti F, Mithbaokar P, Dharmalingam G, Berlingieri S, et al. Transcriptional gene network inference from a massive dataset elucidates transcriptome organization and gene function. Nucleic Acids Res. 2011;39(20):8677–88.

29. Capell A, Liebscher S, Fellerer K, Brouwers N, Willem M, Lammich S, et al. Rescue of progranulin deficiency associated with frontotemporal lobar degeneration by alkalizing reagents and inhibition of vacuolar ATPase. J Neurosci. 2011;31(5):1885–94.

30. Hu F, Padukkavidana T, V??gter CB, Brady OA, Zheng Y, Mackenzie IR, et al. Sortilin-mediated endocytosis determines levels of the frontotemporal dementia protein, progranulin. Neuron. 2010;68(4):654–67.

31. Zhou X, Sun L, de Oliveira FB, Qi X, Brown WJ, Smolka MB, et al. Prosaposin facilitates sortilin-independent lysosomal trafficking of progranulin. J Cell Biol. 2015;210(6):991–1002.

32. Zheng Y, Brady OA, Meng PS, Mao Y, Hu F. C-terminus of progranulin interacts with the beta-propeller region of sortilin to regulate progranulin trafficking. PLoS One. 2011;6(6).

33. Pankiv S, Clausen TH, Lamark T, Brech A, Bruun JA, Outzen H, et al. p62/SQSTM1 binds directly to Atg8/LC3 to facilitate degradation of ubiquitinated protein aggregates by autophagy*[S]. J Biol Chem. 2007;282(33):24131–45.

34. Tanaka Y, Chambers JK, Matsuwaki T, Yamanouchi K, Nishihara M. Possible involvement of lysosomal dysfunction in pathological changes of the brain in aged progranulin-deficient mice - 40478_2014_Article_78.pdf. 2014;1–15.

35. Wils H, Kleinberger G, Pereson S, Janssens J, Capell A, Van Dam D, et al. Cellular ageing, increased mortality and FTLD-TDP-associated neuropathology in progranulin knockout mice. J Pathol. 2012;228(1):67–76.

36. Götzl JK, Mori K, Damme M, Fellerer K, Tahirovic S, Kleinberger G, et al.

Common pathobiochemical hallmarks of progranulin-associated frontotemporal lobar degeneration and neuronal ceroid lipofuscinosis. Acta Neuropathol. 2014;127(6):845–60.

37. Ahmed Z, Sheng H, Xu Y, Lin W-L, Innes AE, Gass J, et al. Accelerated Lipofuscinosis and Ubiquitination in Granulin Knockout Mice Suggest a Role for Progranulin in Successful Aging. Am J Pathol. 2010;177(1):311–24.

38. Yin F, Dumont M, Banerjee R et al. Behavioral deficits and progressive neuropathology in progranulin-deficient mice: a mouse model of frontotemporal dementia. FASEB J. 2010;24(12):4639–47.

39. Ghoshal N, Dearborn JT, Wozniak DF, Cairns NJ. Core features of frontotemporal dementia recapitulated in progranulin knockout mice. Neurobiol Dis. 2012;45(1):395–408.

40. Petkau TL, Neal SJ, Milnerwood A, Mew A, Hill AM, Orban P, et al. Synaptic dysfunction in progranulin-deficient mice. Neurobiol Dis. 2012;45(2):711–22.

41. Cruchaga C, Graff C, Chiang H-H, Wang J, Hinrichs AL, Spiegel N, et al. Association of TMEM106B gene polymorphism with age at onset in granulin mutation carriers and plasma granulin protein levels. Arch Neurol. 2011;68(5):581–6.

42. Finch N, Carrasquillo MM, Baker M, Rutherford NJ, Coppola G, Dejesus-Hernandez M, et al. TMEM106B regulates progranulin levels and the penetrance of FTLD in GRN mutation carriers. Neurology. 2011;76(5):467–74.

43. Van Der Zee J, Van Langenhove T, Kleinberger G, Sleegers K, Engelborghs S, Vandenberghe R, et al. TMEM106B is associated with frontotemporal lobar degeneration in a clinically diagnosed patient cohort. Brain. 2011;134(3):808–15.

44. Van Deerlin VM, Sleiman PM a, Martinez-Lage M, Chen-Plotkin A, Wang L-S, Graff-Radford NR, et al. Common variants at 7p21 are associated with frontotemporal lobar degeneration with TDP-43 inclusions. Nat Genet. 2010;42(3):234–9.

45. Gallagher MD, Suh E, Grossman M, Elman L, McCluskey L, Van Swieten JC, et al. TMEM106B is a genetic modifier of frontotemporal lobar degeneration with C9orf72 hexanucleotide repeat expansions. Acta Neuropathol. 2014;127(3):407–18.

46. Ash PEA, Bieniek KF, Gendron TF, Caulfield T, Lin WL, DeJesus-Hernandez M, et al. Unconventional Translation of C9ORF72 GGGGCC Expansion Generates Insoluble Polypeptides Specific to c9FTD/ALS. Neuron. 2013;77:639–46.

47. Chen-Plotkin AS, Unger TL, Gallagher MD, Bill E, Kwong LK, Volpicelli-Daley L, et al. TMEM106B, the risk gene for frontotemporal dementia, is regulated by the microRNA-132/212 cluster and affects progranulin pathways. J Neurosci. 2012;32(33):11213–27.

48. Brady OA, Zheng Y, Murphy K, Huang M, Hu F. The frontotemporal lobar degeneration risk factor, TMEM106B, regulates lysosomal morphology and function. Hum Mol Genet. 2013;22(4):685–95.

49. Lang CM, Fellerer K, Schwenk BM, Kuhn PH, Kremmer E, Edbauer D, et al. Membrane orientation and subcellular localization of transmembrane protein 106B (TMEM106B), a major risk factor for frontotemporal lobar degeneration. J Biol Chem. 2012;287(23):19355–65.

50. Stagi M, Klein ZA, Gould TJ, Bewersdorf J, Strittmatter SM. Lysosome size, motility and stress response regulated by fronto-temporal dementia modifier TMEM106B. Mol Cell Neurosci. 2014;61:226–40.

51. Schwenk BM, Lang CM, Hogl S, Tahirovic S, Orozco D, Rentzsch K, et al. The FTLD risk factor TMEM106B and MAP6 control dendritic trafficking of lysosomes. EMBO J. 2014;33(5):450–67.

52. Zhou X, Sun L, Brady OA, Murphy KA, Hu F. Elevated TMEM106B levels exaggerate lipofuscin accumulation and lysosomal dysfunction in aged mice with progranulin deficiency. Acta Neuropathol Commun. 2017;5(1):9.

53. Skibinski G, Parkinson NJ, Brown JM, Chakrabarti L, Lloyd SL, Hummerich H, et al. Mutations in the endosomal ESCRTIII-complex subunit CHMP2B in frontotemporal dementia. Nat Genet. 2005;37(8):806–8.

54. Urwin H, Josephs KA, Rohrer JD, MacKenzie IR, Neumann M, Authier A, et al. FUS pathology defines the majority of tau-and TDP-43-negative frontotemporal lobar degeneration. Acta Neuropathol. 2010;120(1):33–41.

55. Parkinson N, Ince PG, Smith MO, Highley R, Skibinski G, Andersen PM, et al. ALS phenotypes with mutations in CHMP2B (charged multivesicular body protein 2B). Neurology. 2006;67(6):1074–7.

56. Tsang HTH, Connell JW, Brown SE, Thompson A, Reid E, Sanderson CM. A systematic analysis of human CHMP protein interactions: Additional MIT domain-containing proteins bind to multiple components of the human ESCRT III complex. Genomics. 2006;88(3):333–46.

57. Fader CM, Colombo MI. Autophagy and multivesicular bodies: two closely related partners. Cell Death Differ. 2009;16(1):70–8.

58. Shim S, Kimpler LA, Hanson PI. Structure/function analysis of four core

ESCRT-III proteins reveals common regulatory role for extreme C-terminal domain. Traffic. 2007;8(8):1068–79.

59. van der Zee J, Urwin H, Engelborghs S, Bruyland M, Vandenberghe R, Dermaut B, et al. CHMP2B C-truncating mutations in frontotemporal lobar degeneration are associated with an aberrant endosomal phenotype in vitro. Hum Mol Genet. 2008;17(2):313–22.

60. Stuchell-Brereton MD, Skalicky JJ, Kieffer C, Karren MA, Ghaffarian S, Sundquist WI. ESCRT-III recognition by VPS4 ATPases. Nature. 2007;449(7163):740–4.

61. Takayuki Obita, Suraj Saksena, Sara Ghazi-Tabatabai, David J. Gill, Olga Perisic, Scott D. Emt RLW. Structural basis for selective recognition of ESCRT-III by the AAA ATPase Vps4. Nature. 2007;449:735–40.

62. Wollert T, Wunder C, Lippincott-schwartz J, Hurley JHJH, H J. Membrane scission by the ESCRT-III complex. Nature. 2009;458(7235):172–7.

63. Lu Y, Zhang Z, Sun D, Sweeney ST, Gao FB. Syntaxin 13, a genetic modifier of mutant CHMP2B in frontotemporal dementia, is required for autophagosome maturation. Mol Cell. 2013;52(2):264–71.

64. West RJH, Lu Y, Marie B, Gao FB, Sweeney ST. Rab8, POSH, and TAK1 regulate synaptic growth in a Drosophila model of frontotemporal dementia. J Cell Biol. 2015;208(7):931–47.

65. Filimonenko M, Stuffers S, Raiborg C, Yamamoto A, Malerød L, Fisher EMC, et al. Functional multivesicular bodies are required for autophagic clearance of protein aggregates associated with neurodegenerative disease. J Cell Biol. 2007;179(3):485–500.

66. Lee JA, Liu L, Gao FB. Autophagy defects contribute to neurodegeneration induced by dysfunctional ESCRT-III. Vol. 5, Autophagy. 2009. p. 1070–2.

67. Ghazi-Noori S, Froud KE, Mizielinska S, Powell C, Smidak M, Fernandez De Marco M, et al. Progressive neuronal inclusion formation and axonal degeneration in CHMP2B mutant transgenic mice. Brain. 2012;135(3):819–32.

68. Krasniak CS, Ahmad ST. The role of CHMP2BIntron5 in autophagy and frontotemporal dementia. Brain Res. 2016;1649:151–7.

69. Vernay A, Therreau L, Blot B, Risson V, Dirrig-Grosch S, Waegaert R, et al. A transgenic mouse expressing CHMP2Bintron5 mutant in neurons develops histological and behavioural features of amyotrophic lateral sclerosis and frontotemporal dementia. Hum Mol Genet. 2016;ddw182.

70. Nielsen TT, Mizielinska S, Hasholt L, Isaacs AM, Nielsen JE. Reversal of pathology in CHMP2B-mediated frontotemporal dementia patient cells using RNA interference. J Gene Med. 2012;14(8):521–9.

71. Clayton EL, Mizielinska S, Edgar JR, Nielsen TT, Marshall S, Norona FE, et al. Frontotemporal dementia caused by CHMP2B mutation is characterised by neuronal lysosomal storage pathology. Acta Neuropathol. 2015;130(4):511–23.

72. Watts GDJ, Wymer J, Kovach MJ, Mehta SG, Mumm S, Darvish D, et al. Inclusion body myopathy associated with Paget disease of bone and frontotemporal dementia is caused by mutant valosin-containing protein. Nat Genet. 2004;36(4):377–81.

73. Guyant-Mar??chal L, Laquerri??re A, Duyckaerts C, Dumanchin C, Bou J, Dugny F, et al. Valosin-containing protein gene mutations: Clinical and neuropathologic features. Neurology. 2006;67(4):644–51.

74. Forman MS, Mackenzie IR, Cairns NJ, Swanson E, Boyer PJ, Drachman DA, et al. Novel ubiquitin neuropathology in frontotemporal dementia with valosin-containing protein gene mutations. J Neuropathol Exp Neurol. 2006;65(6):571–81.

75. Schröder R, Watts GDJ, Mehta SG, Evert BO, Broich P, Fließbach K, et al. Mutant valosin-containing protein causes a novel type of frontotemporal dementia. Ann Neurol. 2005;57(3):457–61.

76. Neumann M, Mackenzie IR, Cairns NJ, Boyer PJ, Markesbery WR, Smith CD, et al. TDP-43 in the ubiquitin pathology of frontotemporal dementia with VCP gene mutations. J Neuropathol Exp Neurol. 2007;66(2):152–7.

77. Johnson JO, Mandrioli J, Benatar M, Abramzon Y, Van Deerlin VM, Trojanowski JQ, et al. Exome Sequencing Reveals VCP Mutations as a Cause of Familial ALS. Neuron. 2010;68(5):857–64.

78. Gonzalez MA, Feely SM, Speziani F, Strickland A V., Danzi M, Bacon C, et al. A novel mutation in VCP causes Charcot-Marie-Tooth Type 2 disease. Brain. 2014;137(11):2897–902.

79. Jentsch S, Rumpf S. Cdc48 (p97): a “molecular gearbox” in the ubiquitin pathway? Trends Biochem Sci. 2007;32(1):6–11.

80. Rabinovich E, Kerem A, Fröhlich K-U, Diamant N, Bar-Nun S. AAA-ATPase p97/Cdc48p, a cytosolic chaperone required for endoplasmic reticulum-associated protein degradation. Mol Cell Biol. 2002;22(2):626–34.

81. Song C, Wang Q, Song C, Rogers TJ. Valosin-containing protein (VCP/p97) is capable of unfolding polyubiquitinated proteins through its ATPase domains.

Biochem Biophys Res Commun. 2015;463(3):453–7.

82. Lim PJ, Danner R, Liang J, Doong H, Harman C, Srinivasan D, et al. Ubiquilin and p97/VCP bind erasin, forming a complex involved in ERAD. J Cell Biol. 2009;187(2):201–17.

83. Ye Y, Meyer HH, Rapoport T a. The AAA ATPase Cdc48/p97 and its partners transport proteins from the ER into the cytosol. Nature. 2001;414(6864):652–6.

84. Pleasure IT, Black MM, Keen JH. Valosin-containing protein, VCP, is a ubiquitous clathrin-binding protein. Nature. 1993;365(6445):459–62.

85. Ramanathan HN, Ye Y. The p97 ATPase associates with EEA1 to regulate the size of early endosomes. Cell Res. 2012;22(2):346–59.

86. Ju JS, Fuentealba RA, Miller SE, Jackson E, Piwnica-Worms D, Baloh RH, et al. Valosin-containing protein (VCP) is required for autophagy and is disrupted in VCP disease. J Cell Biol. 2009;187(6):875–88.

87. Tresse E, Salomons FA, Vesa J, Bott LC, Kimonis V, Yao TP, et al. VCP/p97 is essential for maturation of ubiquitin-containing autophagosomes and this function is impaired by mutations that cause IBMPFD. Autophagy. 2010;6(2):217–27.

88. Ritz D, Vuk M, Kirchner P, Bug M, Schütz S, Hayer A, et al. Endolysosomal sorting of ubiquitylated caveolin-1 is regulated by VCP and UBXD1 and impaired by VCP disease mutations. Nat Cell Biol. 2011;13(9):1116–23.

89. Badadani M, Nalbandian A, Watts GD, Vesa J, Kitazawa M, Su H, et al. VCP associated inclusion body myopathy and paget disease of bone knock-in mouse model exhibits tissue pathology typical of human disease. PLoS One. 2010;5(10).

90. Custer SK, Neumann M, Lu H, Wright AC, Taylor JP. Transgenic mice expressing mutant forms VCP/p97 recapitulate the full spectrum of IBMPFD including degeneration in muscle, brain and bone. Hum Mol Genet. 2010;19(9):1741–55.

91. Müller JMM, Deinhardt K, Rosewell I, Warren G, Shima DT. Targeted deletion of p97 (VCP/CDC48) in mouse results in early embryonic lethality. Biochem Biophys Res Commun. 2007;354(2):459–65.

92. Buchan JR, Kolaitis RM, Taylor JP, Parker R. XEukaryotic stress granules are cleared by autophagy and Cdc48/VCP function. Cell. 2013;153(7):1461–74.

93. Weihl CC, Temiz P, Miller SE, Watts G, Smith C, Forman M, et al. TDP-43 accumulation in inclusion body myopathy muscle suggests a common

pathogenic mechanism with frontotemporal dementia. J Neurol Neurosurg Psychiatry. 2008;79(10):1186–9.

94. Fecto F. Mutations in Familial and Sporadic Amyotrophic Lateral Sclerosis. Arch Neurol. 2011;68(11):1440–6.

95. Deng H-X, Chen W, Hong S-T, Boycott KM, Gorrie GH, Siddique N, et al. Mutations in UBQLN2 cause dominant X-linked juvenile and adult-onset ALS and ALS/dementia. Nature. 2011;477(7363):211–5.

96. Freischmidt A, Müller K, Ludolph AC, Weishaupt JH, Andersen PM. Association of Mutations in TBK1 With Sporadic and Familial Amyotrophic Lateral Sclerosis and Frontotemporal Dementia. JAMA Neurol. 2016;3–6.

97. Weishaupt JH, Waibel S, Birve A, Volk AE, Mayer B, Meyer T, et al. A novel optineurin truncating mutation and three glaucoma-associated missense variants in patients with familial amyotrophic lateral sclerosis in Germany. Neurobiol Aging. 2013;34(5):1516.e9-1516.e15.

98. Williams KL, McCann EP, Fifita JA, Zhang K, Duncan EL, Leo PJ, et al. Novel TBK1 truncating mutation in a familial amyotrophic lateral sclerosis patient of Chinese origin. Neurobiol Aging. 2015;36(12):3334.e1-3334.e5.

99. Maruyama H, Morino H, Ito H, Izumi Y, Kato H, Watanabe Y, et al. Mutations of optineurin in amyotrophic lateral sclerosis. Nature. 2010;465(7295):223–6.

100. Kovacs GG, van der Zee J, Hort J, Kristoferitsch W, Leitha T, Höftberger R, et al. Clinicopathological description of two cases with SQSTM1 gene mutation associated with frontotemporal dementia. Neuropathology. 2016;36(1):27–38.

101. Pottier C, Bieniek KF, Finch NC, van de Vorst M, Baker M, Perkersen R, et al. Whole-genome sequencing reveals important role for TBK1 and OPTN mutations in frontotemporal lobar degeneration without motor neuron disease. Acta Neuropathol. 2015;130(1):77–92.

102. Arai T, Nonaka T, Hasegawa M, Akiyama H, Yoshida M, Hashizume Y, et al. Neuronal and glial inclusions in frontotemporal dementia with or without motor neuron disease are immunopositive for p62. Neurosci Lett. 2003;342(1–2):41–4.

103. Kuusisto E, Kauppinen T, Alafuzoff I. Use of p62/SQSTM1 antibodies for neuropathological diagnosis. Neuropathol Appl Neurobiol. 2008;34(2):169–80.

104. Nakano T, Nakaso K, Nakashima K, Ohama E. Expression of ubiquitin-binding protein p62 in ubiquitin-immunoreactive intraneuronal inclusions in amyotrophic lateral sclerosis with dementia: Analysis of five autopsy cases with broad clinicopathological spectrum. Acta Neuropathol. 2004;107(4):359–64.

105. Korolchuk VI, Menzies FM, Rubinsztein DC. A novel link between autophagy and the ubiquitin-proteasome system. Autophagy. 2009;5(6):862–3.

106. Seibenhener M, Babu J. Sequestosome 1 / p62 Is a Polyubiquitin Chain Binding Protein Involved in Ubiquitin Proteasome Degradation. Mol Cell Biol. 2004;24(18):8055–68.

107. Rea SL, Walsh JP, Layfield R, Ratajczak T, Xu Jiake J. New insights into the role of sequestosome 1/p62 mutant proteins in the pathogenesis of paget's disease of bone. Endocr Rev. 2013;34(4):501–24.

108. Rogov V, Dötsch V, Johansen T, Kirkin V. Interactions between Autophagy Receptors and Ubiquitin-like Proteins Form the Molecular Basis for Selective Autophagy. Mol Cell. 2014;53(2):167–78.

109. Johansen T, Lamark T. Selective autophagy mediated by autophagic adapter proteins. Autophagy. 2011;7(3):279–96.

110. Matsumoto G, Wada K, Okuno M, Kurosawa M, Nukina N. Serine 403 phosphorylation of p62/SQSTM1 regulates selective autophagic clearance of ubiquitinated proteins. Mol Cell. 2011;44(2):279–89.

111. Pilli M, Arko-Mensah J, Ponpuak M, Roberts E, Master S, Mandell MA, et al. TBK-1 Promotes Autophagy-Mediated Antimicrobial Defense by Controlling Autophagosome Maturation. Immunity. 2012;37(2):223–34.

112. Lim J, Lachenmayer ML, Wu S, Liu W, Kundu M, Wang R, et al. Proteotoxic stress induces phosphorylation of p62/SQSTM1 by ULK1 to regulate selective autophagic clearance of protein aggregates. PLoS Genet. 2015;11(2):e1004987.

113. Ro SH, Semple IA, Park H, Park H, Park HW, Kim M, et al. Sestrin2 promotes Unc-51-like kinase 1 mediated phosphorylation of p62/sequestosome-1. FEBS J. 2014;281(17):3816–27.

114. Paine MG, Babu JR, Seibenhener ML, Wooten MW. Evidence for p62 aggregate formation: Role in cell survival. FEBS Lett. 2005;579(22):5029–34.

115. Bjørkøy G, Lamark T, Brech A, Outzen H, Perander M, Øvervatn A, et al. p62/SQSTM1 forms protein aggregates degraded by autophagy and has a protective effect on huntingtin-induced cell death. J Cell Biol. 2005;171(4):603–14.

116. Komatsu M, Waguri S, Koike M, Sou Y shin, Ueno T, Hara T, et al. Homeostatic Levels of p62 Control Cytoplasmic Inclusion Body Formation in Autophagy-Deficient Mice. Cell. 2007;131(6):1149–63.

117. Kwok CT, Morris A, de Belleroche JS. Sequestosome-1 (SQSTM1) sequence

variants in ALS cases in the UK: prevalence and coexistence of SQSTM1 mutations in ALS kindred with PDB. Eur J Hum Genet. 2014;22(4):492–6.

118. Teyssou E, Takeda T, Lebon V, Boillée S, Doukouré B, Bataillon G, et al. Mutations in SQSTM1 encoding p62 in amyotrophic lateral sclerosis: Genetics and neuropathology. Acta Neuropathol. 2013;125(4):511–22.

119. Rubino E, Chio A, Rogaeva E, Galimberti D, Bruni AC, St PH. SQSTM1 mutations in frontotemporal lobar degeneration and amyotrophic lateral sclerosis. 2012;

120. Haack TB, Ignatius E, Calvo-Garrido J, Iuso A, Isohanni P, Maffezzini C, et al. Absence of the Autophagy Adaptor SQSTM1/p62 Causes Childhood-Onset Neurodegeneration with Ataxia, Dystonia, and Gaze Palsy. Am J Hum Genet. 2016;735–43.

121. Babu JR, Geetha T, Wooten MW. Sequestosome 1/p62 shuttles polyubiquitinated tau for proteasomal degradation. J Neurochem. 2005;94(1):192–203.

122. Zhang Y-J, Gendron TF, Xu Y-F, Ko L-W, Yen S-H, Petrucelli L. Phosphorylation regulates proteasomal-mediated degradation and solubility of TAR DNA binding protein-43 C-terminal fragments. Mol Neurodegener. 2010 Jan;5:33.

123. Ko HS, Uehara T, Tsuruma K, Nomura Y. Ubiquilin interacts with ubiquitylated proteins and proteasome through its ubiquitin-associated and ubiquitin-like domains. FEBS Lett. 2004;566(1–3):110–4.

124. N'Diaye E-N, Kajihara KK, Hsieh I, Morisaki H, Debnath J, Brown EJ. PLIC proteins or ubiquilins regulate autophagy-dependent cell survival during nutrient starvation. EMBO Rep. 2009;10(2):173–9.

125. Rothenberg C, Srinivasan D, Mah L, Kaushik S, Peterhoff CM, Ugolino J, et al. Ubiquilin functions in autophagy and is degraded by chaperone-mediated autophagy. Hum Mol Genet. 2010;19(16):3219–32.

126. Cassel JA, Reitz AB. Ubiquilin-2 (UBQLN2) binds with high affinity to the C-terminal region of TDP-43 and modulates TDP-43 levels in H4 cells: Characterization of inhibition by nucleic acids and 4-aminoquinolines. Biochim Biophys Acta - Proteins Proteomics. 2013;1834(6):964–71.

127. Majcher V, Goode A, James V, Layfield R. Autophagy receptor defects and ALS-FTLD. Mol Cell Neurosci. 2015;66(Part A):43–52.

128. Gilpin KM, Chang L, Monteiro MJ. ALS-linked mutations in ubiquilin-2 or hnRNPA1 reduce interaction between ubiquilin-2 and hnRNPA1. Hum Mol

Genet. 2015;24(9):2565–77.

129. Wu Q, Liu M, Huang C, Liu X, Huang B, Li N, et al. Pathogenic Ubqln2 gains toxic properties to induce neuron death. Acta Neuropathol. 2014;129(3):417–28.

130. Le NTT, Chang L, Kovlyagina I, Georgiou P, Safren N, Braunstein KE, et al. Motor neuron disease, TDP-43 pathology, and memory deficits in mice expressing ALS-FTD-linked UBQLN2 mutations. Proc Natl Acad Sci U S A. 2016;201608432.

131. Ceballos-Diaz C, Rosario AM, Park H-J, Chakrabarty P, Sacino A, Cruz PE, et al. Viral expression of ALS-linked ubiquilin-2 mutants causes inclusion pathology and behavioral deficits in mice. Mol Neurodegener. 2015;10(1):25.

132. Huang B, Wu Q, Zhou H, Huang C, Xia XG. Increased Ubqln2 expression causes neuron death in transgenic rats. J Neurochem. 2016;285–93.

133. Walters KJ, Kleijnen MF, Goh AM, Wagner G, Howley PM. Structural studies of the interaction between ubiquitin family proteins and proteasome subunit S5a. Biochemistry. 2002;41(6):1767–77.

134. Hjerpe R, Bett JS, Keuss MJ, Solovyova A, McWilliams TG, Johnson C, et al. UBQLN2 Mediates Autophagy-Independent Protein Aggregate Clearance by the Proteasome. Cell. 2016;166(4):935–49.

135. Osaka M, Ito D, Suzuki N. Disturbance of proteasomal and autophagic protein degradation pathways by amyotrophic lateral sclerosis-linked mutations in ubiquilin 2. Biochem Biophys Res Commun. 2016;472(2):324–31.

136. Xia Y, Yan LH, Huang B, Liu M, Liu X, Huang C. Pathogenic mutation of UBQLN2 impairs its interaction with UBXD8 and disrupts endoplasmic reticulum-associated protein degradation. J Neurochem. 2014;129(1):99–106.

137. Iguchi Y, Katsuno M, Ikenaka K, Ishigaki S, Sobue G. Amyotrophic lateral sclerosis: An update on recent genetic insights. J Neurol. 2013;260(11):2917–27.

138. Wild P, Farhan H, McEwan DG, Wagner S, Rogov V V., Brady NR, et al. Phosphorylation of the Autophagy. Science (80-). 2011;333(July):228–33.

139. Wong YC, Holzbaur ELF. Optineurin is an autophagy receptor for damaged mitochondria in parkin-mediated mitophagy that is disrupted by an ALS-linked mutation. Proc Natl Acad Sci U S A. 2014;111(42):E4439-48.

140. Korac J, Schaeffer V, Kovacevic I, Clement AM, Jungblut B, Behl C, et al. Ubiquitin-independent function of optineurin in autophagic clearance of protein

aggregates. J Cell Sci. 2013;126(2):580–92.

141. Liu Z, Chen P, Gao H, Gu Y, Yang J, Peng H, et al. Ubiquitylation of Autophagy Receptor Optineurin by HACE1 Activates Selective Autophagy for Tumor Suppression. Cancer Cell. 2014;26(1):106–20.

142. Morton S, Hesson L, Peggie M, Cohen P. Enhanced binding of TBK1 by an optineurin mutant that causes a familial form of primary open angle glaucoma. FEBS Lett. 2008;582(6):997–1002.

143. Chalasani MLS, Kumari A, Radha V, Swarup G. E50K-OPTN-induced retinal cell death involves the Rab GTPase-activating protein, TBC1D17 mediated block in autophagy. PLoS One. 2014;9(4).

144. Borghero G, Pugliatti M, Marrosu F, Marrosu MG, Murru MR, Floris G, et al. TBK1 is associated with ALS and ALS-FTD in Sardinian patients. Neurobiol Aging. 2016;43:1–5.

145. Gijselinck I, Van Mossevelde S, van der Zee J, Sieben A, Philtjens S, Heeman B, et al. Loss of *TBK1* is a frequent cause of frontotemporal dementia in a Belgian cohort. Neurology. 2015;85(24):2116–25.

146. Le Ber I, De Septenville A, Millecamps S, Camuzat A, Caroppo P, Couratier P, et al. TBK1 mutation frequencies in French frontotemporal dementia and amyotrophic lateral sclerosis cohorts. Neurobiol Aging. 2015;36(11):3116.e5-3116.e8.

147. Tsai PC, Liu YC, Lin KP, Liu YT, Liao YC, Hsiao CT, et al. Mutational analysis of TBK1 in Taiwanese patients with amyotrophic lateral sclerosis. Neurobiol Aging. 2016;40:191.e11-6.

148. Oakes JA, Davies MC, Collins MO. TBK1: a new player in ALS linking autophagy and neuroinflammation. 2017;1–10.

149. Minegishi Y, Nakayama M, Iejima D, Kawase K, Iwata T. Significance of optineurin mutations in glaucoma and other diseases. Prog Retin Eye Res. 2016;55:149–81.

150. Moore AS, Holzbaur ELF. Dynamic recruitment and activation of ALS-associated TBK1 with its target optineurin are required for efficient mitophagy. Proc Natl Acad Sci U S A. 2016;1–10.

151. Dejesus-hernandez M, Mackenzie IR, Boeve BF, Boxer AL, Baker M, Rutherford NJ, et al. Supplemental Information Expanded GGGGCC Hexanucleotide Repeat in Noncoding Region of C9ORF72 Causes Chromosome 9p-Linked FTD and ALS. 72.

152. Renton AE, Majounie E, Waite A, Simón-Sánchez J, Rollinson S, Gibbs JR, et al. A hexanucleotide repeat expansion in C9ORF72 is the cause of chromosome 9p21-linked ALS-FTD. Neuron. 2011;72:257–68.

153. Gijselinck I, Van Langenhove T, van der Zee J, Sleegers K, Philtjens S, Kleinberger G, et al. A C9orf72 promoter repeat expansion in a Flanders-Belgian cohort with disorders of the frontotemporal lobar degeneration-amyotrophic lateral sclerosis spectrum: A gene identification study. Lancet Neurol. 2012;11:54–65.

154. Majounie E, Renton AE, Mok K, Dopper EGP, Waite A, Rollinson S, et al. Frequency of the C9orf72 hexanucleotide repeat expansion in patients with amyotrophic lateral sclerosis and frontotemporal dementia: A cross-sectional study. Lancet Neurol. 2012;11(4):323–30.

155. van der Zee J, Gijselinck I, Dillen L, Van Langenhove T, Theuns J, Engelborghs S, et al. A Pan-European Study of the C9orf72 Repeat Associated with FTLD: Geographic Prevalence, Genomic Instability, and Intermediate Repeats. Hum Mutat. 2013;34(2):363–73.

156. Al-Sarraj S, King A, Troakes C, Smith B, Maekawa S, Bodi I, et al. P62 positive, TDP-43 negative, neuronal cytoplasmic and intranuclear inclusions in the cerebellum and hippocampus define the pathology of C9orf72-linked FTLD and MND/ALS. Acta Neuropathol. 2011;122(6):691–702.

157. Brettschneider J, Van Deerlin VM, Robinson JL, Kwong L, Lee EB, Ali YO, et al. Pattern of ubiquilin pathology in ALS and FTLD indicates presence of C9ORF72 hexanucleotide expansion. Acta Neuropathol. 2012;123(6):825–39.

158. King A, Maekawa S, Bodi I, Troakes C, Al-Sarraj S. Ubiquitinated, p62 immunopositive cerebellar cortical neuronal inclusions are evident across the spectrum of TDP-43 proteinopathies but are only rarely additionally immunopositive for phosphorylation-dependent TDP-43. Neuropathology. 2011;31(3):239–49.

159. Mahoney CJ, Beck J, Rohrer JD, Lashley T, Mok K, Shakespeare T, et al. Frontotemporal dementia with the C9ORF72 hexanucleotide repeat expansion: Clinical, neuroanatomical and neuropathological features. Brain. 2012;135(3):736–50.

160. Mori K, Weng S-M, Arzberger T, May S, Rentzsch K, Kremmer E, et al. The C9orf72 GGGGCC repeat is translated into aggregating dipeptide-repeat proteins in FTLD/ALS. Science. 2013;339:1335–8.

161. DeJesus-Hernandez M, Mackenzie IR, Boeve BF, Boxer AL, Baker M, Rutherford NJ, et al. Expanded GGGGCC Hexanucleotide Repeat in Noncoding Region of C9ORF72 Causes Chromosome 9p-Linked FTD and

ALS. Neuron. 2011;72:245–56.

162. Lagier-Tourenne C, Baughn M, Rigo F, Sun S, Liu P, Li H-R, et al. Targeted degradation of sense and antisense C9orf72 RNA foci as therapy for ALS and frontotemporal degeneration. Proc Natl Acad Sci U S A. 2013;110(47):E4530-9.

163. Mizielinska S, Lashley T, Norona FE, Clayton EL, Ridler CE, Fratta P, et al. C9orf72 frontotemporal lobar degeneration is characterised by frequent neuronal sense and antisense RNA foci. Acta Neuropathol. 2013;126(6):845–57.

164. Gendron TF, Bieniek KF, Zhang YJ, Jansen-West K, Ash PEA, Caulfield T, et al. Antisense transcripts of the expanded C9ORF72 hexanucleotide repeat form nuclear RNA foci and undergo repeat-associated non-ATG translation in c9FTD/ALS. Acta Neuropathol. 2013;126(6):829–44.

165. Freibaum BD, Lu Y, Lopez-Gonzalez R, Kim NC, Almeida S, Lee K-H, et al. GGGGCC repeat expansion in C9orf72 compromises nucleocytoplasmic transport. Nature. 2015;525(7567):129–33.

166. Gendron TF, Belzil V V, Zhang Y-J, Petrucelli L. Mechanisms of toxicity in C9FTLD/ALS. Acta Neuropathol. 2014 Mar;127(3):359–76.

167. Zhang K, Donnelly CJ, Haeusler AR, Grima JC, Machamer JB, Steinwald P, et al. The C9orf72 repeat expansion disrupts nucleocytoplasmic transport. Nature. 2015;525(7567):56–61.

168. Khosravi B, Hartmann H, May S, Möhl C, Ederle H, Michaelsen M, et al. Cytoplasmic poly-GA aggregates impair nuclear import of TDP-43 in *C9orf72* ALS/FTLD. Hum Mol Genet. 2016;0(0):ddw432.

169. Zhang Y-J, Gendron TF, Grima JC, Sasaguri H, Jansen-West K, Xu Y-F, et al. C9ORF72 poly(GA) aggregates sequester and impair HR23 and nucleocytoplasmic transport proteins. Nat Neurosci. 2016;19(5):668–77.

170. Lee KH, Zhang P, Kim HJ, Mitrea DM, Sarkar M, Freibaum BD, et al. C9orf72 Dipeptide Repeats Impair the Assembly, Dynamics, and Function of Membrane-Less Organelles. Cell. 2016;167(3):774–788.e17.

171. Fratta P, Poulter M, Lashley T, Rohrer JD, Polke JM, Beck J, et al. Homozygosity for the C9orf72 GGGGCC repeat expansion in frontotemporal dementia. Acta Neuropathol. 2013;126(3):401–9.

172. van Blitterswijk M, Gendron TF, Baker MC, DeJesus-Hernandez M, Finch NCA, Brown PH, et al. Novel clinical associations with specific C9ORF72 transcripts in patients with repeat expansions in C9ORF72. Acta Neuropathol.

2015;130(6):863–76.

173. Waite AJ, Bäumer D, East S, Neal J, Morris HR, Ansorge O, et al. Reduced C9orf72 protein levels in frontal cortex of amyotrophic lateral sclerosis and frontotemporal degeneration brain with the C9ORF72 hexanucleotide repeat expansion. Neurobiol Aging. 2014;35.

174. Therrien M, Rouleau GA, Dion PA, Parker JA. Deletion of C9ORF72 results in motor neuron degeneration and stress sensitivity in C. elegans. PLoS One. 2013;8.

175. Ciura S, Lattante S, Le Ber I, Latouche M, Tostivint H, Brice A, et al. Loss of function of C9orf72 causes motor deficits in a zebrafish model of amyotrophic lateral sclerosis. Ann Neurol. 2013;74:180–7.

176. Koppers M, Blokhuis AM, Westeneng HJ, Terpstra ML, Zundel CAC, Vieira De Sá R, et al. C9orf72 ablation in mice does not cause motor neuron degeneration or motor deficits. Ann Neurol. 2015;78(3):426–38.

177. Burberry A, Suzuki N, Wang JY, Moccia R, Mordes DA, Stewart MH, et al. Loss-of-function mutations in the C9ORF72 mouse ortholog cause fatal autoimmune disease. Sci Transl Med. 2016;8(347):347ra93.

178. ORourke JG, Bogdanik L, Yanez A, Lall D, Wolf AJ, Muhammad AKMG, et al. C9orf72 is required for proper macrophage and microglial function in mice. Science (80-). 2016;351(6279):1324–9.

179. Atanasio A, Decman V, White D, Ramos M, Ikiz B, Lee H-C, et al. C9orf72 ablation causes immune dysregulation characterized by leukocyte expansion, autoantibody production, and glomerulonephropathy in mice. Sci Rep. 2016;6(November 2015):23204.

180. Sullivan PM, Zhou X, Robins AM, Paushter DH, Kim D, Smolka MB, et al. The ALS/FTLD associated protein C9orf72 associates with SMCR8 and WDR41 to regulate the autophagy-lysosome pathway. Acta Neuropathol Commun. 2016;4(1):51.

181. Sudria-Lopez E, Koppers M, de Wit M, van der Meer C, Westeneng HJ, Zundel CAC, et al. Full ablation of C9orf72 in mice causes immune system-related pathology and neoplastic events but no motor neuron defects. Acta Neuropathol. 2016;132(1):145–7.

182. Jiang J, Zhu Q, Gendron TF, Saberi S, McAlonis-Downes M, Seelman A, et al. Gain of Toxicity from ALS/FTD-Linked Repeat Expansions in C9ORF72 Is Alleviated by Antisense Oligonucleotides Targeting GGGGCC-Containing RNAs. Neuron. 2016;90(3):535–50.

183. Farg MA, Sundaramoorthy V, Sultana JM, Yang S, Atkinson RAK, Levina V, et al. C9ORF72, implicated in amytrophic lateral sclerosis and frontotemporal dementia, regulates endosomal trafficking. Hum Mol Genet. 2014;23(13):3579–95.

184. Sellier C, Campanari M-L, Julie Corbier C, Gaucherot A, Kolb-Cheynel I, Oulad-Abdelghani M, et al. Loss of C9ORF72 impairs autophagy and synergizes with polyQ Ataxin-2 to induce motor neuron dysfunction and cell death. EMBO J. 2016;35(Icm):1–22.

185. Yang M, Liang C, Swaminathan K, Herrlinger S, Lai F, Shiekhattar R, et al. A C9ORF72/SMCR8-containing complex regulates ULK1 and plays a dual role in autophagy. Sci Adv. 2016;2(9):e1601167–e1601167.

186. Webster CP, Smith EF, Bauer CS, Moller A, Guillaume M, Ferraiuolo L, et al. The C9orf72 protein interacts with Rab 1 a and the ULK 1 complex to regulate initiation of autophagy. EMBO J. 2016;35(15):1–21.

187. Ugolino J, Ji YJ, Conchina K, Chu J, Nirujogi RS, Pandey A, et al. No Title. 2016;

188. Amick J, Roczniak-Ferguson A, Ferguson SM. C9orf72 binds SMCR8, localizes to lysosomes and regulates mTORC1 signaling. Mol Biol Cell. 2016;72.

189. Maharjan N, Kunzli C, Buthey K SS. C9ORF72 Regulates stress granule formation and its deficiency impairs stress granule assembly, hypersensitizing cells to stress. Hum Mol Genet. 2016;25(15):3341–60.

190. Sivadasan R, Hornburg D, Drepper C, Frank N, Jablonka S, Hansel A, et al. C9ORF72 interaction with cofilin modulates actin dynamics in motor neurons. Nat Neurosci. 2016;19(12):1610–8.

191. Snowden JS, Hu Q, Rollinson S, Halliwell N, Robinson A, Davidson YS, et al. The most common type of FTLD-FUS (aFTLD-U) is associated with a distinct clinical form of frontotemporal dementia but is not related to mutations in the FUS gene. Acta Neuropathol. 2011;122(1):99–110.

192. Lagier-Tourenne C, Polymenidou M, Cleveland DW. TDP-43 and FUS/TLS: Emerging roles in RNA processing and neurodegeneration. Hum Mol Genet. 2010;19(R1):46–64.

193. Bosco DA, Lemay N, Ko HK, Zhou H, Burke C, Kwiatkowski TJ, et al. Mutant FUS proteins that cause amyotrophic lateral sclerosis incorporate into stress granules. Hum Mol Genet. 2010;19(21):4160–75.

194. Thomas M, Alegre-Abarrategui J, Wade-Martins R. RNA dysfunction and

aggrephagy at the centre of an amyotrophic lateral sclerosis/frontotemporal dementia disease continuum. Brain. 2013;136(5):1345–60.

195. Cruts M, Theuns J, Van Broeckhoven C. Locus-specific mutation databases for neurodegenerative brain diseases. Hum Mutat. 2012;33(9):1340–4.

196. Edor Kabashi, Paul Valdmanis, Partrick Dion. Dan Spiegelman, Brendan J McConkey, Christine Vande Velde, Jean-Peirre Bouchard, Lucette Lacomblez, Ksenia Pochigaeva, Francois Salachas, Pierre-Francois Pradat, William Camu, Vincent Meininger, Nicolas Dupre GAR. TARDBP mutations in individuals with sporadic and familial amyotrophoc lateral sclerosis. Nat Genet. 2008;40(5):572–4.

197. Huang C-C, Bose JK, Majumder P, Lee K-H, Huang J-TJ, Huang JK, et al. Metabolism and mis-metabolism of the neuropathological signature protein TDP-43. J Cell Sci. 2014;127(Pt 14):3024–38.

198. Xia Q, Wang H, Hao Z, Fu C, Hu Q, Gao F, et al. TDP-43 loss of function increases TFEB activity and blocks autophagosome–lysosome fusion. EMBO J. 2016;35(2):121–42.

199. Monahan Z, Shewmaker F, Pandey UB. Stress granules at the intersection of autophagy and ALS. Vol. 1649, Brain Research. 2016. p. 189–200.

200. Bose JK, Huang CC, Shen CKJ. Regulation of autophagy by neuropathological protein TDP-43. J Biol Chem. 2011;286(52):44441–8.

201. Molliex A, Temirov J, Lee J, Coughlin M, Kanagaraj AP, Kim HJ, et al. Phase Separation by Low Complexity Domains Promotes Stress Granule Assembly and Drives Pathological Fibrillization. Cell. 2015;163(1):123–33.

202. Murakami T, Qamar S, Lin JQ, Schierle GSK, Rees E, Miyashita A, et al. ALS/FTD Mutation-Induced Phase Transition of FUS Liquid Droplets and Reversible Hydrogels into Irreversible Hydrogels Impairs RNP Granule Function. Neuron. 2015;88(4):678–90.

203. Li YR, King OD, Shorter J, Gitler AD. Stress granules as crucibles of ALS pathogenesis. J Cell Biol. 2013;201(3):361–72.

204. Taylor JP, Brown RH, Cleveland DW. Decoding ALS: from genes to mechanism. Nature. 2016;539(7628):197–206.

205. Zhou Y, Liu S, Liu G, Öztürk A, Hicks GG. ALS-Associated FUS Mutations Result in Compromised FUS Alternative Splicing and Autoregulation. PLoS Genet. 2013;9(10).

206. Ryu HH, Jun MH, Min KJ, Jang DJ, Lee YS, Kim HK, et al. Autophagy

regulates amyotrophic lateral sclerosis-linked fused in sarcoma-positive stress granules in neurons. Neurobiol Aging. 2014;35(12):2822–31.

207. Gal J, Zhang J, Kwinter DM, Zhai J, Jia H, Jia J, et al. Nuclear localization sequence of FUS and induction of stress granules by ALS mutants. Neurobiol Aging. 2011;32(12):2323.e27-2323.e40.

208. Ling S-C, Polymenidou M, Cleveland DW. Converging mechanisms in ALS and FTD: disrupted RNA and protein homeostasis. Neuron. 2013 Aug 7;79(3):416–38.

209. Dormann D, Haass C. TDP-43 and FUS: A nuclear affair. Trends Neurosci. 2011;34(7):339–48.

210. Patel A, Lee HO, Jawerth L, Maharana S, Jahnel M, Hein MY, et al. A Liquid-to-Solid Phase Transition of the ALS Protein FUS Accelerated by Disease Mutation. Cell. 2015;162(5):1066–77.

211. Soo KY, Sultana J, King AE, Atkinson R, Warraich ST, Sundaramoorthy V, et al. ALS-associated mutant FUS inhibits macroautophagy which is restored by overexpression of Rab1. Cell death Discov. 2015;1(July):15030.

212. Van Swieten J, Spillantini MG. Hereditary frontotemporal dementia caused by Tau gene mutations. Brain Pathol. 2007;17(1):63–73.

213. Kuusisto E, Salminen A, Alafuzoff I. Ubiquitin-binding protein p62 is present in neuronal and glial inclusions in human tauopathies and synucleinopathies. Neuroreport. 2001;12(10):2085–90.

214. Ramesh Babu J, Lamar Seibenhener M, Peng J, Strom AL, Kemppainen R, Cox N, et al. Genetic inactivation of p62 leads to accumulation of hyperphosphorylated tau and neurodegeneration. J Neurochem. 2008;106(1):107–20.

215. Thomas Arendt, , Jens T. Stieler MH. Tau and tauopathies. Brain Res Bull. 2016;126(3):238–92.

216. David DC, Layfield R, Serpell L, Narain Y, Goedert M, Spillantini MG. Proteasomal degradation of tau protein. J Neurochem. 2002;83(1):176–85.

217. Hatakeyama S, Matsumoto M, Kamura T, Murayama M, Chui DH, Planel E, et al. U-box protein carboxyl terminus of Hsc70-interacting protein (CHIP) mediates poly-ubiquitylation preferentially on four-repeat Tau and is involved in neurodegeneration of tauopathy. J Neurochem. 2004;91(2):299–307.

218. Dolan PJ, Johnson GVW. A caspase cleaved form of tau is preferentially degraded through the autophagy pathway. J Biol Chem. 2010;285(29):21978–

87.

219. Hamano T, Gendron TF, Causevic E, Yen SH, Lin WL, Isidoro C, et al. Autophagic-lysosomal perturbation enhances tau aggregation in transfectants with induced wild-type tau expression. Eur J Neurosci. 2008;27(5):1119–30.

220. Berger Z, Ravikumar B, Menzies FM, Oroz LG, Underwood BR, Pangalos MN, et al. Rapamycin alleviates toxicity of different aggregate-prone proteins. Hum Mol Genet. 2006;15(3):433–42.

221. Krüger U, Wang Y, Kumar S, Mandelkow EM. Autophagic degradation of tau in primary neurons and its enhancement by trehalose. Neurobiol Aging. 2012;33(10):2291–305.

222. Schaeffer V, Goedert M. Stimulation of autophagy is neuroprotective in a mouse model of human tauopathy. Autophagy. 2012;8(11):1686–7.

223. Polito V a, Li H, Martini-Stoica H, Wang B, Yang L, Xu Y, et al. Selective clearance of aberrant tau proteins and rescue of neurotoxicity by transcription factor EB. EMBO Mol Med. 2014;6(9):1142–60.

224. Witman GB, Cleveland DW, Weingarten MD, Kirschner MW. Tubulin requires tau for growth onto microtubule initiating sites (flagella/in vitro assembly/electron microscopy). Cell Biol. 1976;73(11):4070–4.

225. Weingarten MD, Lockwood AH, Hwo SY, Kirschner MW. A protein factor essential for microtubule assembly. Proc Natl Acad Sci U S A. 1975;72(5):1858–62.

226. Adams SJ, Crook RJP, Deture M, Randle SJ, Innes AE, Yu XZ, et al. Overexpression of wild-type murine tau results in progressive tauopathy and neurodegeneration. Am J Pathol. 2009;175(4):1598–609.

227. Santacruz K, Lewis J, Spires T, Paulson J, Kotilinek L, Ingelsson M, et al. Tau suppression in a neurodegenerative mouse model improves memory function. Science. 2005;309(5733):476–81.

228. Love S, Bridges LR, Case CP. Neurofibrillary tangles in Niemann-Pick disease type C. Brain. 1995;118:119–29.

229. AUER I, SCHMIDT M, LEE V et al. PAIRED-HELICAL-FILAMENT-TAU (PHFTAU) IN NIEMANN-PICK TYPE-C DISEASE IS SIMILAR TO PHFTAU IN ALZHEIMERS-DISEASE. Acta Neuropathol. 1995;90:547–51.

230. Perlson E, Maday S, Fu M meng, Moughamian AJ, Holzbaur ELF. Retrograde axonal transport: Pathways to cell death? Trends Neurosci. 2010;33(7):335–44.

CHAPTER 2

THE ALS/FTLD ASSOCIATED PROTEIN C9ORF72 ASSOCIATES WITH SMCR8 AND WDR41 TO REGULATE THE AUTOPHAGY-LYSOSOME PATHWAY

This work was submitted 6 May 2016 and first published 18 May 2016 DOI10.1186/s40478-016-0324-5. The manuscript was published as Sullivan PM, Zhou X, Robins AM, Kim D, Smolka M, and Hu F. The ALS/FTLD associated protein C9orf72 associates with SMCR8 and WDR41 to regulate the autophagy-lysosome pathway. *Acta Neuropathologica Communications*. 2016;4:51. **DOI:** 10.1186/s40478-016-0324-5.

2.1 Abstract

Hexanucleotide repeat expansion in the C9orf72 gene is a leading cause of frontotemporal lobar degeneration (FTLD) with amyotrophic lateral sclerosis (ALS). Reduced expression of C9orf72 has been proposed as a possible disease mechanism. However, the cellular function of C9orf72 remains to be characterized. Here we report the identification of two binding partners of C9orf72: SMCR8 and WDR41. We show that WDR41 interacts with the C9orf72/SMCR8 heterodimer and WDR41 is tightly associated with the Golgi complex. We further demonstrate that C9orf72/SMCR8/WDR41 associates with the FIP200/ Ulk1 complex, which is essential for autophagy initiation. C9orf72 deficient mice, generated using the CRISPR/Cas9 system, show severe inflammation in multiple organs, including lymph node, spleen and liver. Lymph node enlargement and severe splenomegaly are accompanied with macrophage infiltration. Increased levels of autophagy and lysosomal proteins and autophagy defects were detected in both the spleen and liver of C9orf72 deficient mice, supporting an in vivo role of C9orf72 in regulating the autophagy/lysosome pathway.

In summary, our study elucidates potential physiological functions of C9orf72 and disease mechanisms of ALS/FTLD.

2.2 Introduction

Frontotemporal lobar degeneration (FTLD) and amyotrophic lateral sclerosis (ALS) are two devastating neurodegenerative diseases, which due to overlaps in clinical presentations, pathological features, and genetic causes, are considered two manifestations of a continuous disease spectrum [1-6].

Many novel genes have been recently associated with ALS/FTLD [5, 7]. Among these, hexanucleotide repeat expansion in the C9orf72 gene has been shown to be the main cause of ALS/FTLD [8-10], for which three disease mechanisms have been proposed: toxicity of RNA foci formed by RNA repeats, toxicity induced by dipeptide repeat aggregation as a result of repeat associated non-ATG mediated RNA translation (RAN), and reduced expression of the C9orf72 gene [11, 12]. Recently, many animal models have been established to investigate repeat associated gain of toxicity [13-18] as well as the physiological functions of C9orf72 in mammals. While neuron and glia specific C9orf72 ablation or intracerebral mRNA knockdown does not seem to cause motor neuron disease in mouse models [19, 20], two recent studies on whole body C9orf72 deficient mice demonstrate that C9orf72 deficiency results in severe immune dysregulation [21, 22], suggesting that loss of C9orf72 function could lead to mis-regulated inflammatory responses.

Despite many attempts at characterizing the exact molecular function of C9orf72, its cellular role is still not entirely clear. Bioinformatics studies have predicted C9orf72 to be a member of DENN domain containing proteins which typically function as guanine exchange factors for Rab GTPases, key regulators of membrane trafficking

in eukaryotic cells [23, 24]. One study has demonstrated physical interactions between C9orf72 and Rab7 and Rab11, GTPases involved in late endosome maturation or endosome recycling, respectively, and a role of C9orf72 in autophagy regulation [25]. However, direct regulation of these Rab GTPases by C9orf72 was not demonstrated in this study [25].

In order to gain insight into C9orf72 function, we performed a proteomic screen for C9orf72 binding partners. We showed that C9orf72 forms a tight complex with SMCR8, another DENN domain containing protein [24], and WDR41, a WD40 repeat protein. We further demonstrated the physical interaction between C9orf72/SMCR8/WDR41 and the FIP200/Ulk1/ATG13/ATG101 complex, which is an essential regulator of autophagy initiation. Our results are consistent with two recent reports on the C9orf72/SMCR8/WDR41 interaction published while this manuscript was under preparation [26, 27]. Furthermore, our data from C9orf72 deficient mice support a role of C9orf72 in immune regulation and the autophagy-lysosome pathway.

2.3 Results

C9orf72 forms a complex with SMCR8 and WDR41

In humans, two C9orf72 protein isoforms are generated from three alternatively spliced transcripts, a long form (C9-L) and a short form (C9-S), with multiple studies showing that the protein and mRNA level of the C9-L form are decreased in C9/ALS patients [28-30]. To decipher the protein interaction network of C9orf72, a SILAC (stable isotope labeling of amino acids in cell culture) based proteomic screen was performed in the neuroblastoma cells line neuro-2a (N2a) using GFP-C9orf72 (C9-L) as the bait and GFP as a control (Fig. 2-1a, Fig. 2-S1). Several proteins were found to be enriched in the C9orf72 immunoprecipitations (IPs) (Fig. 2-1b, Table 2-S1). The top

two hits from the screen were SMCR8 and WDR41, two proteins of unknown functions (Fig. 2-1b). Interestingly, like C9orf72, SMCR8 was also predicted to contain a DENN domain [24]. The interaction between C9orf72, SMCR8, and WDR41 was verified using co-IPs in transfected HEK293T cells (Fig. 2-2a-c). SMCR8 strongly interacts with GFP-C9orf72 but not GFP in the co-IP experiment (Fig. 2-2a). Moreover, co-expression of C9orf72 consistently increases the level of SMCR8, suggesting that C9orf72 might stabilize overexpressed SMCR8. However, the short isoform of human C9orf72 (C9-S) does not bind SMCR8 (Fig. 2-2a). Thus we focus on the C9-L form for the rest of the study (hereafter referred to as C9orf72). While we failed to detect any interaction between WDR41 and C9orf72 or SMCR8 when WDR41 is expressed with either C9orf72 or SMCR8 alone, WDR41 strongly co-immunoprecipitates with C9orf72 and SMCR8 when C9orf72 and SMCR8 are co-expressed, suggesting that WDR41 interacts only with the C9orf72/SMCR8 heterodimer (Fig. 2-2b-c).

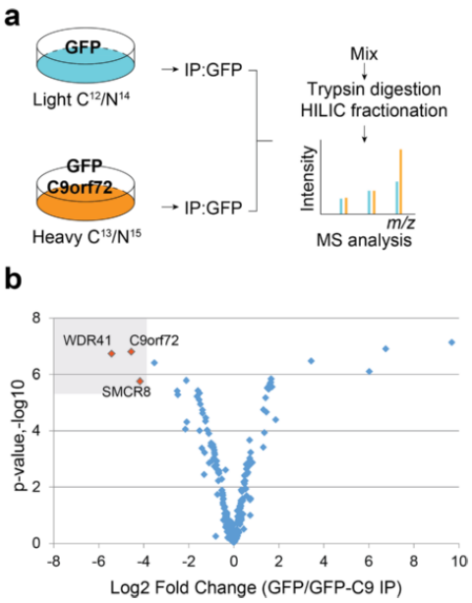

Figure 2-1: SILAC proteomic screen for C9orf72 binding partners.
a. Schematic workflow of SILAC proteomic screen used to identify C9orf72 protein interactions. **b.** Volcano plot of SILAC hits. Hits with more than 10 peptides are plotted. Top hits identified in the heavy fraction are highlighted.

Protein	Log2 fold change (GFP/GFP-C9orf72 IP)	P Value	Count	Count H	Count L
WDR41	-5.43	1.85E-07	23	22	1
3110043O21RIK	-4.55	1.58E-07	144	114	30
SMCR8	-4.17	1.75E-06	64	57	7
VDAC3	-3.58	3.89E-07	29	25	4
SLC25A4	-2.52	3.87E-06	20	15	5
SLC25A5	-2.49	5.23E-06	50	33	17
CHCHD3	-2.15	8.81E-05	14	11	3
SLC25A12	-2.11	1.64E-06	29	22	7
IMMT	-2.09	4.91E-05	27	23	4
SLC3A2	-1.64	6.02E-06	16	11	5
SLC25A12	-1.60	3.73E-06	17	13	4
LOC100046151	-1.54	7.94E-06	14	7	7
FAR1	-1.52	9.92E-05	14	11	3
SLC25A11	-1.52	4.62E-06	11	8	3
DNAJA1	-1.49	1.15E-05	38	29	9
GCN1L1	-1.41	4.18E-04	18	16	2
DNAJB11	-1.39	1.82E-05	14	9	5
DNAJA2	-1.39	2.42E-05	27	21	6
KARS	-1.32	3.61E-03	13	10	3
ASS1	-1.30	6.00E-04	13	10	3
TUBA4A	-1.25	4.60E-05	11	6	5
SLC25A4	-1.24	3.49E-05	59	34	25
MTAP1B	-1.18	9.49E-05	79	57	22
SLC25A4	-1.11	1.27E-04	24	13	11
NSF	-1.09	1.41E-03	11	7	4
2310079N02RIK	-1.02	3.44E-04	15	10	5
TUBA1A	-1.01	2.73E-04	30	17	13

Table 2-S1: List of hits from the SILAC proteomic screen. Proteins with more than ten peptides and Log2 fold change (GFP/GFP-C9orf72) <-1.00 are listed. Count: total number of peptides identified; Count H: number of peptides in the heavy fraction; Count L: number of peptides in the light fraction.

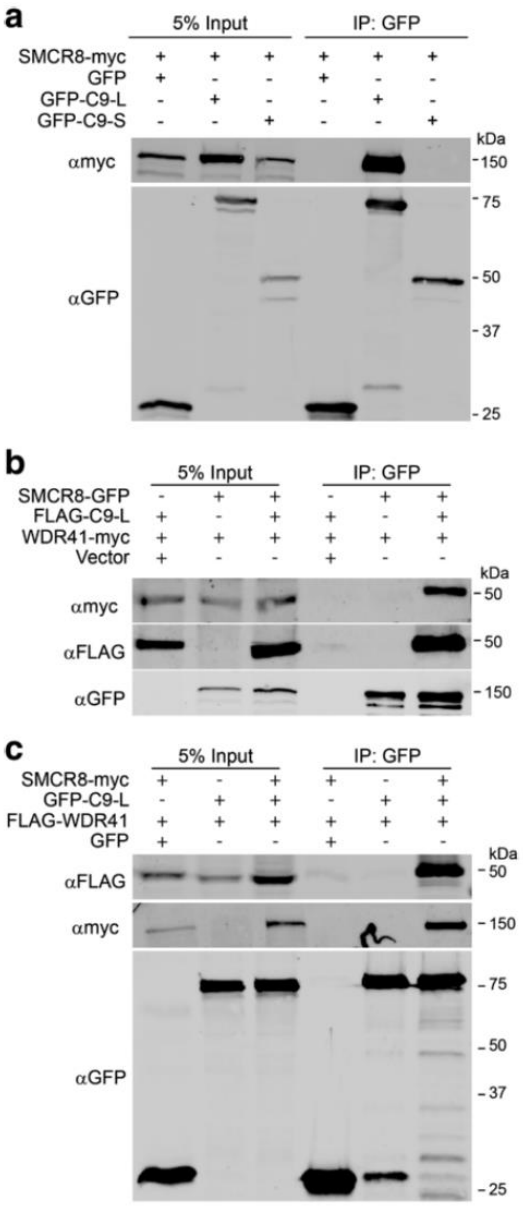

Figure 2-2: Co-immunoprecipitation between C9orf72, SMCR8 and WDR41

a. GFP-tagged human C9orf72 isoform I (GFP-C9-L) or isoform II (GFP-C9-S) were overexpressed with SMCR8-myc in HEK293T cells and immunoprecipitated by anti-GFP beads. **b.** SMCR8-GFP and WDR41-myc were coexpressed with or without FLAG-C9-L and the lysates were immunoprecipitated using anti-GFP antibodies. **c.** GFP-C9-L and FLAG-WDR41 were co-expressed with or without SMCR8-myc as indicated and the lysates were immunoprecipitated using anti-GFP antibodies.

Cellular localization of C9orf72, SMCR8 and WDR41

To gain insight into the cellular function of the C9orf72/SMCR8/WDR41 complex, we expressed these proteins in HeLa cells and examined their distribution within the cell. Both C9orf72 and SMCR8 show diffuse cytoplasmic localization, when expressed alone or together (Fig. 2-3a and 2-3b). Nuclear localization was observed for C9orf72, especially the GFP-tagged C9orf72 but not SMCR8 (Fig. 2-3a and 2-3b). WDR41 also shows diffuse cytoplasmic distribution (Fig. 2-3a and 2-3c). However, careful examination reveals enrichment of WDR41 at the cis-Golgi, which is confirmed when labelled by the cis-Golgi protein GPP130 (Fig. 2-3c). This is further supported by treatment of cells with BrefeldinA, which causes the Golgi to collapse. Even after such treatment, WDR41 remains colocalized with GPP130, indicating that WDR41 is tightly associated with the Golgi membrane. Similar results were obtained after treatment with nocodazole, a microtubule destabilizing drug that causes the Golgi to disperse (Fig. 2-3c).

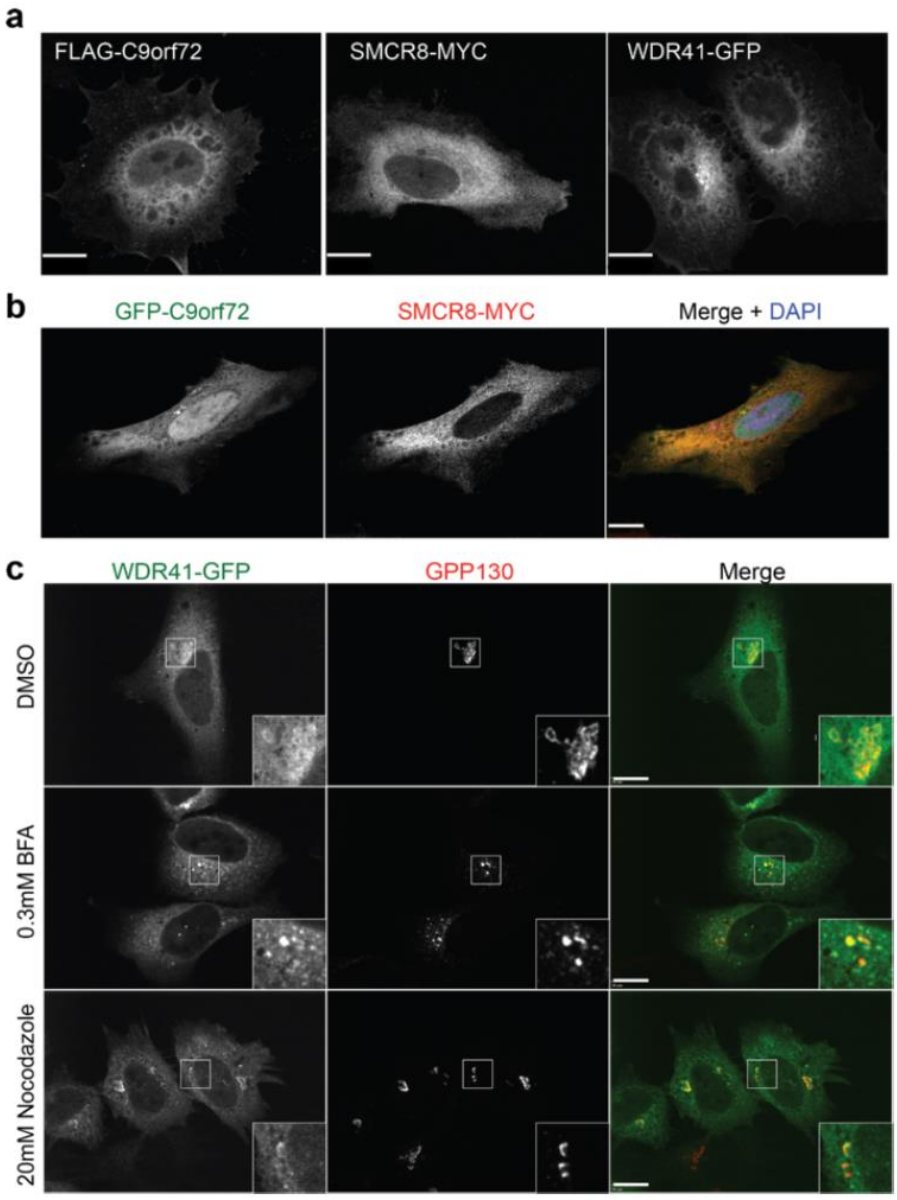

Figure 2-3: Cellular localization of C9orf72, SMCR8 and WDR41.
a. HeLa cells were transfected with FLAG-C9orf72 (C9-L), SMCR8-myc or WDR41-GFP. Cells were stained with anti-FLAG or anti-myc to visualize FLAG-C9orf72 or SMCR8-myc, respectively. Maximum projection images from confocal sections are shown. Scale bar=10µm **b.** HeLa cells were transfected with GFP-C9orf72 and SMCR8-myc. Cells were stained with anti-myc antibodies to visualize SMCR8-myc. **c.** WDR41-GFP expressing HeLa cells were treated with DMSO control, 0.3mM BrefeldinA (BFA), or 20mM Nocodazole for 2 hours. Cells were stained with anti-GPP130 antibodies to label cis-Golgi. Single confocal images are shown for b and c. Scale bar=10µm.

Interaction of C9orf72/SMCR8/WDR41 with the FIP200 autophagy initiation complex

A previously reported proteomics screen identified SMCR8 as a binding partner for FIP200 (also called RB1CC1) [31], a protein involved in autophagy initiation [32]. However, the interaction between SMCR8 and FIP200 is barely detectable by co-IP when only these two proteins are overexpressed (Fig. 2-4a). Interestingly, we found that co-transfection of C9orf72 and SMCR8 allows much stronger binding of SMCR8 to FIP200, which is further enhanced by WDR41 overexpression, suggesting that C9orf72/SMCR8/WDR41 forms a ternary complex to interact with FIP200 (Fig. 2-4a). The weaker binding between SMCR8 and FIP200 when SMCR8 is expressed alone in HEK293T cells is most likely explained by very low endogenous levels of C9orf72 and WDR41 (Fig. 2-4a and Fig. 2-S1). Ulk1, a kinase that interacts with FIP200 in the autophagy initiation complex [32], binds the C9orf72/SMCR8/WDR41 in a similar manner as FIP200 (Fig. 2-4a). Furthermore, C9orf72, SMCR8 and WDR41 are all detected in the FIP200 immunoprecipitates (Fig. 2-4b). ATG13 and ATG101, two other proteins associated with FIP200/Ulk1 also interact with C9orf72/SMCR8/WDR41 (Fig. 2-4c and 2-4d). These data support that the formation of the C9orf72/SMCR8/WDR41 complex allows their interaction with the FIP200/Ulk1/ATG13/ATG101 complex (Fig. 2-4e).

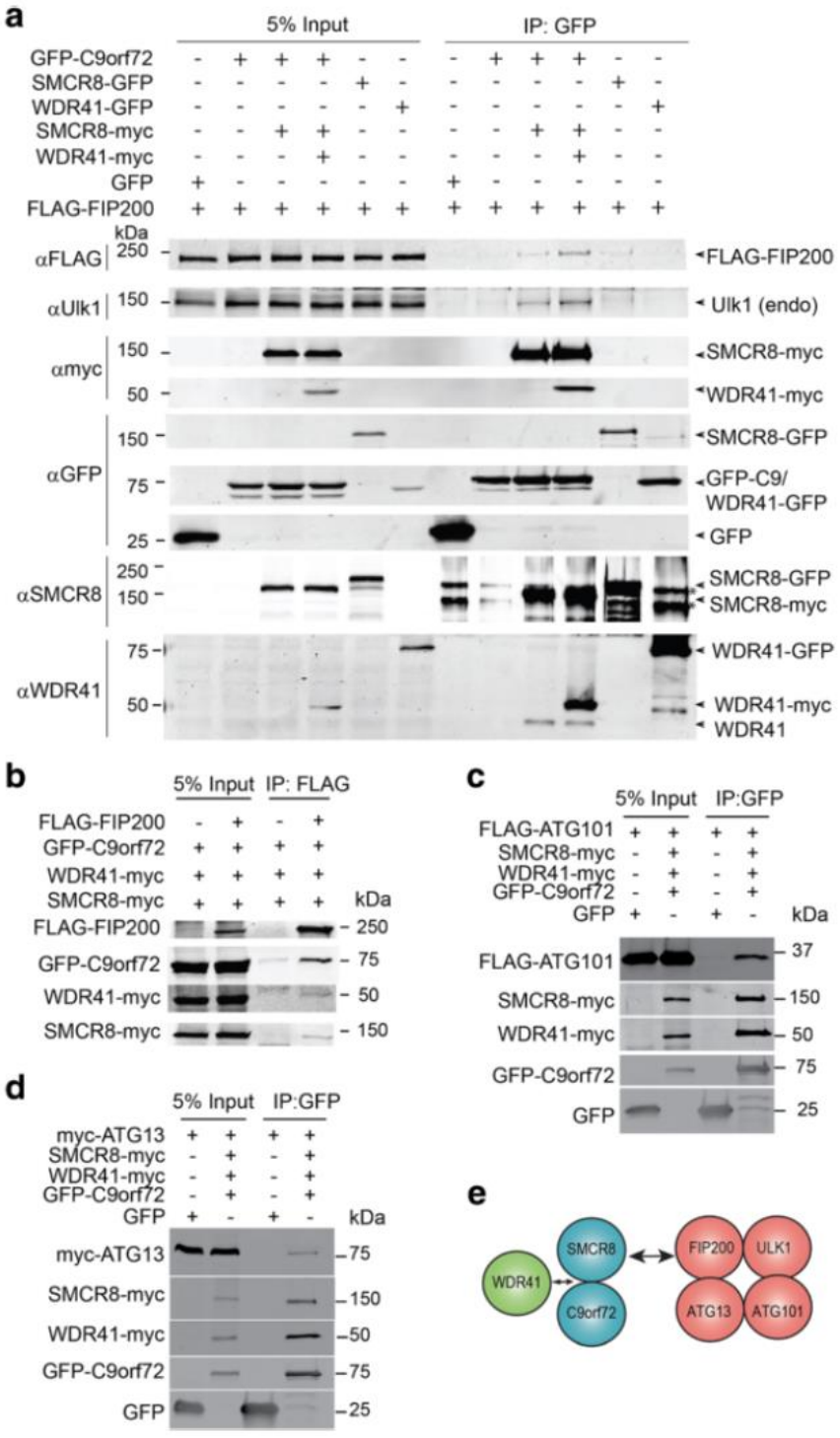

Figure 2-4: The C9orf72/SMCR8/WDR41 complex interacts with FIP200/Ulk1. a. Co-immunoprecipitation between C9orf72/SMCR8/WDR41 and FIP200 and Ulk1. HEK293T cells were transfected with FLAG-FIP200 and C9orf72, SMCR8 and/or WDR41 as indicated. Cells were lysed 40hrs after transfection and lysates were

(continued from previous page) immunoprecipated with anti-GFP antibodies. Lysates and immunoprecipitates were analyzed by Western blots as indicated. * indicated non-specific bands recognized by anti SMCR8 antibodies in the IP products. Representative images from 3 independent experiments are shown. **b.** Co-immunoprecipitation between C9orf72/SMCR8/WDR41 and FIP200. HEK293T cells were transfected as indicated and lysed and immunoprecipitated using anti-FLAG antibodies. Lysates and immunoprecipitates were analyzed by Western blots. **c, d.** Co-immunoprecipitation between C9orf72/SMCR8/WDR41 and ATG101 (c) or ATG13 (d). HEK293T cells were transfected as indicated and lysed and immunoprecipitated using anti-GFP antibodies. Lysates and immunoprecipitates were analyzed by Western blots. **e.** Schematic drawing of the interaction between C9orf72/SMCR8/WDR41 and the FIP200/Ulk1 complex. WDR41 interacts with the C9orf72/SMCR8 dimer to form ternary complex, which then interacts with the FIP200/Ulk1/ATG13/ATG101 complex.

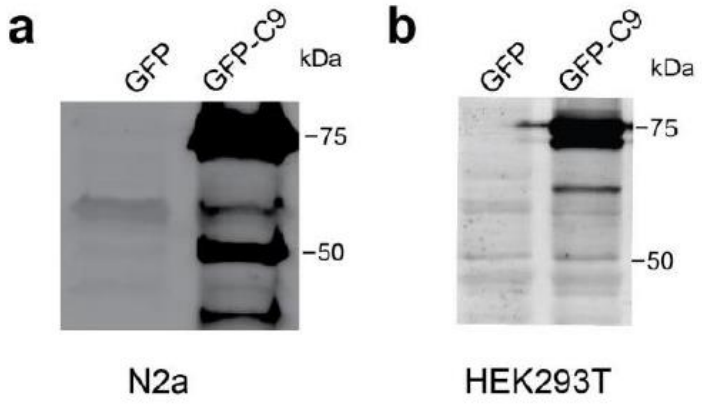

Figure 2-S1: Levels of endogenous versus overexpressed C9orf72 in N2a and HEK293T cells. N2a (a) and HEK293T (b) cells were transfected with GFP control or GFP-C9orf72. Cells were lysed two days after transfection and lysates were subjected to Western blot using anti-C9orf72 antibodies (Proteintech) to determine the levels of endogenous versus overexpressed C9orf72.

Generation and characterization of C9orf72 deficient mice

Three protein isoforms of mouse C9orf72 homolog (I, 55kDa; II, 35kDa and III; 50kDa) have been identified with isoform I (55kDa), the functional homolog of C9-L in humans, being the dominant form in most tissues [33, 34]. In order to investigate the function of C9orf72 in vivo, we generated C9orf72 deficient mice using the CRISPR/Cas9 system [35, 36]. Guide RNA targeted close to the start codon of the mouse C9orf72 isoform I and III was co-injected with the Cas9 mRNA into the pronuclei of fertilized eggs (Fig. 2-5a). All the offspring displayed Cas9 mediated cleavage and editing from non-homologous end joining mediated repair. We chose one founder containing a one-nucleotide deletion at the beginning of the C9orf72 open reading frame, resulting in a frame shift at residue 33 that produces a stop codon at amino acid 40 (Fig. 2-5b). Based on the splicing patterns, the one nucleotide deletion should cause the loss of protein products for C9orf72 isoforms I (55kDa) and III (50kDa), but should not affect isoform II (35kDa). Indeed, Western blot using several antibodies shows loss of C9orf72 isoform I protein in homozygous offspring from the above-mentioned founder (Fig. 2-5c, and Fig. 2-S2). We failed to detect isoform II and III in our Western blots with all the C9orf72 antibodies tested and thus we cannot determine whether these isoforms are affected by the CRISPR/Cas9 editing. While C9orf72 isoform I is detectable in all tissues examined, its level is highest in spleen, followed by kidney, brain, and heart, and much lower in the liver and muscle (Fig. 2-5c). This expression pattern is consistent with a recent publication demonstrating the highest levels of C9orf72 in $CD11b^+$ myeloid cells [22].

Our C9orf72 deficient mice do not have any apparent growth defects (data not shown) but display an obvious lymph node and spleen enlargement phenotype (Fig. 2-5d), consistent with recent reports on another two independent lines of C9orf72 knockout mice [21, 22] . While occasional mild splenomegaly was observed in the 2

month old C9orf72 deficient mice, this phenotype becomes more severe with age, with the 4-5 month old C9orf72 deficient mouse having a spleen 2-3 times the size of its littermate control (Fig. 2-5d and Fig. 2-S3). This is also seen in two of the 10 month old founder mice from the CRISPR mediated editing (Fig. 2-S3). The liver also shows slight enlargement but there are no obvious gross anatomical defects in the brain of C9orf72 deficient mice (data not shown).

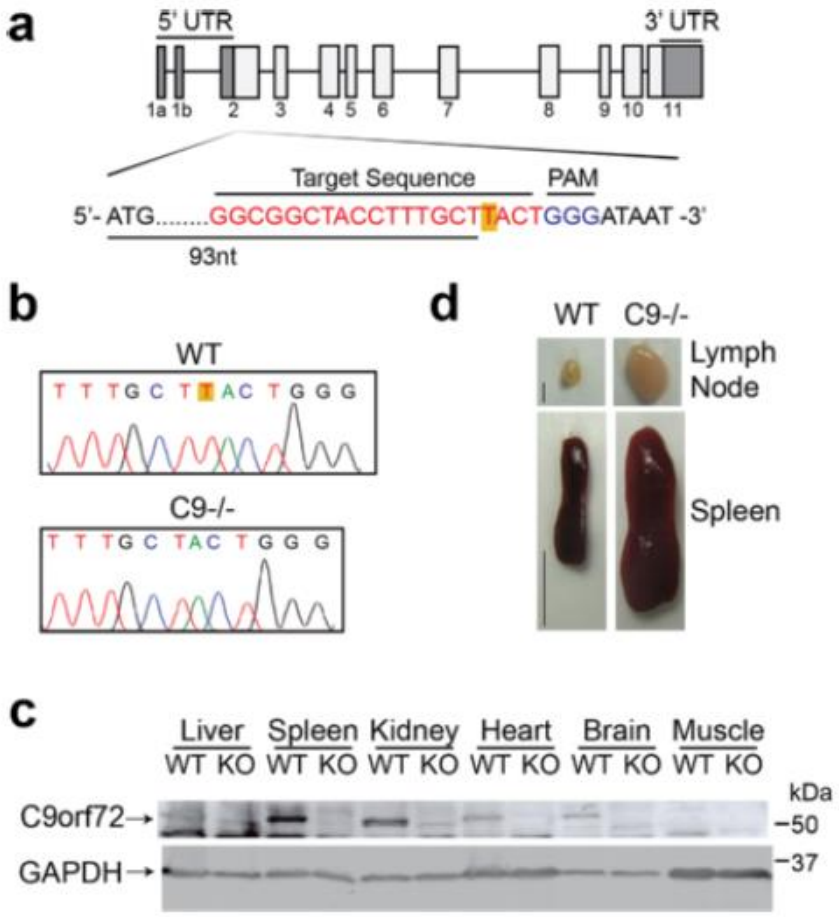

Figure 2-5: Generation of C9orf72 deficient mice. a. Schematic drawing of the mouse homologue of C9orf72, 3110043O21RIK, and the site targeted for editing by CRISPR/Cas9. **b.** Sequencing traces of wildtype (top) and edited (bottom) C9orf72 from genomic PCR show a one nucleotide deletion (highlighted with yellow) near the (continued from previous page) Cas9 cleavage site. **c.** Western blot analysis of C9orf72 protein levels in wild type (WT) and C9orf72-/- (KO) mouse tissues with anti-C9-L antibodies. **d.** Representative images of cervical lymph nodes and spleen from 4-5 months old WT and C9orf72-/- mice. Scale bar=2 mm (lymph node); 1 cm (spleen).

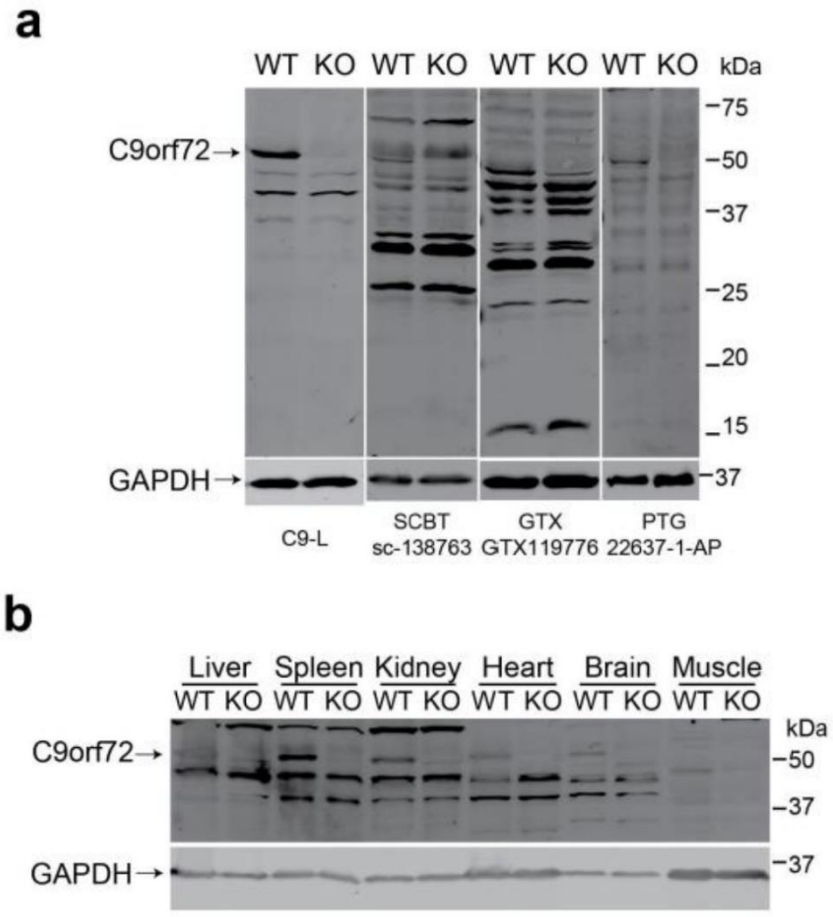

Figure 2-S2: Absence of C9orf72 isoform I in the C9orf72 CRISPR targeted mice. **a**. Western blot of brain lysate from wild type (WT) or C9orf72 deficient (KO) mice using various C9orf72 antibodies as indicated. **b.** Western blot analysis of C9orf72 protein levels in WT and KO mouse tissues with anti0C9-L antibodies.

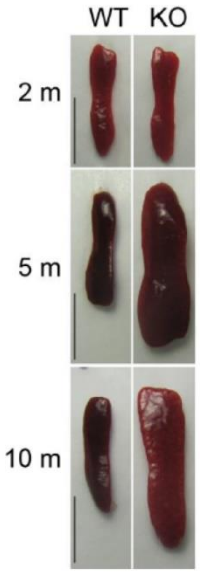

Figure 2-S3: C9orf72 deficiency in mice leads to age dependent spleen enlargement. Representative images of spleen dissected form 2 month, 5 month, and 10 month old WT and C9orf72-/- mice are shown. Scale bar=1 cm.

Hematoxylin and eosin (H&E) staining of the C9orf72 deficient spleen reveals enlarged germinal centers (GCs) and abundant extramedullary hematopoietic cells (Fig. 2-6a). High magnification shows the enlarged GCs are packed with immature immune cells, among which plasma cells are often observed (Fig. 2-6a). Several types of hematopoietic cells are enriched in the red pulp (Fig. 2-6a). Immunostaining with anti-CD68 antibodies shows macrophage accumulation or infiltration in the red pulp of the spleen (Fig. 2-6b), which is also seen in the peripheral regions of cervical lymph nodes (Fig. 2-7a) and to a lesser extent, liver of C9orf72 deficient mice at 4 months of age (Fig. 2-8b). In C9orf72-/- liver tissues, infiltrated immune cells were observed in both hepatic portal area and hepatic parenchyma (Fig. 2-8a). Surrounding by the infiltrated immune cells, necrotic hepatocytes are occasionally seen in C9orf72-/- liver tissues (Fig. 2-8a). Despite macrophage infiltration in multiple peripheral organs, microglia, the counterpart of macrophages in the central nervous system, do not show any obvious changes in number and morphology in the C9orf72 deficient mice (Fig. 2-9).

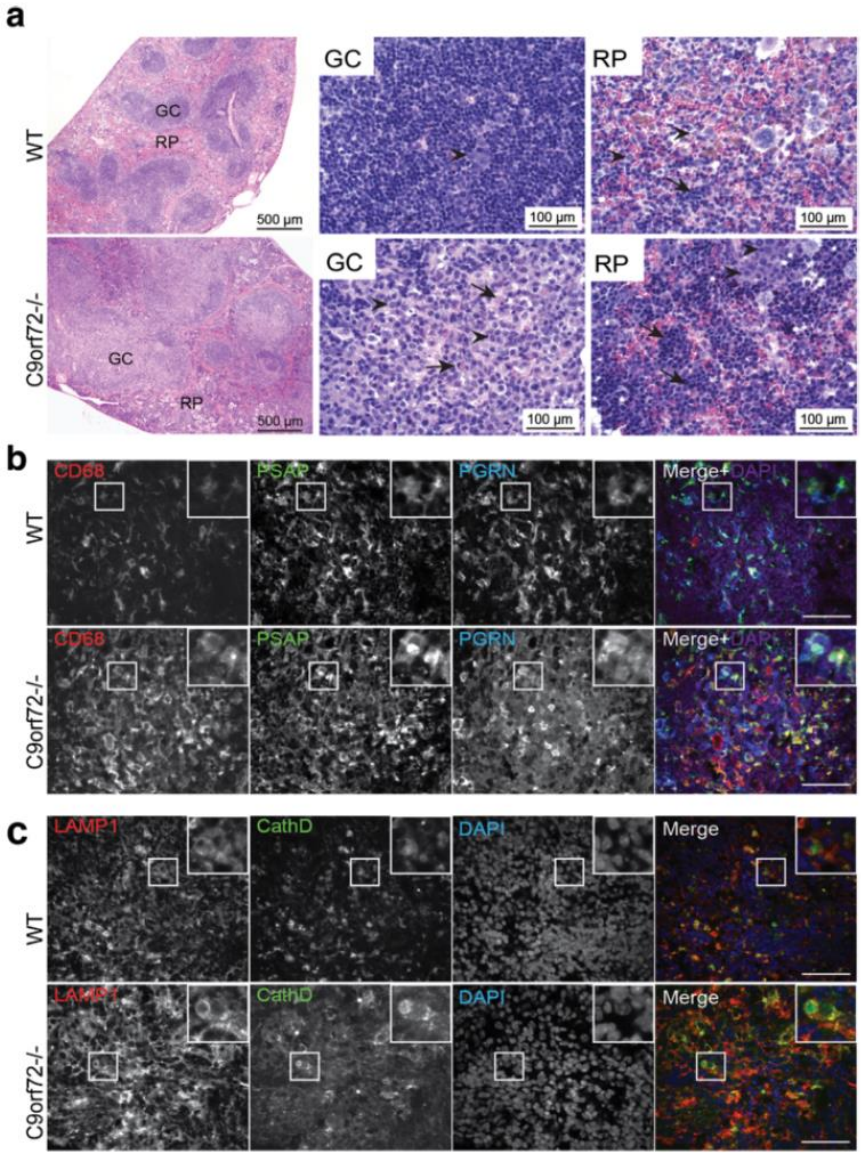

Figure 2-6: C9orf72 deficiency in mice results in an enlarged spleen phenotype and macrophage infiltration into the spleen.

a. H&E staining of spleen tissues from 5 month old of WT or C9orf72 -/- mouse with zoomed images of germinal center (GC) and red pulp (RP). (GC): Arrows indicate plasma cells and the arrowheads indicate immature immune cells). (RP): arrowheads indicate myeloid precursors; arrows indicate erythroid precursors. Scale bar=500 µm (100 µm in the zoomed in images for GC and RP) b. Immunostaining of 4 month old spleen sections (red pulp region) of WT and C9orf72-/- mice with anti-mouse CD68, prosaposin (PSAP), and progranulin (PGRN) antibodies. Nuclei are labelled with DAPI. Insert shows representative CD68+ macrophage cells. Representative pictures from three pairs of mice are shown. Scale bar=40 µm. c. Immunostaining of 4 month old spleen sections (red pulp region) of WT and C9orf72-/- mice with anti-mouse -

(continued from previous page) Lamp1, and cathepsin D (CathD) antibodies. Nuclei are labelled with DAPI. Insert shows representative cells. Representative pictures from three pairs of mice are shown. Scale bar=40 µm.

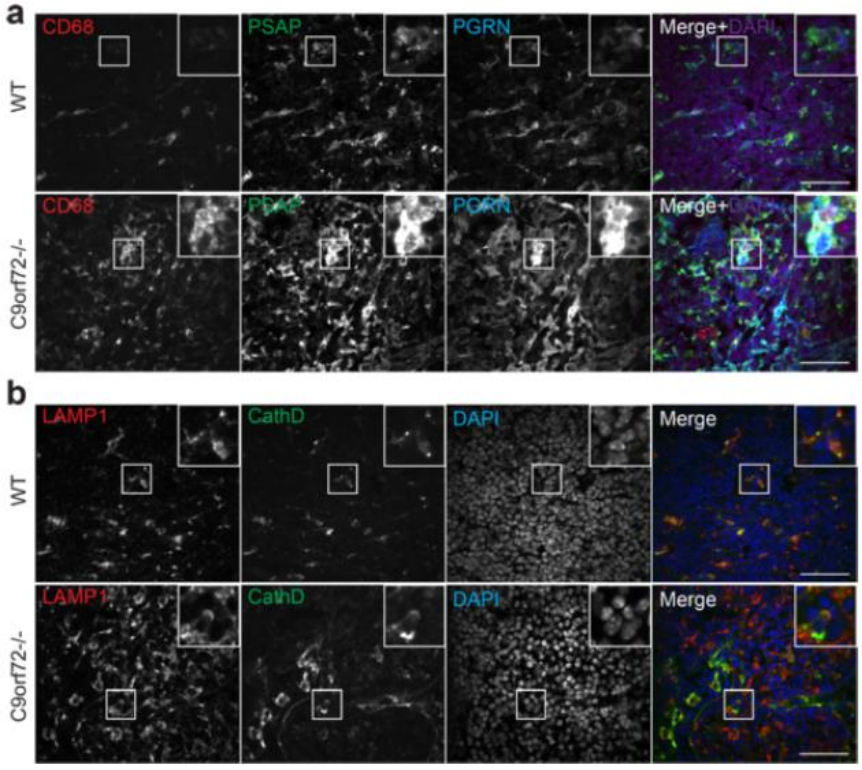

Figure 2-7: Increased macrophage infiltration and lysosomal proteins in the cervical lymph node of C9orf72 deficient mice.
a. Immunostaining of 4 month old cervical lymph nodes sections (peripheral region) of WT and C9orf72-/- mice with anti-mouse CD68, prosaposin (PSAP), and progranulin (PGRN) antibodies. Nuclei is labelled with DAPI. Insert shows representative CD68+ macrophage cells. Representative pictures from three pairs of mice are shown. Scale bar=40 µm. **b**. Immunostaining of 4 month old cervical lymph nodes sections (peripheral region) of WT and C9orf72-/- mice with anti-mouse Lamp1, and cathepsin D (CathD) antibodies. Nuclei are labelled with DAPI. Insert shows representative cells. Representative pictures from three pairs of mice are shown. Scale bar=40 µm.

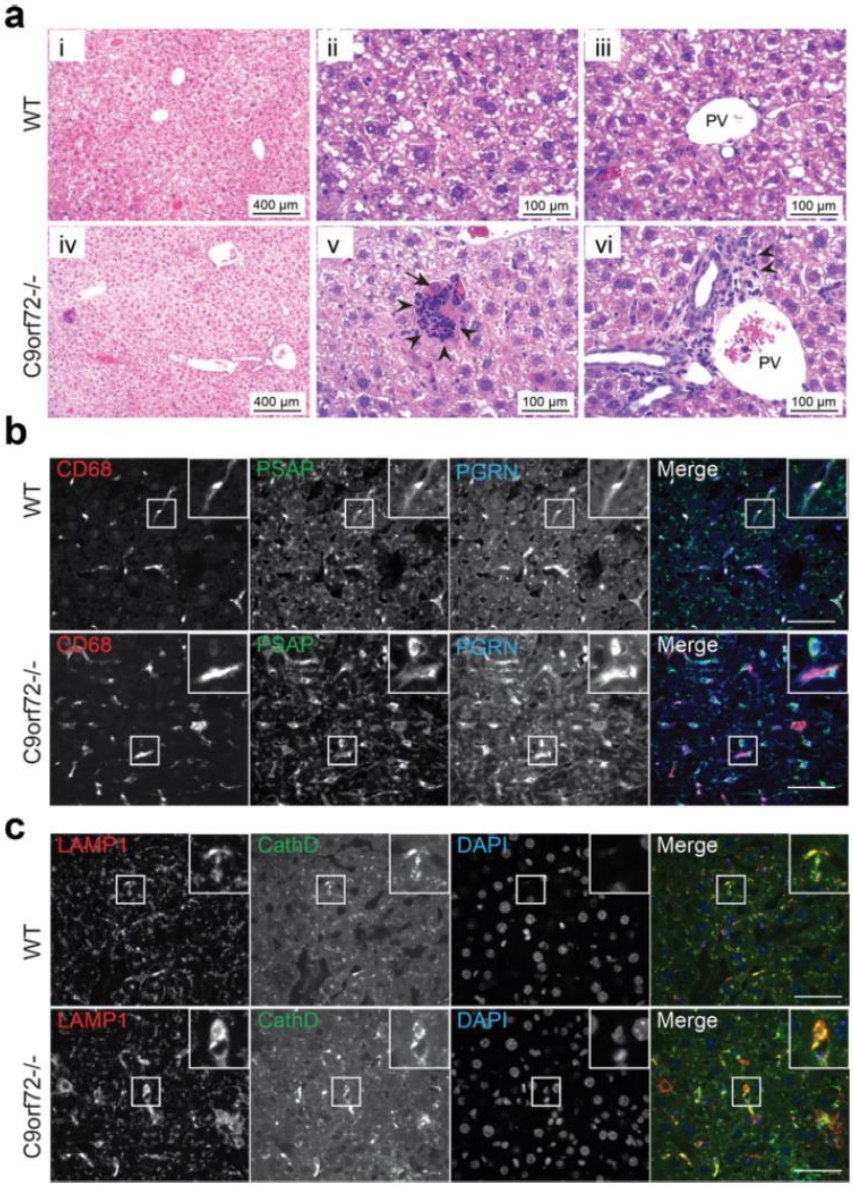

Figure 2-8: C9 deficiency in mice results in macrophage infiltration and increased levels of lysosomal proteins in the liver.

a. H&E staining of liver tissues from 10 month old of WT or C9orf72 -/- mouse. (ii) and (iii) are high power magnification images of the hepatic parenchyma, arrowhead indicates infiltrated immune cells; arrow points to necrotic hepatocyte. (v) and (vi) are high power magnification images of the hepatic portal area, arrowhead indicates infiltrated immune cells. PV, portal vein. Scale bar: 500 µm in (i) and (iv), 100 µm in (ii, iii, v, vi) **b.** Immunostaining of 4 month old liver sections of WT and C9orf72-/- mice with anti-mouse CD68, prosaposin (PSAP), and progranulin (PGRN) antibodies. Nuclei are labelled with DAPI. Insert shows representative CD68+ macrophage cells.

(continued from previous page) Representative pictures from three pairs of mice are shown. Scale bar=40 µm. **c**. Immunostaining of 4 month old liver sections of WT and C9orf72-/- mice with anti-(continued from previous page) mouse Lamp1, and cathepsin D (CathD) antibodies. Nuclei are labelled with DAPI. Insert shows representative cells. Representative pictures from three pairs of mice are shown. Scale bar=40 µm.

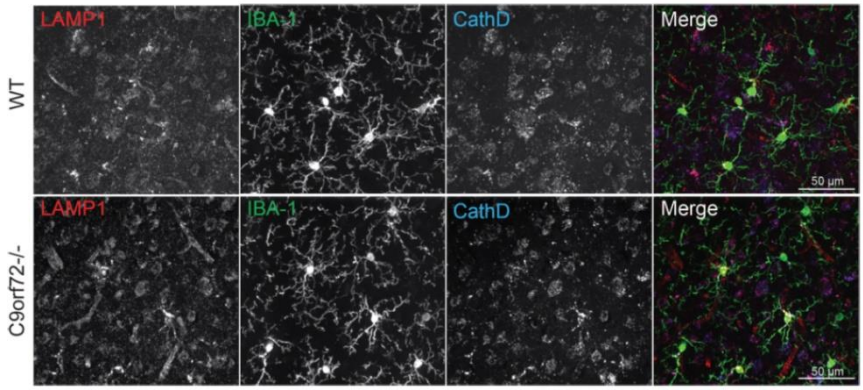

Figure 2-9: Microglia do not show any obvious abnormalities in C9orf72 deficient mice.
Brain sections from 10 month old WT and C9orf72-/- mice were stained with anti-LAMP1, Iba1 and cathepsin D antibodies. Similar results were seen with 5 month old C9orf72-/- mouse. Scale bar=50µm.

Autophagy and lysosome defects in the C9orf72 deficient mice

Because C9orf72/SMCR8/WDR41 co-immunoprecipitates with the FIP200/Ulk1/ATG13/ATG101 complex, we investigated possible autophagy/lysosome defects in the C9orf72 deficient mice. Interestingly, Ulk1 deficiency has also been reported to result in splenomegaly [37]. Western blot analysis showed significantly increased levels of several proteins involved in the autophagy/lysosomal pathway in spleen and liver lysates of the 2 month old C9orf72 deficient mice compared to littermate controls, including LC3-I, LAMP1, and prosaposin (PSAP), even before the appearance of an obvious splenomegaly phenotype, suggesting that autophagy/lysosome defects might precede anatomical spleen abnormalities (Fig. 2-10a, 2-10b). Although no obvious changes in lysosomal morphology were seen in the C9orf72-/- macrophages, increased levels of the lysosomal proteins progranulin (PGRN), PSAP, LAMP1 and cathepsin D (CathD) are seen in CD68 positive macrophages in the lymph nodes, spleen and liver of C9orf72 deficient mice (Fig. 2-6, 2-7, and 2-8). This might suggest that loss of C9orf72 causes a defect in the lysosome that requires upregulation of lysosomal proteins to compensate. Conversion of LC3-I to LC3-II is an indicator of autophagy initiation [38]. Although LC3-I levels are dramatically increased in C9orf72 deficient spleen lysates, LC3-II levels are significantly reduced in C9orf72 deficient spleen lysates (Fig. 2-10a, 2-10b), suggesting that loss of C9orf72 causes a defect in autophagy initiation. Despite these changes in multiple peripheral tissues, brain lysates do not show any apparent increases in autophagy or lysosomal proteins in the 2 month old C9orf72 deficient mice compared to controls (Fig. 2-10a, 2-10b).

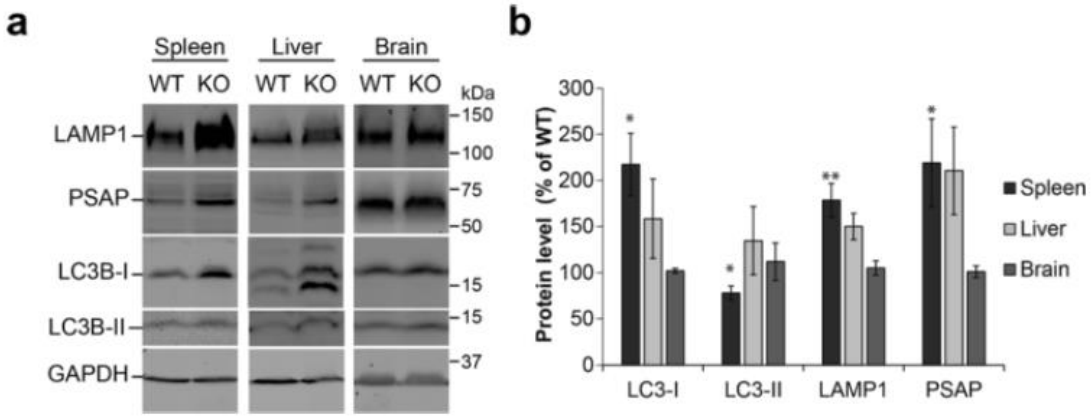

Figure 2-10: C9orf72 deficiency in mice leads to increased levels of autophagy-lysosome proteins in the spleen. a. Western blot analysis of tissue lysates from spleen, liver, and brain of WT and knockout mice. Representative pairs are shown. **b.** Quantification of autophagy and lysosomal protein levels in knockout mice relative to WT controls. Data are presented as Mean $\pm$ SEM, n=3-6. *, $p < 0.05$; **, $p<0.01$.

2.4 Discussion

The cellular function of C9orf72 has been under intensive investigation since hexanucleotide repeat expansion in the C9orf72 gene was shown to be the main cause of ALS/FTLD [8-10], with reduced C9orf72 expression proposed as one of the disease mechanisms [11]. In this study, we searched for protein interactors for C9orf72 and identified SMCR8 and WDR41 as two binding partners of C9orf72, consistent with two recently published reports [26, 27]. We further demonstrated that C9orf72/SMCR8/WDR41 interacts with the FIP200/Ulk1/ATG13/ATG101 complex involved in autophagy initiation. Our data also showed that C9orf72 deficient mice display defects in autophagy/lysosome pathway, supporting a critical role of C9orf72 in

autophagy/lysosome regulation.

Many other genes involved in membrane trafficking and autophagy have been associated with ALS/FTLD, including TBK1, OPTN, SQSTM1/p62, UBQLN2, VCP/p97 and CHMP2B [39-42]. Progranulin, the gene mutated in a vast majority of FTLD with ubiquitin positive TDP-43 aggregates, was recently shown to play a critical role in regulating lysosomal function [43, 44] and the progranulin protein was shown to reside in the lysosome [45, 46]. TMEM106B, a risk factor for FTLD with progranulin mutations, also regulates lysosomal morphology and function [47-51]. Our current results further support that dysfunction in the autophagy lysosome pathway is implicated in the disease progression of ALS/FTLD caused by C9orf72 mutations. C9orf72 deficiency in C. elegans and zebrafish has been shown to result in locomotion defects [52, 53], supporting the notion that C9orf72 haploinsufficiency could contribute to ALS/FTLD progression. While neuron and glia specific C9orf72 ablation or intracerebral mRNA knockdown does not seem to cause motor neuron disease in mouse models [19, 20], our data and recent data by others consistently demonstrate that whole body C9orf72 deficiency produces severe immune dysregulation in mice [21, 22]. In one study, lysosomal abnormalities were also observed in microglia isolated from C9orf72 deficient mice and in the motor cortex and spinal cord of ALS patients with C9orf72 mutations [22]. These findings strongly suggest that C9orf72 may regulate motor neuron survival through regulation of inflammatory responses by affecting autophagy-lysosomal function of microglia and macrophages. In contrast, our studies failed to detect any obvious abnormalities of microglia in our C9orf72 deficient mice (Fig. 9). It is possible that this may simply be due to our mice not being old enough (10 months old) for us to detect a microglial phenotype. It is also likely that microglial abnormalities may become apparent in the C9orf72 deficient mice upon additional insults to the nervous system.

The physical interaction between the C9orf72/SMCR8/WDR41 complex and the autophagy initiation complex FIP200/Ulk1/ATG13/ATG101 (Fig. 4) suggests that C9orf72/SMCR8/WDR41 might regulate autophagy through the FIP200/Ulk1/ATG13/ATG101 complex. However, exactly how C9orf72/SMCR8/WDR41 regulates autophagy remains unclear. It is interesting that WDR41 is enriched at the Golgi, as the ER-Golgi intermediate compartment has been shown to serve as a key membrane source for autophagosome biogenesis [54]. One possibility is that C9orf72/SMCR8/WDR41 serves as a substrate and a downstream signaling component after Ulk1 activation. Interestingly, SMCR8 was shown to be a substrate for Ulk1 in a recent study [27]. This observation together with reduced autophagy initiation in C9or72-/- spleen tissues argues that C9orf72/SMCR8/WDR41 functions downstream of Ulk1 activation during autophagy activation. Autophagy defects in C9orf72-/- mice might trigger upregulation of autophay/lysosome genes to compensate for the defect. Although we failed to identify any Rab GTPases as C9orf72 interactors in our proteomic screen, C9orf72/SMCR8/WDR41 was shown to interact with Rab8a and Rab39b and functions as a guanine nucleotide exchange factor (GEF) for Rab GTPases in a recent study [27]. However, the effect of Ulk1 phosphorylation on the GEF activities remains to be determined. Future endeavors are needed to further understand the mechanistic functions and regulations of C9orf72/SMCR8/WDR41 complex at molecular and cellular levels. More studies are also needed to characterize neuronal and microglial phenotypes due to C9orf72 loss, possibly upon additional challenges, to explain how C9orf72 deficiency contributes to ALS/FTLD progression.

2.5 Conclusions

We describe the identification of two binding partners for C9orf72: SMCR8 and WDR41. We demonstrated that C9orf72/SMCR8/WDR41 interacts with the FIP200/Ulk1/ATG13/ATG101 complex. We also generated C9orf72 deficient mice and showed that loss of C9orf72 leads to macrophage infiltration in multiple organs. Additionally, C9orf72 deficiency leads to autophagy defects and increased levels of many lysosomal proteins, supporting a critical role of C9orf72 in regulating autophagy/lysosomal pathway and inflammation in vivo.

2.6 Material and methods

DNA and Plasmids - Human C9orf72 (C9-L), WDR41 and SMCR8 cDNAs were from the human ORFome 8.1 library and cloned into pQCXIN, pEGFP-N1 or pEGFP-N2, respectively, with an N-terminal (C9orf72) or C-terminal (WDR41 and SMCR8) GFP tag. WDR41 and SMCR8 were also cloned into pcDNA3.1 myc his A (Invitrogen) to generate C-terminal myc his tagged constructs. Additionally, C9orf72 and WDR41 were cloned into p3xFLAG-CMV7.1 (Sigma) to generate N-terminal FLAG tagged constructs. Myc-ATG13, FLAG-ATG101 and p3xFLAG-CMV10-hFIP200 were obtained from Addgene (plasmid #31965, 22877 and 24300, respectively).

Pharmacological Reagents and Antibodies - The following primary antibodies were used in this study: anti-FLAG (M2) and anti-myc (9E10) from Sigma-Aldrich, anti-GAPDH from Abcam (ab8245), anti-LC3B (GTX127375) and anti-C9orf72 (GTX119776) from GeneTex, anti-Cathepsin D (sc-6486), anti-Ulk1 (sc-33182) and anti-C9orf72 (sc-138763) from Santa Cruz Biotechnology, anti-C9orf72 (AP12928b) and anti-FIP200 (17250-1-AP) from Proteintech, anti-SMCR8 from Bethyl

Laboratories, anti-WDR41 from Abgent, rat anti-CD68 from AbD Serotec, sheep anti-progranulin from R&D systems and anti-mouse LAMP1 (553792) from BD Biosciences. Anti-mouse prosaposin antibody was generated by Pocono Rabbit Farm and Laboratory and was previously characterized [46]. Anti-C9orf72-long isoform [30] was a gift from Dr. Janice Robertson (University of Toronto); anti-GFP antibody was a gift from Dr. Anthony Bretscher (Cornell University); and anti-GPP130 was a gift from Dr. William Brown (Cornell University). The following secondary antibodies were used: donkey anti-mouse 800 and donkey anti-rabbit 800 from LI-COR, AlexaFluor donkey anti-goat 680, donkey anti-rabbit 680, donkey anti-mouse 680, and donkey anti-rat 680 from Invitrogen, and donkey anti-mouse 568 from Biotium. Hoechst stain was obtained from Invitrogen. Brefeldin A (BFA), bafilomycin A1 (Bfa1) and nocodazole were obtained from Sigma-Aldrich and used at a final concentration of 300 μM, 50nM and 20mM, respectively.

Mouse strains - C9orf72 knockout mice were produced using CRISPR/Cas9 genome editing with a guide RNA (gRNA) targeting exon 2 of mouse gene 3110043O21RIK. C57BL/6J x FvB/N mouse embryos were injected with gRNA and Cas9 mRNA at the Cornell Transgenic Core Facility. Editing was confirmed by sequencing PCR products from genomic DNA and loss of protein products was determined by Western blot of tissue lysate. Offspring from the founder containing 1bp deletion were used for the study except the 10 month old founder mice. The following primers were used to genotype C9orf72 knockout mice: 5'- gcggctacctttgcttac -3' (WT forward), 5'- tggcggctacctttgcta -3 (KO forward) and 5'- tgcccaggagacacaacata -3' (common reverse).

Cell Culture and DNA Transfection - HEK293T cells were maintained in Dulbecco's Modified Eagle's Medium (Cellgro) supplemented with 10% fetal bovine serum (Gibco) and 1% Penicillin–Streptomycin (Invitrogen) in a humidified incubator

at 37ºC and 5% CO_2. Cells were transiently transfected with polyethyleneimine as described [55].

Immunoprecipitation and protein analysis- Cells were lysed in 50 mM Tris pH 8.0, 150 mM NaCl, 1% Triton X-100, and 0.1% deoxycholic acid with protease inhibitors (Roche). Lysates were incubated with GFP-Trap beads (ChromoTek) or anti-FLAG antibody conjugated beads (Sigma-Aldrich) for 2-3 hours at 4°C. Beads were washed 3 times with 50 mM Tris pH 8.0, 150 mM NaCl, and 1% Triton X-100. Samples were denatured in 2xSDS sample buffer (4% SDS, 20% glycerol, 100 mM Tris pH 6.8, 0.2 g/L bromophenol blue) by boiling for 3 minutes. Samples were run on 8% or 12% polyacrylamide gels and transferred to PVDF membranes (Millipore). Membranes were blocked in either Odyssey Blocking Buffer (LI-COR Biosciences) or 5% non-fat milk in PBS for 1 hour followed by incubation with primary antibodies overnight at 4°C. Membranes were washed 3 times with Tris-buffered saline with 0.1% Tween-20 (TBST) then incubated with secondary antibody for 2 hours at room temperature. Membranes were washed 3 times with TBST and imaged using an Odyssey Infrared Imaging System (LI-COR Biosciences).

To quantify protein levels in tissue samples, tissues were homogenized in RIPA buffer (50 mM Tris pH 8.0, 150 mM NaCl, 1% Triton X-100, 0.1% SDS and 0.1% deoxycholic acid) with protease inhibitors on ice and then equal volume of 2X SDS sample buffer was added before sonication. 50µg of each protein sample was loaded onto a 12% poly-acrylamide gel. Blots were analyzed by LiCor Odyssey system and normalized to GAPDH.

SILAC and mass spectrometry analysis- N2a cells were grown a minimum of five generations in DMEM with 10% dialyzed FBS (Sigma) supplemented with either light (C12, N14 arginine and lysine) or heavy (C13, N15 arginine and lysine) amino acids. The heavy cells were transfected in two 15 cm dishes with GFP-C9orf72

expression constructs while the light cells were transfected with pEGFP-C1 as a control. Two days after transfection, cells were lysed in 50mM Tris pH8.0, 150mM NaCl, 1% Triton, 0.1% deoxycholic acid with protease inhibitors (Roche). The lysates were subject to anti-GFP immunoprecipitation using GFP-Trap beads (ChromoTek). The presence of GFP and GFP-C9orf72 in immunoprecipitated samples was confirmed by SDS-PAGE and Krypton staining (Invitrogen). Samples were then combined and boiled 5 minutes with 1% DTT followed by alkylation by treating samples with a final concentration of 28 mM iodoacetamide. Proteins were precipitated on ice for 30 minutes with a mixture of 50% acetone/49.9% ethanol/0.1% acetic acid. Proteins were pelleted and washed with this buffer, re-precipitated on ice, and dissolved in 8M urea/50 mM Tris pH 8.0 followed by dilution with three volumes of 50 mM Tris pH 8.0/150 mM NaCl. Proteins were digested overnight at 37º C with 1 μg mass-spec grade Trypsin (Promega). The resulting peptide samples were cleaned up for mass spectrometry by treatment with 10% formic acid and 10% trifluoroacetic acid (TFA) and washed twice with 0.1% acetic acid on pre-equilibrated Sep-Pak C18 cartridges (Waters). Samples were eluted with 80% acetonitrile (ACN)/0.1% acetic acid into silanized vials (National Scientific) and evaporated using a SpeedVac. Samples were re-dissolved in H2O with ~1% formic acid and 70% ACN. Peptides were separated using hydrophilic interaction liquid chromatography (HILIC) on an Ultimate 300 LC (Dionex). Each fraction was evaporated with a SpeedVac and resuspended in 0.1% TFA with 0.1 pM angiotensin internal standard. Samples were run on a Thermo LTQ Orbitrap XL mass spectrometer and data analyzed using the SORCERER system (Sage-N research).

Hematoxylin and eosin (H&E) staining - Mouse tissues were fixed with 4% formaldehyde. After dehydration with 70% ethanol, tissues were embedded with paraffin. The tissues were sliced to 8μm. Followed by deparaffiinization with xylene and ethanol (100%, 95%, 80%) and rehydration with tap water, the slides were stained

in hematoxalin for 3 minutes, destained with acid ethanol and rinsed with tap water, and then stained with eosin for 30 seconds. The slides were then dehydrated with ethanol and xylene and mounted.

Immunofluorescence microscopy- HeLa cells grown on glass coverslips were fixed in 3.7% paraformaldehyde for 15 minutes, washed 3 times with PBS, and permeabilized and blocked in Odyssey Blocking Buffer with 0.05% saponin or 0.1% Triton for 20 minutes. Primary antibodies diluted in blocking buffer with 0.05% saponin were applied to the cells overnight at 4°C. Coverslips were washed 3 times with PBS. Secondary antibodies and Hoechst stain diluted in blocking buffer with 0.05% saponin were applied to the cells for 2 hours at room temperature. Coverslips were washed and mounted onto slides with Fluoromount G (Southern Biotech). Images were acquired on a CSU-X spinning disc confocal microscope (Intelligent Imaging Innovations) with an HQ2 CCD camera (Photometrics) using a 100x objective.

Mouse tissues were perfused and fixed with 4% formaldehyde. After gradient dehydration with 15% and 30% sucrose, tissues were embedded with OCT compound (Sakura Finetek USA) and sectioned with Cryotome. For the immunostaining, tissue sections were permeabilized and blocked in Odyssey blocking buffer with 0.05% saponin for 1 hour. Primary antibodies were incubated in blocking buffer overnight at 4ºC. Sections were washed and incubated in secondary antibodies conjugated to Alexaflour 488, 568, or 660 (Invitrogen). Sections were washed three more times and coverslips mounted onto slides with Fluoromount G (Southern Biotech). Images were acquired on a CSU-X spinning disc confocal microscope (Intelligent Imaging Innovations) with an HQ2 CCD camera (Photometrics) using a 40x objective.

Statistical analysis -The data were presented as mean ± SEM. Two-group analysis was performed using the Student's t test. P-values <0.05 were considered statistically significant.

REFERENCES

1. Liscic, R.M., et al., *ALS and FTLD: two faces of TDP-43 proteinopathy.* Eur J Neurol, 2008. **15**(8): p. 772-80.

2. Verma, A., *Tale of two diseases: amyotrophic lateral sclerosis and frontotemporal dementia.* Neurol India, 2014. **62**(4): p. 347-51.

3. Ferrari, R., et al., *FTD and ALS: a tale of two diseases.* Curr Alzheimer Res, 2011. **8**(3): p. 273-94.

4. Achi, E.Y. and S.A. Rudnicki, *ALS and Frontotemporal Dysfunction: A Review.* Neurol Res Int, 2012. **2012**: p. 806306.

5. Ling, S.C., M. Polymenidou, and D.W. Cleveland, *Converging mechanisms in ALS and FTD: disrupted RNA and protein homeostasis.* Neuron, 2013. **79**(3): p. 416-38.

6. Burrell, J.R., et al., *The frontotemporal dementia-motor neuron disease continuum.* Lancet, 2016.

7. Rademakers, R. and M. van Blitterswijk, *Motor neuron disease in 2012: Novel causal genes and disease modifiers.* Nat Rev Neurol, 2013. **9**(2): p. 63-4.

8. Wood, H., *A hexanucleotide repeat expansion in C9ORF72 links amyotrophic lateral sclerosis and frontotemporal dementia.* Nat Rev Neurol, 2011. **7**(11): p. 595.

9. Renton, A.E., et al., *A hexanucleotide repeat expansion in C9ORF72 is the cause of chromosome 9p21-linked ALS-FTD.* Neuron, 2011. **72**(2): p. 257-68.

10. DeJesus-Hernandez, M., et al., *Expanded GGGGCC hexanucleotide repeat in noncoding region of C9ORF72 causes chromosome 9p-linked FTD and ALS.* Neuron, 2011. **72**(2): p. 245-56.

11. Rohrer, J.D., et al., *C9orf72 expansions in frontotemporal dementia and amyotrophic lateral sclerosis.* Lancet Neurol, 2015. **14**(3): p. 291-301.

12. Le Ber, I., *Frontotemporal lobar dementia and amyotrophic lateral sclerosis associated with c9orf72 expansion.* Rev Neurol (Paris), 2015. **171**(6-7): p. 475-81.

13. Peters, O.M., et al., *Human C9ORF72 Hexanucleotide Expansion Reproduces RNA Foci and Dipeptide Repeat Proteins but Not Neurodegeneration in BAC Transgenic Mice.* Neuron, 2015. **88**(5): p. 902-9.

14. O'Rourke, J.G., et al., *C9orf72 BAC Transgenic Mice Display Typical Pathologic Features of ALS/FTD.* Neuron, 2015. **88**(5): p. 892-901.

15. Tran, H., et al., *Differential Toxicity of Nuclear RNA Foci versus Dipeptide Repeat Proteins in a Drosophila Model of C9ORF72 FTD/ALS.* Neuron, 2015. **87**(6): p. 1207-14.

16. Chew, J., et al., *Neurodegeneration. C9ORF72 repeat expansions in mice cause TDP-43 pathology, neuronal loss, and behavioral deficits.* Science, 2015. **348**(6239): p. 1151-4.

17. Liu, Y., et al., *C9orf72 BAC Mouse Model with Motor Deficits and Neurodegenerative Features of ALS/FTD.* Neuron, 2016.

18. Jiang, J., et al., *Gain of Toxicity from ALS/FTD-Linked Repeat Expansions in C9ORF72 Is Alleviated by Antisense Oligonucleotides Targeting GGGGCC-Containing RNAs.* Neuron, 2016.

19. Koppers, M., et al., *C9orf72 ablation in mice does not cause motor neuron degeneration or motor deficits.* Ann Neurol, 2015. **78**(3): p. 426-38.

20. Lagier-Tourenne, C., et al., *Targeted degradation of sense and antisense C9orf72 RNA foci as therapy for ALS and frontotemporal degeneration.* Proc Natl Acad Sci U S A, 2013. **110**(47): p. E4530-9.

21. Atanasio, A., et al., *C9orf72 ablation causes immune dysregulation characterized by leukocyte expansion, autoantibody production, and glomerulonephropathy in mice.* Sci Rep, 2016. **6**: p. 23204.

22. O'Rourke, J.G., et al., *C9orf72 is required for proper macrophage and microglial function in mice.* Science, 2016. **351**(6279): p. 1324-9.

23. Levine, T.P., et al., *The product of C9orf72, a gene strongly implicated in neurodegeneration, is structurally related to DENN Rab-GEFs.* Bioinformatics, 2013. **29**(4): p. 499-503.

24. Zhang, D., et al., *Discovery of Novel DENN Proteins: Implications for the Evolution of Eukaryotic Intracellular Membrane Structures and Human Disease.* Front Genet, 2012. **3**: p. 283.

25. Farg, M.A., et al., *C9ORF72, implicated in amytrophic lateral sclerosis and frontotemporal dementia, regulates endosomal trafficking.* Hum Mol Genet, 2014. **23**(13): p. 3579-95.

26. Xiao, S., et al., *C9orf72 isoforms in Amyotrophic Lateral Sclerosis and Frontotemporal Lobar Degeneration.* Brain Res, 2016.

27. Sellier, C., et al., *Loss of C9ORF72 impairs autophagy and synergizes with polyQ Ataxin-2 to induce motor neuron dysfunction and cell death.* Embo J, 2016.

28. Belzil, V.V., et al., *Reduced C9orf72 gene expression in c9FTD/ALS is caused by histone trimethylation, an epigenetic event detectable in blood.* Acta Neuropathol, 2013. **126**(6): p. 895-905.

29. Waite, A.J., et al., *Reduced C9orf72 protein levels in frontal cortex of amyotrophic lateral sclerosis and frontotemporal degeneration brain with the C9ORF72 hexanucleotide repeat expansion.* Neurobiol Aging, 2014. **35**(7): p. 1779 e5-1779 e13.

30. Xiao, S., et al., *Isoform-specific antibodies reveal distinct subcellular localizations of C9orf72 in amyotrophic lateral sclerosis.* Ann Neurol, 2015. **78**(4): p. 568-83.

31. Behrends, C., et al., *Network organization of the human autophagy system.* Nature, 2010. **466**(7302): p. 68-76.

32. Stanley, R.E., M.J. Ragusa, and J.H. Hurley, *The beginning of the end: how scaffolds nucleate autophagosome biogenesis.* Trends Cell Biol, 2014. **24**(1): p. 73-81.

33. Atkinson, R.A., et al., *C9ORF72 expression and cellular localization over mouse development.* Acta Neuropathol Commun, 2015. **3**: p. 59.

34. Suzuki, N., et al., *The mouse C9ORF72 ortholog is enriched in neurons known to degenerate in ALS and FTD.* Nat Neurosci, 2013. **16**(12): p. 1725-7.

35. Cong, L., et al., *Multiplex genome engineering using CRISPR/Cas systems.* Science, 2013. **339**(6121): p. 819-23.

36. Mali, P., et al., *RNA-guided human genome engineering via Cas9.* Science, 2013. **339**(6121): p. 823-6.

37. Kundu, M., et al., *Ulk1 plays a critical role in the autophagic clearance of mitochondria and ribosomes during reticulocyte maturation.* Blood, 2008. **112**(4): p. 1493-502.

38. Klionsky, D.J., et al., *Guidelines for the use and interpretation of assays for monitoring autophagy (3rd edition).* Autophagy, 2016. **12**(1): p. 1-222.

39. Ju, J.S., et al., *Valosin-containing protein (VCP) is required for autophagy and is disrupted in VCP disease.* J Cell Biol, 2009. **187**(6): p. 875-88.

40. Rusten, T.E. and A. Simonsen, *ESCRT functions in autophagy and associated disease.* Cell Cycle, 2008. **7**(9): p. 1166-72.

41. Lee, J.A. and F.B. Gao, *ESCRT, autophagy, and frontotemporal dementia.* BMB Rep, 2008. **41**(12): p. 827-32.

42. Peters, O.M., M. Ghasemi, and R.H. Brown, Jr., *Emerging mechanisms of molecular pathology in ALS.* J Clin Invest, 2015. **125**(5): p. 1767-79.

43. Smith, K.R., et al., *Strikingly Different Clinicopathological Phenotypes Determined by Progranulin-Mutation Dosage.* Am J Hum Genet, 2012. **90**(6): p. 1102-7.

44. Canafoglia, L., et al., *Recurrent generalized seizures, visual loss, and palinopsia as phenotypic features of neuronal ceroid lipofuscinosis due to progranulin gene mutation.* Epilepsia, 2014. **55**(6): p. e56-9.

45. Hu, F., et al., *Sortilin-mediated endocytosis determines levels of the frontotemporal dementia protein, progranulin.* Neuron, 2010. **68**(4): p. 654-67.

46. Zhou, X., et al., *Prosaposin facilitates sortilin-independent lysosomal trafficking of progranulin.* J Cell Biol, 2015. **210**(6): p. 991-1002.

47. Brady, O.A., et al., *The frontotemporal lobar degeneration risk factor, TMEM106B, regulates lysosomal morphology and function.* Hum Mol Genet, 2013. **22**(4): p. 685-95.

48. Chen-Plotkin, A.S., et al., *TMEM106B, the Risk Gene for Frontotemporal Dementia, Is Regulated by the microRNA-132/212 Cluster and Affects Progranulin Pathways.* J Neurosci, 2012. **32**(33): p. 11213-27.

49. Lang, C.M., et al., *Membrane orientation and subcellular localization of transmembrane protein 106B (TMEM106B), a major risk factor for frontotemporal lobar degeneration.* J Biol Chem, 2012. **287**(23): p. 19355-65.

50. Stagi, M., et al., *Lysosome size, motility and stress response regulated by fronto-temporal dementia modifier TMEM106B.* Mol Cell Neurosci, 2014. **61**: p. 226-40.

51. Jun, M.H., et al., *TMEM106B, a frontotemporal lobar dementia (FTLD) modifier, associates with FTD-3-linked CHMP2B, a complex of ESCRT-III.* Mol Brain, 2015. **8**: p. 85.

52. Ciura, S., et al., *Loss of function of C9orf72 causes motor deficits in a zebrafish model of amyotrophic lateral sclerosis.* Ann Neurol, 2013. **74**(2): p. 180-7.

53. Therrien, M., et al., *Deletion of C9ORF72 results in motor neuron degeneration and stress sensitivity in C. elegans.* PLoS ONE, 2013. **8**(12): p. e83450.

54. Ge, L., et al., *The ER-Golgi intermediate compartment is a key membrane source for the LC3 lipidation step of autophagosome biogenesis.* Elife, 2013. **2**: p. e00947.

55. Vancha, A.R., et al., *Use of polyethyleneimine polymer in cell culture as attachment factor and lipofection enhancer.* BMC Biotechnol, 2004. **4**: p. 23.

CHAPTER 3

IDENTIFICATION OF C9ORF72-SMCR8-WDR41 COMPLEX BINDING PROTEINS

3.1 ABSTRACT

The C9orf72 gene has been found to be the leading genetic cause of ALS/FTLD. One proposed mechanism leading from genetic mutation to disease, is that insufficient protein expression contributes to development of neurodegeneration. To better understand the role of C9orf72 protein in disease, more needs to be known about what this protein normally does in the cell. To understand more about C9orf72's protein network, several SILAC screen were used to identify additional protein binding partners of C9orf72/SMCR8/WDR41 complex. While several interactions have been validated, the physiological importance of these interactions remains unknown.

3.2 INTRODUCTION

Intronic hexanucleotide repeat expansion in the gene C9orf72 was identified as a leading cause of two related neurodegenerative diseases, ALS and FTLD[1, 2]. One proposed model of how this mutation leads to disease is through haploinsufficiency of the protein product of C9orf72. In order to understand the contribution of C9orf72 haploinsufficiency, we sought to discover the cellular function of C9orf72. By employing stable isotope labeling of amino acids in cell culture (SILAC) with mass spectrometry, we identified many potential protein interactions. We published data

characterizing the interaction between C9orf72, SMCR8, and WDR41. Here, I describe additional C9orf72 protein interactions based on mass spectrometry results and C9orf72 domain structure predictions.

3.3 Results

C9orf72 SILAC-MS identifies potential protein interactions

To discover which proteins the C9orf72-SMCR8-WDR41 complex interacts with, we performed several SILAC based mass spectrometry experiments. First, using light amino acid-labeled GFP and heavy amino acid GFP-C9orf72 overexpressed in N2a cells. SILAC experiments were also conducted in HEK293T cells by either co-expressing GFP-C9orf72 with SMCR8-GFP or expressing WDR41-GFP alone. Tables 3-1, 3-2, and 3-3 show the top hits from each of these three experiments.

GFP-C9orf72 in N2a cells

orf	gene	Count H	Count L	gmean
ALPPL2	ALPPL2	2	0	0.0121
MMS19	MMS19	2	0	0.0207
FSIP2	FSIP2	2	0	0.0341
FARSA	FARSA	2	0	0.0345
ALKBH3	ALKBH3	2	0	0.0469
WDR41	WDR41	9	1	0.0509
C9ORF72	**C9ORF72**	**152**	**53**	**0.0552**
SORT1	SORT1	4	0	0.0575
FAM82A2	FAM82A2	2	0	0.059
LAMC1	LAMC1	2	0	0.0602
SMCR8	SMCR8	26	3	0.0641
YME1L1	YME1L1	4	0	0.0648
DNAJC11	DNAJC11	3	0	0.0838
VDAC3	VDAC3	28	5	0.0978
SSR1	SSR1	2	2	0.0987
DERL1	DERL1	1	1	0.1111
COL5A2	COL5A2	4	0	0.1115
TBC1D15	TBC1D15	2	1	0.113
RRM1	RRM1	2	1	0.1298
AKAP8	AKAP8	2	1	0.1428
RABIF	RABIF	1	1	0.1656
SLC25A4,SLC25A5,SLC5A6	"291-SLC25A4	15	6	0.1813
ERGIC1	ERGIC1	4	0	0.1854
SLC25A5	SLC25A5	31	18	0.1863

Table 3-1: List of protein interactions by SILAC analysis of GFP-C9orf72 binding partners in N2a cells. Count H: number of peptides in the heavy fraction; Count L: number of peptides in the light fraction. Peptides with a gmean score <0.2 are listed. Bait proteins are listed in bold.

GFP-C9orf72 + SMCR8-GFP in HEK293T cells

orf	gene	Count H	Count L	gmean
PHB2	PHB2	2	0	0.0191
TCP1	TCP1	3	0	0.0191
SLC25A10	SLC25A10	2	0	0.0417
"83858-ATAD3B,ATAD3A"	"83858-ATAD3B	2	0	0.0722
ATAD3A	ATAD3A	4	0	0.0881
"84617-TUBB6,TUBB2B,TUBBA,TUBB2C"	"84617-TUBB6	2	0	0.0932
CIAO1	CIAO1	4	0	0.1196
TUBB2B	TUBB2B	2	0	0.1317
HAX1	HAX1	2	0	0.1382
"7277-TUBA4A,TUBA1A,TUBAC,TUBA3D,TUBA1C,TUBA8,TUA1B"	"7277-TUBA4A	3	0	0.1679
DNAJA1	DNAJA1	14	0	0.1706
DNAJC11	DNAJC11	2	0	0.1816
"3320-HSP90AA1,HSP90AA5P"	"3320-HSP90AA1	3	0	0.1818
"291-SLC25A4,SLC25A5,SLC5A6"	"291-SLC25A4	4	1	0.2240
AIFM1	AIFM1	17	1	0.2376
DNAJA2	DNAJA2	10	0	0.2502
MMS19	MMS19	5	0	0.2567
SLC25A5	SLC25A5	7	2	0.2572
RNF219	RNF219	2	0	0.2602
SLC25A13	SLC25A13	11	0	0.2700
C9ORF72	**C9ORF72**	**25**	**10**	**0.2807**
"6182-MRPL12,SLC25A10"	"6182-MRPL12	7	0	0.2866
"3327-HSP90AB3P,HSP90AB1"	"3327-HSP90AB3P	3	0	0.3002
WDR41	WDR41	27	5	0.3080
"219293-ATAD3C,ATAD3A"	"219293-ATAD3C	2	0	0.3149
TUBB4	TUBB4	4	0	0.3168
EMD	EMD	6	1	0.3449
DPM1	DPM1	2	0	0.3636
"83858-ATAD3B,ATAD3C,ATA3A"	"83858-ATAD3B	3	0	0.3636
FAM96B	FAM96B	2	0	0.3857
NPEPPS	NPEPPS	3	0	0.3968
SMCR8	**SMCR8**	**71**	**32**	**0.4045**
"84617-TUBB6,TUBB2B,TUBB,TUBB8,TUBB2A,TUBB2C,TUB"	"84617-TUBB6	2	0	0.4066
"84617-TUBB6,TUBB4Q,TUBB,TUBBP5,MC	"84617-TUBB6	5	3	0.4121

1R,TUBB3,TUBB2,TUBB4,TUBB8,TUBB2A,TUBB2C,TUBB"				
BAG2	BAG2	6	2	0.4215
TUFM	TUFM	5	0	0.4263
"10382-TUBB4,TUBB4Q,TUBB,TUBB2C,TUBB"	"10382-TUBB4	2	1	0.4329
STUB1	STUB1	5	0	0.4644
"7277-TUBA4A,TUBA1A,TUBAC,TUBA3D,TUBA3E,TUBA1C,TBA4B,TUBA8,TUBA1B"	"7277-TUBA4A	2	1	0.4765
"3324-HSP90AA2,HSP90AA1,SP90AB1"	"3324-HSP90AA2	2	0	0.5143
"7277-TUBA4A,TUBA1A,TUBAC,TUBA3D,TUBA1C,TUBAL3,TBA8,TUBA1B"	"7277-TUBA4A	3	1	0.5222
HSP90AA1	HSP90AA1	7	0	0.5342
KPNB1	KPNB1	2	0	0.5378
PRKDC	PRKDC	28	1	0.5398
PSME3	PSME3	3	0	0.5488
SLC25A3	SLC25A3	8	0	0.5494
RPL23	RPL23	3	2	0.5590
SLC25A11	SLC25A11	7	0	0.5619
ATP5A1	ATP5A1	10	0	0.5721
C1ORF57	C1ORF57	2	0	0.5750
CCT5	CCT5	2	0	0.5892
FAR1	FAR1	2	0	0.5892
CCT8	CCT8	5	0	0.5947
"478-ATP1A3,ATP1A1,ATP1A,ATP1A2"	"478-ATP1A3	2	0	0.6030
"7277-TUBA4A,TUBA1A,TUBAC,TUBA3D,MGC16703,TUBA1CTUBA1B"	"7277-TUBA4A	2	1	0.6045
DNAJA3	DNAJA3	10	1	0.6120
CHCHD3	CHCHD3	3	0	0.6205
"292-SLC25A5,SLC25A6"	"292-SLC25A5	2	1	0.6364
SLC25A6	SLC25A6	1	1	0.6364
"347733-TUBB2B,TUBB2A"	"347733-TUBB2B	4	0	0.6441

Table 3-2: (Previous page) List of protein interactions by SILAC analysis of GFP-C9orf72 with SMCR8-GFP binding partners in HEK293T cells. Count H: number of peptides in the heavy fraction; Count L: number of peptides in the light fraction. Bait proteins are listed in bold.

GFP-WDR41 SILAC

orf	gene	Count H	Count L	gmean
ATAD3B	ATAD3B	2	0	0.01137
HIF1AN	HIF1AN	2	0	0.01137
FAR1	FAR1	2	0	0.02542
XPO1	XPO1	2	0	0.02666
STUB1	STUB1	7	0	0.02968
WDR41	**WDR41**	**65**	**20**	**0.04859**
IMMT	IMMT	4	0	0.05018
SLC25A5	SLC25A5	6	0	0.05259
CCT7	CCT7	2	0	0.05272
"291-SLC25A4,SLC25A6"	"291-SLC25A4	2	0	0.05819
ATAD3A	ATAD3A	4	0	0.06326
ARL1	ARL1	2	0	0.06432
"219293-ATAD3C,ATAD3A"	"219293-ATAD3C	3	0	0.06463
LBR	LBR	2	0	0.06795
SLC25A11	SLC25A11	7	0	0.09676
ATP5C1	ATP5C1	6	1	0.09794
SLC25A22	SLC25A22	2	0	0.10906
"83858-ATAD3B,ATAD3C,ATA3A"	"83858-ATAD3B	3	0	0.1248
DNAJA2	DNAJA2	2	0	0.12892
SMCR8	SMCR8	9	1	0.13076
CCT3	CCT3	5	0	0.13292
DHCR7	DHCR7	2	0	0.13925
PRKDC	PRKDC	28	1	0.1436
DNAJA1	DNAJA1	6	1	0.1559
"292-SLC25A5,SLC25A6"	"292-SLC25A5	2	0	0.16458
SLC25A13	SLC25A13	7	0	0.16727
"291-SLC25A4,SLC25A5,SLC5A6"	"291-SLC25A4	2	1	0.16938
C9ORF72	C9ORF72	6	0	0.17153
TCP1	TCP1	4	0	0.18011
"83858-ATAD3B,ATAD3A"	"83858-ATAD3B	3	0	0.19518
ATP5A1	ATP5A1	4	0	0.19902

Table 3-3: (Previous page) List of protein interactions by SILAC analysis of WDR41-GFP binding partners in HEK293T cells. Count H: number of peptides in the heavy fraction; Count L: number of peptides in the light fraction. Peptides with a gmean score <0.2 are listed. Bait proteins are listed in bold.

MMS19 and Iron-Sulfur Complex Transfer Machinery

Among the top hits identified in both the C9orf72 and C9orf72 with SMCR8 SILAC experiments was MMS19, a protein involved in coordinating the incorporation of iron-sulfur (FeS) clusters into nascent FeS-containing proteins (Table 3-1, Table 3-2, Figure 3-1A) [3, 4]. Interestingly, a previously reported mass spectrometry analysis of MMS19 binding proteins also identified SMCR8, WDR41, and C9orf72 as potential hits [4]. To test this interaction, I co-immunoprecipitated (Co-IP) GFP alone, GFP-C9orf72, or SMCR8-GFP co-expressed MMS19-V5 in HEK293T cells and found that MMS19 was present after C9orf72 and SMCR8 Co-IP but not GFP alone (Figure 3-1B). MMS19 contains several HEAT (Huntingtin, Elongation factor 3, protein phosphatase 2A, and mTOR) domains, several of which are clustered at the C-terminal end of MMS19 and are critical for interacting with apo-proteins about to receive a FeS cluster whereas the rest of the protein coordinates the binding of several proteins involved in FeS transfer (Figure 3-1A) [5]. To test which domain of MMS19 interacts with C9orf72, I made two truncations. One lacks the HEAT repeat domain (ΔHEAT) and another with only the HEAT repeat domain (HRD). Co-IP of FLAG-tagged MMS19 constructs for GFP-C9orf72 showed that the ΔHEAT construct had the strongest interaction with C9orf72 (Figure 3-1C). Finally, to test if components of the C9orf72 complex interacted with other proteins involved in FeS transfer, I conducted a Co-IP for GFP-C9orf72, SMCR8-GFP, or WDR41-GFP in the presence of four additional FeS proteins: NARFL, CIAO1, ANT2, and FAM96B (Figure 3-1D) [4, 6]. Despite one SILAC screen identifying CIAO1 and FAM96B as potential binding partners to C9orf72 and SMCR8 (Table 3-2), the interaction could not be verified by Co-IP in HEK293T cells (Figure 3-1D).

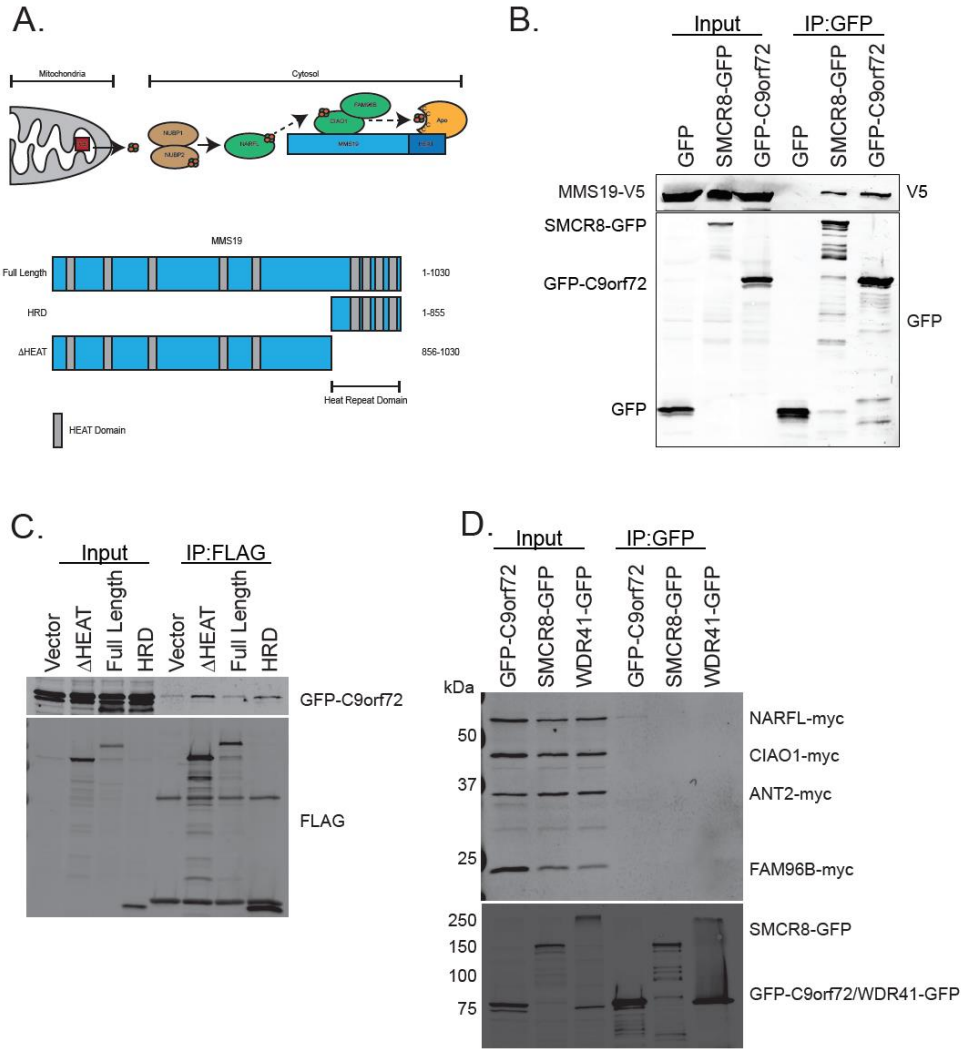

Figure 3-1: C9orf72 complex interaction with MMS19. a. Schematic of the cytosolic iron-sulfur assembly pathway and schematic of MMS19 domain structure. **b**. Western blot results from Co-IP of overexpressed GFP, GFP-C9orf72, or SMCR8-GFP with MMS19-V5 in HEK293T cells. **c**. Western blot of Co-IP with overexpressed FLAG-tagged full length, HEAT, or ΔHEAT Repeat Domain (HRD) MMS19 with GFP-C9orf72. **d**. Western blot of Co-IP between GFP-C9orf72, SMCR8-GFP, or WDR41-GFP and NARFL-myc, CIAO1-myc, ANT2-myc, and FAM96B-myc.

TRiC/Chaperonin Complex

Another protein complex that was identified by SILAC in multiple experiments was the TRiC (T-Complex protein-1 Ring Complex) or CCT (Chaperonin Containing T-Complex Protein-1) complex, an eight-subunit complex that aids in the proper folding of many substrates, including tubulin, actin, and many WD-repeat containing proteins[7, 8]. Furthermore, mutations in the TRiC complex have been associated with sensory neuropathy and genetic disruption of the TRiC complex was shown to delay autophagy initiation by disrupting the actin cytoskeleton[9, 10]. Since WDR41 is predicted to be almost entirely WD-repeats, TRiC may act as a chaperone for WDR41, thus affecting the stability of the C9or72 complex[11, 12]. The C9orf72 complex might also directly interact with TRiC to regulate its function. However, no binding was observed when overexpressed GFP-C9orf72, SMCR8-GFP, and WDR41-GFP were coexpressed and pulled down to identify whether TCP-1α, a component of the TRiC complex, is also pulled down (Figure 3-2A). Additionally, no binding was observed with TCP-1β or TCP-1δ in the presence of overexpressed GFP-C9orf72 and SMCR8-GFP (Figure 3-2B). These data suggest that the C9orf72 complex and TRiC complex do not directly interact. To test whether loss of C9orf72 complex components had any effect on TRiC complex, TCP-1α was blotted in C9orf72, WDR41, or SMCR8 knockout MEF cell lysates (Figure 3-2C). While C9orf72 and WDR41 knockouts did not seem to have any effect, loss of SMCR8 increased the protein levels of TCP-1α (Figure 3-2C).

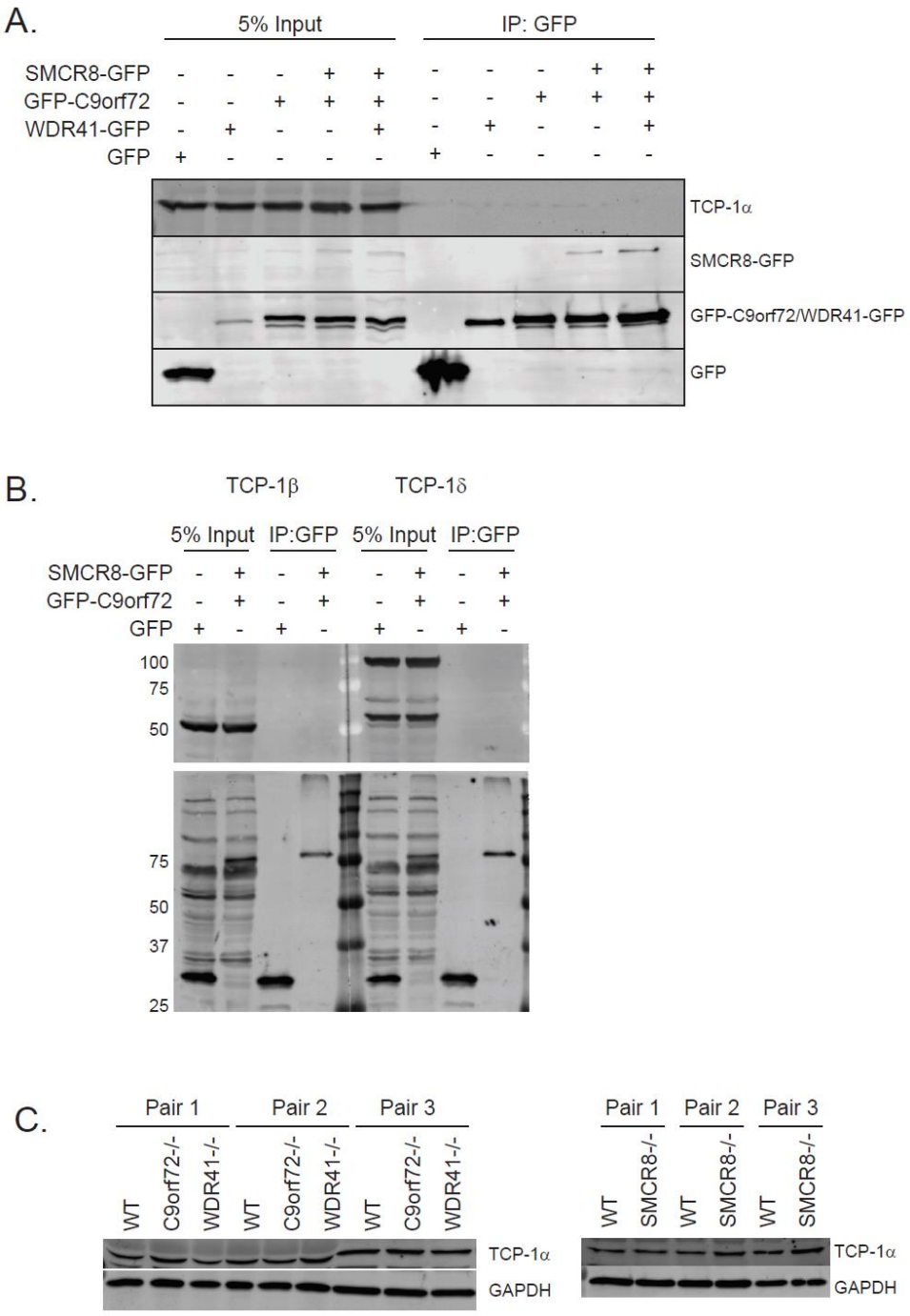

Figure 3-2: C9orf72 does not interact with the Tri/Chaperonin complex. **a**. Western blot for the IP of overexpressed GFP, GFP-C9orf72, SMCR8-GFP, or WDR41-GFP and blotted for endogenous TCP-1α. **b**. Western blot of Co-IP with overexpressed GFP-C9orf72 and SMCR8-GFP for endogenous TCP-1β or TCP-1δ. **c**. Endogenous TCP-1α in 3 sets of either WT, C9orf72-/-, WDR41-/-, or SMCR8-/- mouse embryonic fibroblasts.

Tubulin

Another protein that was found in multiple SILAC experiments was Tubulin (Table 3-2). While tubulin can be a common contaminant in mass spectrometry experiments due to its abundance, overexpressed GFP-C9orf72 and SMCR8-GFP appear to specifically pull down endogenous α-tubulin from HEK293T lysates (Figure 3-3A). Furthermore, this interaction is modulated by nutrient starvation, as FLAG-C9orf72 can better pull down tubulin under amino acid starvation conditions (Figure 3-3B) [13]. Finally, to test whether microtubule structure is disrupted upon C9orf72 knockout, primary cultured macrophages were stained for α-tubulin after nutrient starvation (Figure 3-3C).

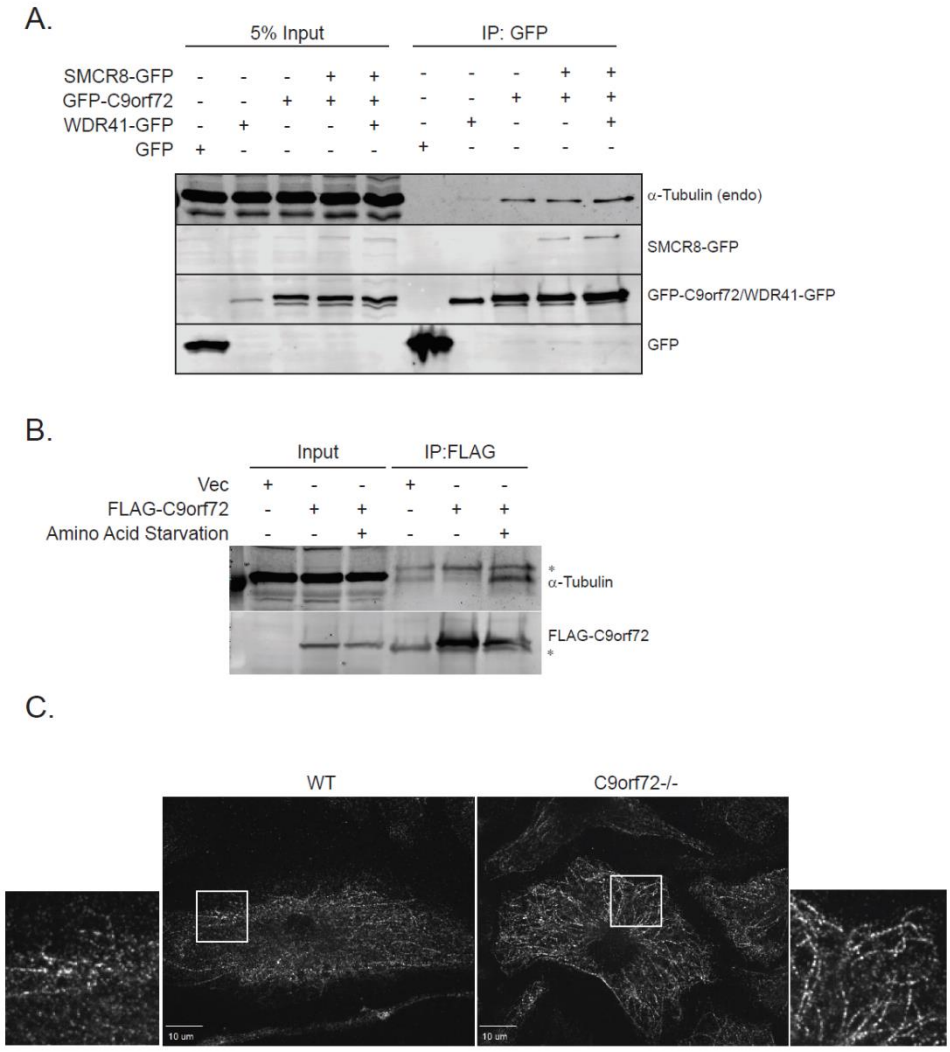

Figure 3-3: C9orf72 interaction with tubulin. a. Western blot for the IP of overexpressed GFP, GFP-C9orf72, SMCR8-GFP, or WDR41-GFP and blotted for endogenous α-tubulin. **b**. Western blot for Co-IP of overexpressed FLAG-C9orf72 for endogenous α-tubulin with or without 60 minutes of amino acid starvation. **c**. WT and C9orf72-/- MEF cells stained fixed and stained for α-tubulin after 60 minutes of amino acid starvation.

Small GTPases

An early characterization of C9orf72 and SMCR8 by structural prediction suggested that they both contain DENN (Differentially Expressed in Normal and Neoplastic) domains (Figure 3-4A), which are commonly found in Rab GTPase GEFs (Guanine Exchange Factors) [14] [15]. Despite no sequence homology to the canonical DENN domains, C9orf72 and SMCR8 were predicted to contain this domain by comparing the predicted secondary structures to that of non-canonical DENN domain containing protein Folliculin (FLCN), which actually acts as a GAP (GTPase Activating Protein) to activate RagC/D by promoting the GDP-bound form of RagC/D [14] [16]. This prediction has led many labs to test C9orf72 and SMCR8 interaction with various Rab GTPases. To date, other labs have proposed that C9orf72 or C9orf72 with SMCR8 interact with Rab1, Rab5, Rab7, Rab8A, and Rab38B [17] [18, 19]. Despite not identifying any Rab GTPases in our SILAC screens, we have also tested a panel of available Rab GTPases for Co-IP with C9orf72, SMCR8, and WDR41. To test for Rab GTPase interactions, GFP-tagged Rabs were pulled down in the presence of FLAG-C9orf72, SMCR8-myc, and WDR41-myc (Figure 3-4B). While no Rab Co-IPs demonstrated clear binding to SMCR8 or WDR41, C9orf72 bound to several Rabs, including Rab5, Rab7, Rab35, and Rab39A.

Since Rab39B was reported as a target of C9orf72 and SMCR8 GEF activity, I further tested the interaction with the related Rab39A by overexpressing combinations of GFP-tagged C9orf72, SMCR8, and WDR41 with myc-tagged Rab39A (Figure 3-5A). Rab39A bound to C9orf72 alone, but bound more strongly to C9orf72 with SMCR8 present while the presence of WDR41 had little effect (Figure 3-5A). To further

characterize this interaction, the interaction of wild type (WT) Rab39A with C9orf72 was compared to constitutively active Rab39A (QL; mimicking GTP-bound, active state) or the dominant negative Rab39A (SN; mimicking GDP/nucleotide free state). C9orf72 and SMCR8 bound most strongly to the WT and constitutively active Rab39A (Figure 3-5B).

Rab5 and Rab7 binding was also previously reported, though with less characterization [17]. In addition to binding WT Rab5 and Rab7, the constitutively active Rab5 shows increased binding to C9orf72 and SMCR8, whereas the dominant negative, inactive Rab7 shows the same binding as WT Rab7 (Figure 3-4C).

The only GTPase identified by SILAC analysis was Arl1, found in the WDR41-GFP screen (Table 3-3). This interaction was also tested by Co-IP using overexpressed GFP-C9orf72, SMCR8-myc, and FLAG-Arl1 in HEK293T cells (Figure 3-6A). However, no binding was observed between Arl1 and C9orf72 with SMCR8. As C9orf72 and SMCR8 were predicted to contain DENN domains based on the structure of FLCN, a Rag GTPase interacting protein, the interaction with Rag GTPases was also tested[16]. Overexpressed GFP-C9orf72 and SMCR8-myc were pulled down from HEK293T lysates and endogenous RagA and RagC were blotted (Figure 3-6B). As with Arl1, no interaction between RagA or RagC and C9orf72 was observed.

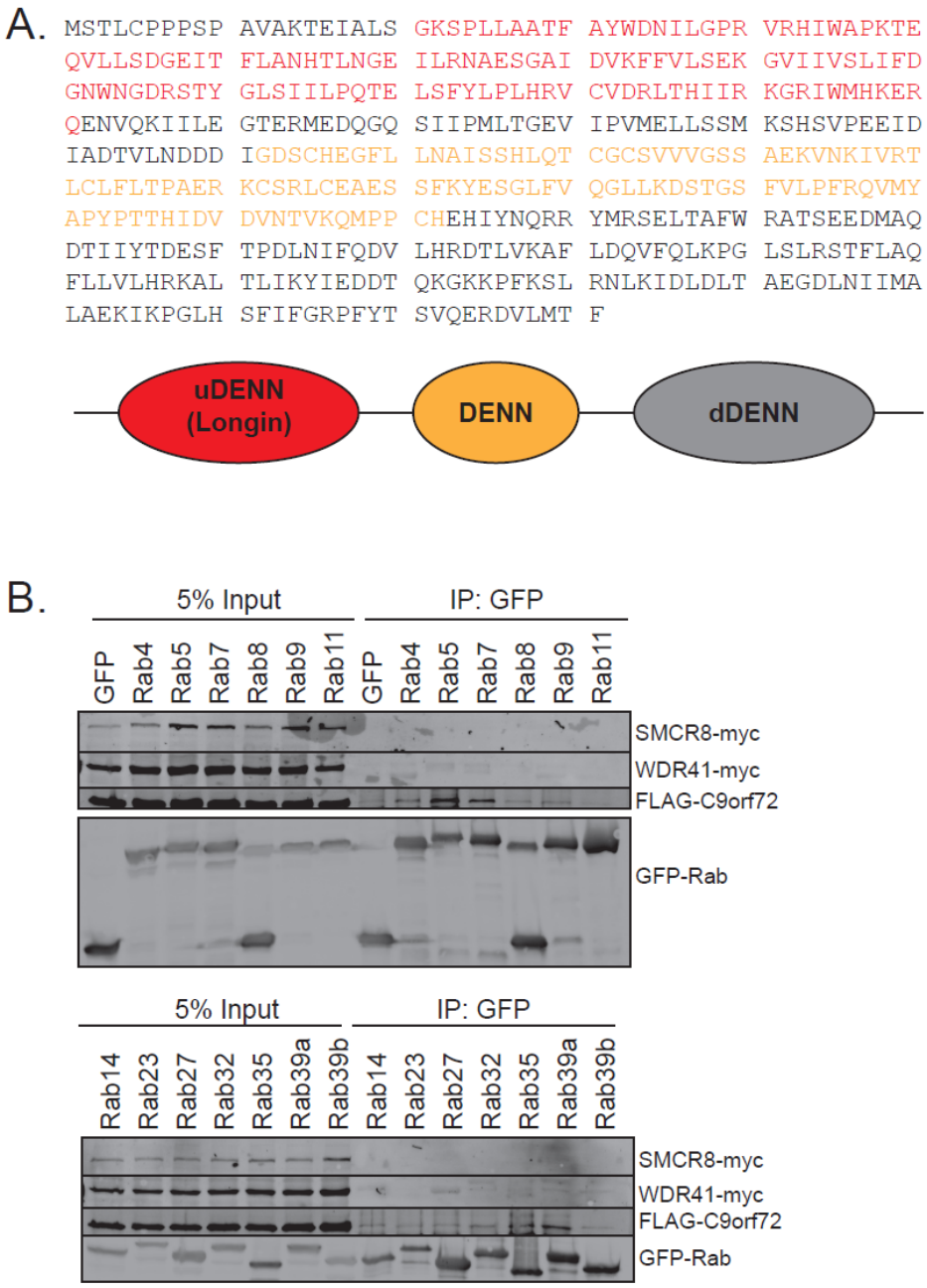

Figure 3-4: C9orf72 is predicted to interact with Rab GTPases through a DENN domain. a. C9orf72 sequence and schematic of predicted domains. Upstream DENN (uDENN) is shown in red, DENN domain in yellow, and dDENN in gray. **b**. Western blot of Co-IP pulling down GFP-tagged Rab GTPases for FLAG-C9orf72, SMCR8-myc, and WDR41-myc.

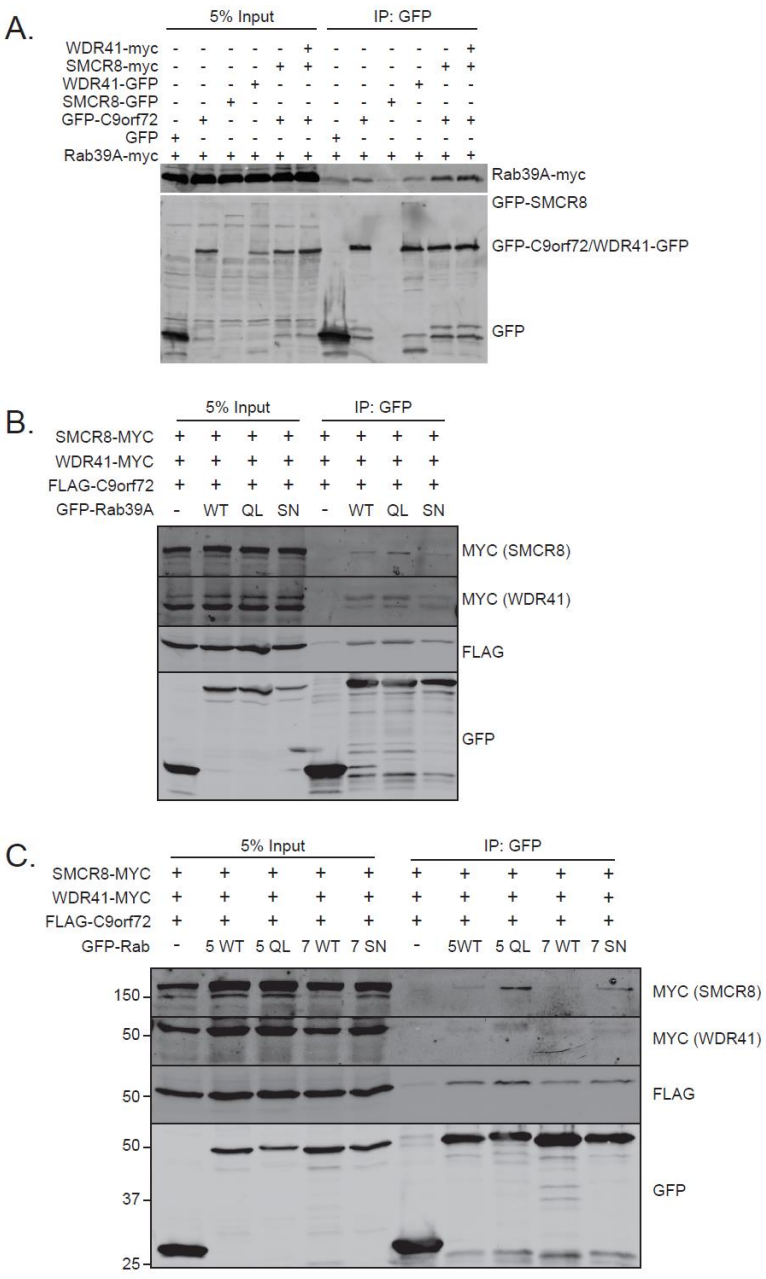

Figure 3-5: C9orf72 interaction with Rab39A, Rab5, and Rab7. a. Western blot for Co-IP from overexpressed GFP-C9orf72, SMCR8-GFP, and/or WDR41-GFP for Rab39A-myc in HEK293T cells. **b**. Western blot for Co-IP with GFP or GFP-tagged Rab39A WT, constitutively active (QL), or dominant negative (SN) for FLAG-C9orf72, SMCR8-myc, and WDR41-myc in HEK293T cells. **c**. Western blot for Co-IP with GFP or GFP-tagged Rab5 WT (5 WT), Rab5 constitutively active (5 QL), Rab7 WT (7 WT), or Rab7 dominant negative (7 SN) for FLAG-C9orf72, SMCR8-myc, or WDR41-myc in HEK293T cells.

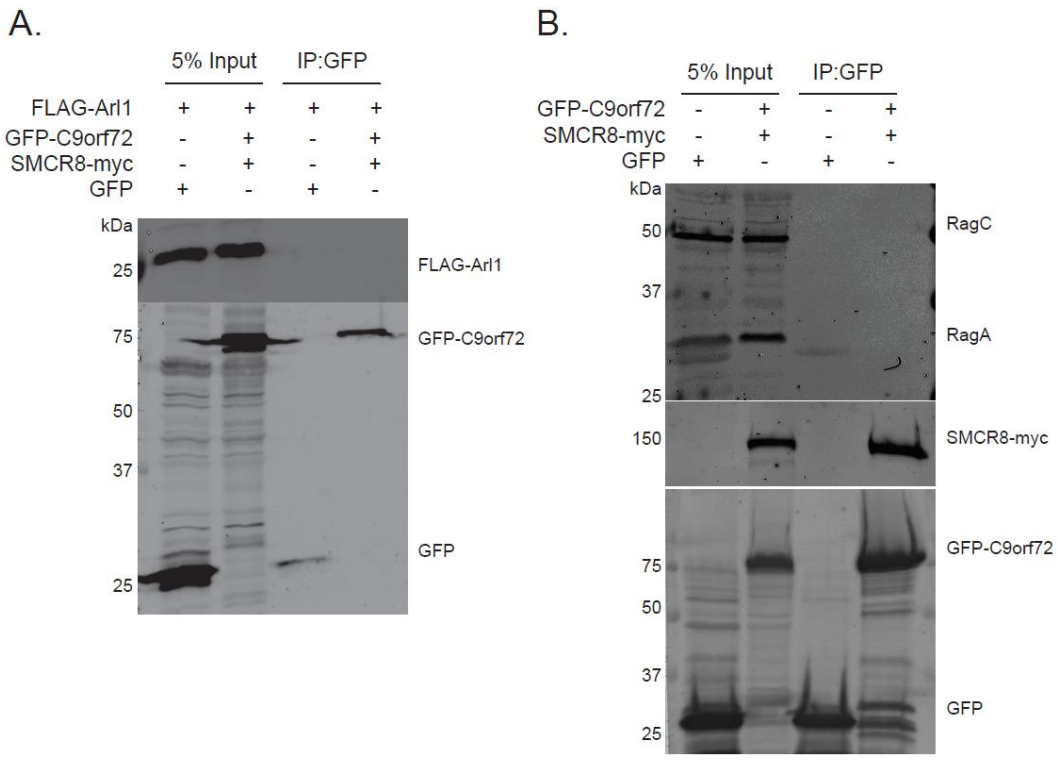

Figure 3-6: C9orf72 does not interact with other small GTPase candidates. a. Western blot for Co-IP between overexpressed GFP or GFP-C9orf72 with SMCR8-myc and FLAG-Arl1 in HEK293T cells. **b**. Western blot of IP of GFP-C9orf72 and SMCR8-myc for endogenous RagA and RagC using CHAPS-based immunoprecipitation buffer.

3.4 CONCLUSIONS AND DISCUSSION

We found that C9orf72 has many potential binding partners beyond SMCR8 and WDR41, with which it forms a tight complex. Here, we report interactions with MMS19, tubulin, Rab5, Rab7, Rab35, and Rab39A. However, beyond verifying these binding partners through Co-IP, we don't yet know the physiological implications of these interactions or the consequences of loss of the C9orf72 complex on these proteins.

The interaction with MMS19 suggests that C9orf72, SMCR8, and/or WDR41 may either play a role in FeS cluster dynamics or be an FeS cluster containing protein. That C9orf72 binds to the ΔHEAT MMS19 construct suggests that C9orf72 plays a regulatory role unlike proteins that bind the HRD of MMS19 to accept an FeS cluster. However, C9orf72, SMCR8, and WDR41 did not bind to additional FeS cluster transport proteins (NARFL, CIAO1, FAM96B, or ANT2) despite CAIO1 and FAM96B also appearing in the SILAC screen results (Table 3-2). Future experiments will need to test whether C9orf72 or SMCR8 contain an FeS cluster. One way to test this is to treat cells with an iron chelator such as desferrioxamine and observe endogenous protein levels of C9orf72 and SMCR8. Most proteins that contain an FeS cluster require it for stability. Purification of these proteins for structural studies or spectroscopic studies can also indicate whether or not they contain an FeS cluster. Given that we see disruption of mTOR signaling (see chapter 4) and that MMS19 has no reported role in the mTOR pathway, the physiological importance of this interaction remains in question.

The TRiC/chaperonin complex did not show binding to C9orf72, SMCR8, or WDR41 by Co-IP even though nearly all of the eight subunit have appeared in the SILAC screens. This may be in part due to the nature of the TRiC complex and the sensitivity of SILAC. The TRiC complex was previously reported to help fold many classes of proteins, including proteins containing WD repeat domains, as WDR41 does[8]. With WDR41 overexpressed, TRiC is likely bound to nascent WDR41 peptides

that are being overproduced by transient expression. As SILAC is highly sensitive, it may be able to pick up a low level of interaction that is too low to detect by Western blotting. Additionally, just as loss of WDR41 or SMCR8 decreases C9orf72 stability, WDR41 is likely destabilized by the loss C9orf72 or SMCR8 and may result in increased TRiC expression to keep WDR41 properly folded, as reported with expression of aggregating poly-Q proteins[20]. While this interaction may provide insight into the synthesis and stability of the C9orf72-SMCR8, WDR41 complex, it is unlikely to be relevant to the main function of the C9orf72 complex.

The interaction between C9orf72 and tubulin was verified by Co-IP and also seems to be regulated by nutrient availability. Microtubules are known to undergo remodeling upon starvation and autophagy induction[13]. This process of remodeling requires additional protein interactions that are often regulated by post-translational modifications (PTM) of tubulin, such as phosphorylation and acetylation. As we see increased binding between C9orf72 and tubulin upon amino acid starvation, the interaction may be dependent on one such PTM. Using antibodies specific to modified tubulin may indicate whether one of these PTM is mediating the interaction. Furthermore, loss of C9orf72 in primary macrophages shows stronger staining for microtubules after nutrient starvation. This may indicate the microtubules are not remodeling properly. Watching microtubule dynamics in knockout cells will be crucial to understanding what effect, if any, loss of the C9orf72 complex has on microtubules. Additionally, cell fractionation for free tubulin dimers and microtubules will be a more quantitative measure of whether loss of C9orf72 is effecting microtubule dynamics.

Finally, the interaction with multiple Rab GTPases continues a major question in the field studying C9orf72. The prediction that C9orf72 and SMCR8 contain DENN domains have led many groups to test the interaction with various Rab GTPases[17-19]. However, no two groups have reported interaction with the same Rab. Furthermore, we

have not found any Rabs in our SILAC screens, suggesting that if there is binding to a Rab, the interaction may be very transient. Our panel of Rabs only include Rab GTPases that we had ready access to and do not include other potential Rabs or classes of small GTPases. Nonetheless, we did identify several Rab GTPases that showed binding to the C9orf72 complex. Rab5 and Rab7 had previously been reported to bind C9orf72, but the physiological implications of this interaction were not described. Rab5 and Rab7 function in the endocytic pathway and play a role in endosome/lysosome maturation.

Rab39B, a paralogue of Rab39A, was also reported to bind C9orf72 and SMCR8. This report also showed GEF activity of C9orf72 and SMCR8 acting on Rab39B and Rab8A[19]. Oddly, we did not see binding to either of these proteins, even in the same conditions described by the earlier report.

We also observed binding to Rab35, which is involved in the endocytic pathway. Interestingly, constitutively active Rab35 can active AKT signaling, upstream of mTOR and autophagy[21, 22]. More detailed experiments will be needed to address which, if any, of these interactions are physiologically important.

3.5 MATERIALS AND METHODS

SILAC and mass spectrometry analysis- N2a or HEK293T cells were grown a minimum of five generations in DMEM with 10% dialyzed FBS (Sigma) supplemented with either light (C12, N14 arginine and lysine) or heavy (C13, N15 arginine and lysine) amino acids. The heavy cells were transfected in two 15 cm dishes with GFP-C9orf72, GFP-C9orf72 with SMCR8-GFP, or WDR41-GFP expression constructs while the light cells were transfected with pEGFP-C1 as a control. Two days after transfection, cells were lysed in 50mM Tris pH8.0, 150mM NaCl, 1% Triton, 0.1% deoxycholic acid with protease inhibitors (Roche). The lysates were subject to anti-GFP immunoprecipitation

using GFP-Trap beads (ChromoTek). The presence of GFP and GFP-C9orf72, SMCR8-GFP, and WDR41-GFP in immunoprecipitated samples was confirmed by SDS-PAGE and Krypton staining (Invitrogen). Samples were then combined and boiled 5 minutes with 1% DTT followed by alkylation by treating samples with a final concentration of 28 mM iodoacetamide. Proteins were precipitated on ice for 30 minutes with a mixture of 50% acetone/49.9% ethanol/0.1% acetic acid. Proteins were pelleted and washed with this buffer, re-precipitated on ice, and dissolved in 8M urea/50 mM Tris pH 8.0 followed by dilution with three volumes of 50 mM Tris pH 8.0/150 mM NaCl. Proteins were digested overnight at 37º C with 1 μg mass-spec grade Trypsin (Promega). The resulting peptide samples were cleaned up for mass spectrometry by treatment with 10% formic acid and 10% trifluoroacetic acid (TFA) and washed twice with 0.1% acetic acid on pre-equilibrated Sep-Pak C18 cartridges (Waters). Samples were eluted with 80% acetonitrile (ACN)/0.1% acetic acid into silanized vials (National Scientific) and evaporated using a SpeedVac. Samples were re-dissolved in H2O with ~1% formic acid and 70% ACN. Peptides were separated using hydrophilic interaction liquid chromatography (HILIC) on an Ultimate 300 LC (Dionex). Each fraction was evaporated with a SpeedVac and resuspended in 0.1% TFA with 0.1 pM angiotensin internal standard. Samples were run on a Thermo LTQ Orbitrap XL mass spectrometer and data analyzed using the SORCERER system (Sage-N research).

DNA and Plasmids **-** Human C9orf72 , WDR41 and SMCR8 cDNAs were from the human ORFome 8.1 library and cloned into pQCXIN, pEGFP-N1 or pEGFP-N2, respectively, with an N-terminal (C9orf72) or C-terminal (WDR41 and SMCR8) GFP tag. WDR41 and SMCR8 were also cloned into pcDNA3.1 myc his A (Invitrogen) to generate C-terminal myc his tagged constructs. Additionally, C9orf72 and WDR41 were cloned into p3xFLAG-CMV7.1 (Sigma) to generate N-terminal FLAG tagged constructs. MMS19 was obtained from the DNAUS Plasmid Repository and cloned into

pcDNA3.1 V5 (Invitrogen) or p3xFLAG-CMV7.1 (Sigma). MMS19 truncations were based on the following amino acids positions: ΔHEAT (1-855) and HRD (856-1030) and were cloned into p3xFLAG-CMV7.1. NARFL, ANT2, CIAO1, and FAM96B were obtained from the human ORFome 8.1 library and cloned into pcDNA3.1 myc his A (Invitrogen) to generate C-terminally tagged constructs. Rab4, Rab5, Rab7, Rab9, and Rab11 in pEGFP vectors were received from Dr. William Brown (Cornell University). Rab8, Rab27A, Rab35, Rab5 Q67L, and Rab7 S22N in pEGFP vectors were received from Dr. Anthony Bretscher (Cornell University). Rab14, Rab23, Rab32, Rab39A, and Rab39B were obtained from the human ORFome 8.1 library and cloned into pEGFP. Rab39A S22N, Rab39A Q72L, Rab39B S22N, and Rab39B Q68L were created by site-directed mutagenesis and confirmed by sequencing. Arl1 was obtained from the human ORFome 8.1 library and cloned into p3xFLAG-CMV7.1.

Pharmacological Reagents and Antibodies **-** The following primary antibodies were used in this study: anti-FLAG (M2) and anti-myc (9E10) from Sigma-Aldrich, anti-GAPDH from Abcam (ab8245), anti-V5 from Invitrogen, anti-TCP-1α (91A) from Santa Cruz Biotechnology, anti-Tubulin from Proteintech Group, RagA (D8B5) and RagC (D31G9) from Cell Signaling Technology, and anti-GFP antibody was a gift from Dr. Anthony Bretscher (Cornell University). The following secondary antibodies were used: donkey anti-mouse 800 and donkey anti-rabbit 800 from LI-COR, AlexaFluor donkey anti-goat 680, donkey anti-rabbit 680, donkey anti-mouse 680, and donkey anti-rat 680 from Invitrogen, and donkey anti-mouse 568 from Biotium. Hoechst stain was obtained from Invitrogen.

Immunoprecipitation and protein analysis- Cells were lysed in 50 mM Tris pH 8.0, 150 mM NaCl, 1% Triton X-100, and 0.1% deoxycholic acid with protease inhibitors (Roche) or in 0.3% CHAPS, 10mM β-glycerol phosphate, 10mM pyrophosphate, 40mM Hepes pH7.4, 2.5mM $MegCl_2$, and EDTA-free protease inhibitor

(Roche). Lysates were incubated with GFP-Trap beads (ChromoTek) or anti-FLAG antibody conjugated beads (Sigma-Aldrich) for 2-3 hours at 4°C. Beads were washed 3 times with 50 mM Tris pH 8.0, 150 mM NaCl, and 1% Triton X-100 or in 0.3% CHAPS, 10mM β-glycerol phosphate, 10mM pyrophosphate, 40mM Hepes pH7.4, 2.5mM $MegCl_2$, 150mM NaCl . Samples were denatured in 2xSDS sample buffer (4% SDS, 20% glycerol, 100 mM Tris pH 6.8, 0.2 g/L bromophenol blue) by boiling for 3 minutes. Samples were run on 12% polyacrylamide gels and transferred to PVDF membranes (Millipore). Membranes were blocked in either Odyssey Blocking Buffer (LI-COR Biosciences) or 5% non-fat milk in PBS for 1 hour followed by incubation with primary antibodies overnight at 4°C. Membranes were washed 3 times with Tris-buffered saline with 0.1% Tween-20 (TBST) then incubated with secondary antibody for 2 hours at room temperature. Membranes were washed 3 times with TBST and imaged using an Odyssey Infrared Imaging System (LI-COR Biosciences).

Cell Culture and DNA Transfection - HEK293T, N2a, and MEF cells were maintained in Dulbecco's Modified Eagle's Medium (Cellgro) supplemented with 10% fetal bovine serum (Gibco) and 1% Penicillin–Streptomycin (Invitrogen) in a humidified incubator at 37ºC and 5% CO_2. Cells were transiently transfected with polyethyleneimine. MEF cells were collected from P0 mouse pups by removing the head and limbs, then dissecting the skin from each pup. The resulting tissue was minced using a razor blade, then suspended in 3 ml trypsin for 30 minutes with pipetting every 10 minutes to mechanically break up the tissues. Trypsin was then quenched with 7 mL of growth media. The total 10 mL volume was then plated in 10cm plates and allowed to grow to 90% confluence before splitting for use. Bone marrow derived macrophages were collected by harvesting mice 2 months of age or older, dissecting femurs, and flushing each femur with DMEM to collect the bone marrow. Cells were triturated by pipetting then passed through a 70 μm filter. Cells were plated in growth media

containing 20% L929 cell conditioned media and used for experiments after 7 days of differentiation.

Immunofluorescence microscopy- MEF cells grown on glass coverslips were fixed in 3.7% paraformaldehyde for 10 minutes, washed 3 times with PBS, and permeabilized and blocked in Odyssey Blocking Buffer with 0.05% saponin. Primary antibodies diluted in blocking buffer with 0.05% saponin were applied to the cells overnight at 4°C. Coverslips were washed 3 times with PBS. Secondary antibodies diluted in blocking buffer with 0.05% saponin were applied to the cells for 2 hours at room temperature. Coverslips were washed and mounted onto slides with Fluoromount G (Southern Biotech). Images were acquired on a CSU-X spinning disc confocal microscope (Intelligent Imaging Innovations) with an HQ2 CCD camera (Photometrics) using a 63x objective.

REFERENCES

1. DeJesus-Hernandez, M., et al., *Expanded GGGGCC hexanucleotide repeat in noncoding region of C9ORF72 causes chromosome 9p-linked FTD and ALS.* Neuron, 2011. **72**(2): p. 245-56.

2. Renton, A.E., et al., *A hexanucleotide repeat expansion in C9ORF72 is the cause of chromosome 9p21-linked ALS-FTD.* Neuron, 2011. **72**(2): p. 257-68.

3. Gari, K., et al., *MMS19 links cytoplasmic iron-sulfur cluster assembly to DNA metabolism.* Science, 2012. **337**(6091): p. 243-5.

4. Stehling, O., et al., *MMS19 assembles iron-sulfur proteins required for DNA metabolism and genomic integrity.* Science, 2012. **337**(6091): p. 195-9.

5. Hatfield, M.D., et al., *Identification of MMS19 domains with distinct functions in NER and transcription.* DNA Repair (Amst), 2006. **5**(8): p. 914-24.

6. van Wietmarschen, N., et al., *The mammalian proteins MMS19, MIP18, and ANT2 are involved in cytoplasmic iron-sulfur cluster protein assembly.* J Biol Chem, 2012. **287**(52): p. 43351-8.

7. Lopez, T., K. Dalton, and J. Frydman, *The Mechanism and Function of Group II Chaperonins.* J Mol Biol, 2015. **427**(18): p. 2919-30.

8. Miyata, Y., et al., *The molecular chaperone TRiC/CCT binds to the Trp-Asp 40 (WD40) repeat protein WDR68 and promotes its folding, protein kinase DYRK1A binding, and nuclear accumulation.* J Biol Chem, 2014. **289**(48): p. 33320-32.

9. Pavel, M., et al., *CCT complex restricts neuropathogenic protein aggregation via autophagy.* Nat Commun, 2016. **7**: p. 13821.

10. Sergeeva, O.A., et al., *Biochemical characterization of mutants in chaperonin proteins CCT4 and CCT5 associated with hereditary sensory neuropathy.* J Biol Chem, 2014. **289**(40): p. 27470-80.

11. Wang, Y., et al., *WDSPdb: a database for WD40-repeat proteins.* Nucleic Acids Res, 2015. **43**(Database issue): p. D339-44.

12. Wang, Y., et al., *A method for WD40 repeat detection and secondary structure prediction.* PLoS One, 2013. **8**(6): p. e65705.

13. Mackeh, R., et al., *Autophagy and microtubules - new story, old players.* J Cell Sci, 2013. **126**(Pt 5): p. 1071-80.

14. Zhang, D., et al., *Discovery of Novel DENN Proteins: Implications for the Evolution of Eukaryotic Intracellular Membrane Structures and Human Disease.* Front Genet, 2012. **3**: p. 283.

15. Levine, T.P., et al., *The product of C9orf72, a gene strongly implicated in neurodegeneration, is structurally related to DENN Rab-GEFs.* Bioinformatics, 2013. **29**(4): p. 499-503.

16. Tsun, Z.Y., et al., *The folliculin tumor suppressor is a GAP for the RagC/D GTPases that signal amino acid levels to mTORC1.* Mol Cell, 2013. **52**(4): p. 495-505.

17. Farg, M.A., et al., *C9ORF72, implicated in amytrophic lateral sclerosis and frontotemporal dementia, regulates endosomal trafficking.* Hum Mol Genet, 2014. **23**(13): p. 3579-95.

18. Webster, C.P., et al., *The C9orf72 protein interacts with Rab1a and the ULK1 complex to regulate initiation of autophagy.* EMBO J, 2016. **35**(15): p. 1656-76.

19. Sellier, C., et al., *Loss of C9ORF72 impairs autophagy and synergizes with polyQ Ataxin-2 to induce motor neuron dysfunction and cell death.* EMBO J, 2016. **35**(12): p. 1276-97.

20. Tam, S., et al., *The chaperonin TRiC controls polyglutamine aggregation and toxicity through subunit-specific interactions.* Nat Cell Biol, 2006. **8**(10): p. 1155-62.

21. Klinkert, K. and A. Echard, *Rab35 GTPase: A Central Regulator of Phosphoinositides and F-actin in Endocytic Recycling and Beyond.* Traffic, 2016. **17**(10): p. 1063-77.

22. Wheeler, D.B., et al., *Identification of an oncogenic RAB protein.* Science, 2015. **350**(6257): p. 211-7.

CHAPTER 4

LOSS OF C9ORF72 BINDING PARTNER SMCR8 DISRUPTS MTOR SIGNALING BY INCREASING AKT ACTIVITY

4.1 Abstract

Intronic hexanucleatide repeat expansions in the gene C9orf72 are associated with ALS/FTLD. To better understand whether C9orf72 haploinsufficiency was involved in disease onset, we set out to elucidate the cellular function of C9orf72. We previously found that C9orf72 binds to SMCR8 and WDR41 and may be involved in regulating autophagy. Furthermore, loss of C9orf72 in mice disrupts the immune system, causing autoimmune-like symptoms. Here, we report that loss of SMCR8, but not WDR41, causes a similar phenotype to C9orf72 knockout and that loss of SMCR8 causes a decrease in lysosomal protein levels due to increased activity of mTOR and AKT. Our results provide additional insight into how the C9orf72-SMCR8-WDR41 complex may function.

4.2 Introduction

C9orf72, a protein associated with ALS/FTLD, forms a complex with two additional proteins: WDR41 and SMCR8[1-6]. While C9orf72 has gained attention over the past few years, the uncharacterized SMCR8 and WDR41 have received less attention and their functions, like C9orf72, remains elusive.

Recent publications confirmed that C9orf72 binds SMCR8, and that these proteins bind to Ulk1[1, 2, 4, 5, 7]. SMCR8 has also been reported to alter both autophagy and mTOR activity, though reports disagree with exactly how this disruption

occurs. [3, 6, 7]. These models propose that C9orf72 and SMCR8 are effectors of Rab1A to help recruit the Ulk1 complex to sites of autophagy initiation while another model suggests that SMCR8 and C9orf72 function at the lysosome and alter mTOR activity due to disruption of normal lysosome activity [3, 7]. Another model suggests that C9orf72 and SMCR8 are GEFs for Rab8A and Rab39B and promote autophagy through the direct activation of these Rabs [1].

To study the C9orf72-SMCR8-WDR41 complex in more mechanistic detail and resolve the discrepancies between recent studies, we generated SMCR8 and WDR41 knockout mice in addition to our C9orf72 knockout mice and characterized the cellular phenotypes of primary knockout cells. We found, like the C9orf72-/- mice, SMCR8-/- causes abnormal immune response. Moreover, loss of SMCR8 increased mTOR and AKT phosphorylation, suggesting that growth factor sensing may be disrupted. Our data suggests that the C9orf72-SMCR8-WDR41 complex may act upstream of AKT to regulate mTOR signaling and that C9orf72 and SMCR8 act together to regulate immune response, whereas WDR41 is dispensable for this function.

4.3 Results

To study the function of the C9orf72-SMCR8-WDR41 complex, we created SMCR8 and WDR41 knockout mice using CRIPR-Cas9. From the founder mice, we choose a mouse line with a 128 base pair (bp) deletion just after the start codon of SMCR8, resulting in a frame shift and early stop codon after 22 amino acids (Figure 4-1A). For the WDR41 mice, we choose a line that contained a 122bp deletion that encompassed the start codon (Figure 4-1B). Since C9orf72-/- mice show splenomegaly by 4 months of age, we checked whether WDR41-/- or SMCR8-/- mice exhibited a

similar phenotype. SMCR8 mice had significantly enlarged spleens by 4 months of age (Figure 4-2A) while the WDR41-/- mice had no spleen enlargement at this age or up to 12 months old (Figure 4-2B and data not shown). When WDR41-/- and C9orf72-/- were crossed to produce double knockout (DKO) mice, there was a slight reduction in spleen/body size compared to C9orf72-/- alone in 9 month old mice, suggesting that loss of WDR41 may rescue some phenotypes of the C9orf72-/- mice (Figure4-2B).

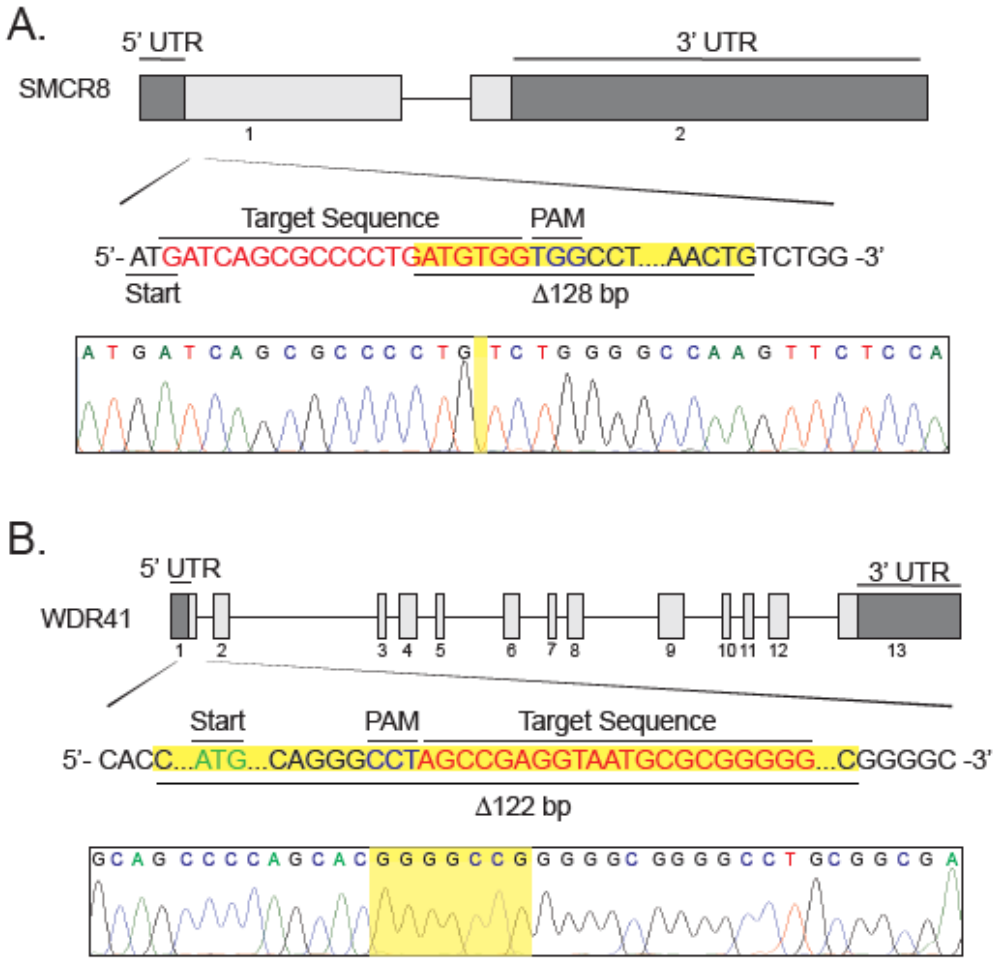

Figure 4-1: CRISPR-Cas9 genome editing produces SMCR8 and WDR41 knockout mice. a. SMCR8 gene schematic and sequence showing start codon (underlined), the gRNA target sequence (red), and deleted region (highlighted in yellow). The DNA sequencing trace is shown below and indicates the location of the deletion (highlighted in yellow). **b**. WDR41 gene schematic, sequence, and trace labeled as in **a**.

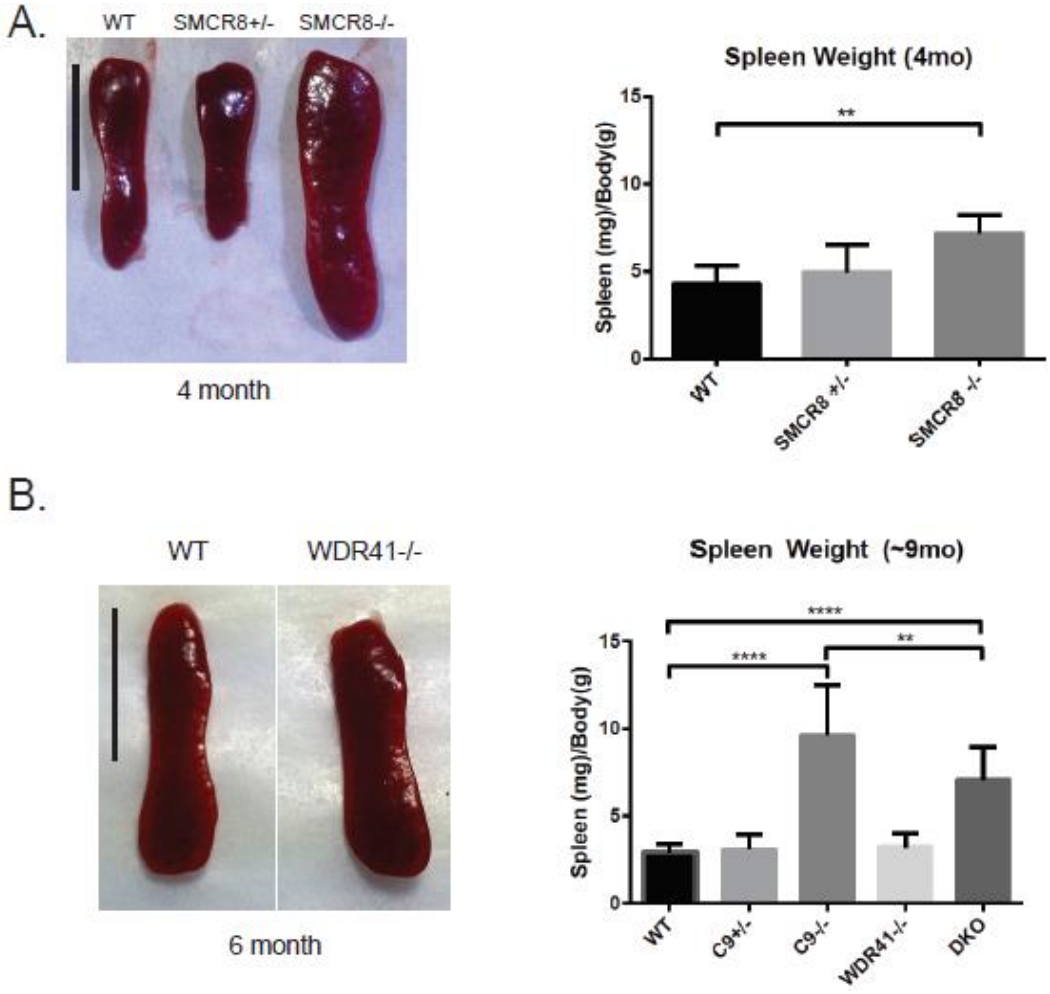

Figure 4-2: Loss of SMCR8, but not WDR41, mimics C9orf72 deletion. A. Representative spleens taken from WT, SMCR8 Heterozygous deletion (+/-) and SMCR8 knockout (-/-) mice. Quantification of spleen weight at 4 months of age (n=3). B. Representative spleens from WT of WDR41-/- at 6 months of age and quantification of spleen weight of WT, C9orf72+/-, C9orf72-/-, WDR41-/- and DKO (n=12-14). ** $p<0.01$; *** $p<0.001$; **** $p<0.0001$. Scale bar = 1cm.

Since these three proteins form a complex and help to stabilize one another, we checked the protein levels of C9orf72 in WDR41 and SMCR8 knockout tissues and MEFs. Loss of either WDR41 (Figure 4-3A) or SMCR8 (Figure 4-3B) led to a decrease in C9orf72 levels. Furthermore, loss of C9orf72, but not WDR41, decreased the protein levels of SMCR8 in MEFs (Figure 4-3C). Finally, looking at mouse tissues, loss of SMCR8 led to decreased C9orf72 protein levels in all analyzed tissues (Figure 4-3D). WDR41 protein levels were not included due to the absence of quality WDR41 antibodies available. These results confirm that each component of the C9orf72 complex is important for its stability.

Our previous work, as well as the work of other groups, have suggested that the C9orf72 complex plays a role in autophagy or mTOR signaling. To test the hypothesis that mTOR activity may be changed, I check the ratio of phosphorylated mTOR at Serine 2448 to total mTOR and found that SMCR8-/- MEF had a greater ratio of p-mTOR than WT (Figure4-4A). If mTOR is more active in SMCR8-/- cells, mTOR should have increased localization at lysosomes. SMCR8-/- MEFs stained for mTOR and a lysosome marker, LAMP1, show increased mTOR signal at the lysosome (Figure 4-4B). Since mTOR is phosphorylated at this site downstream of Pi3K/AKT signaling, we also looked at the phosphorylation of AKT at Ser473 and Thr308. Ser473 of AKT is phosphorylated by PDK1 while Thr308 is phosphorylated by mTORC2. Both of these signaling events are induced by the presence of growth factors. We found that the ratio of p-Ser473 AKT to total AKT is increased, whereas p-Thr308 AKT has less change from WT cells (Figure 4-4A).

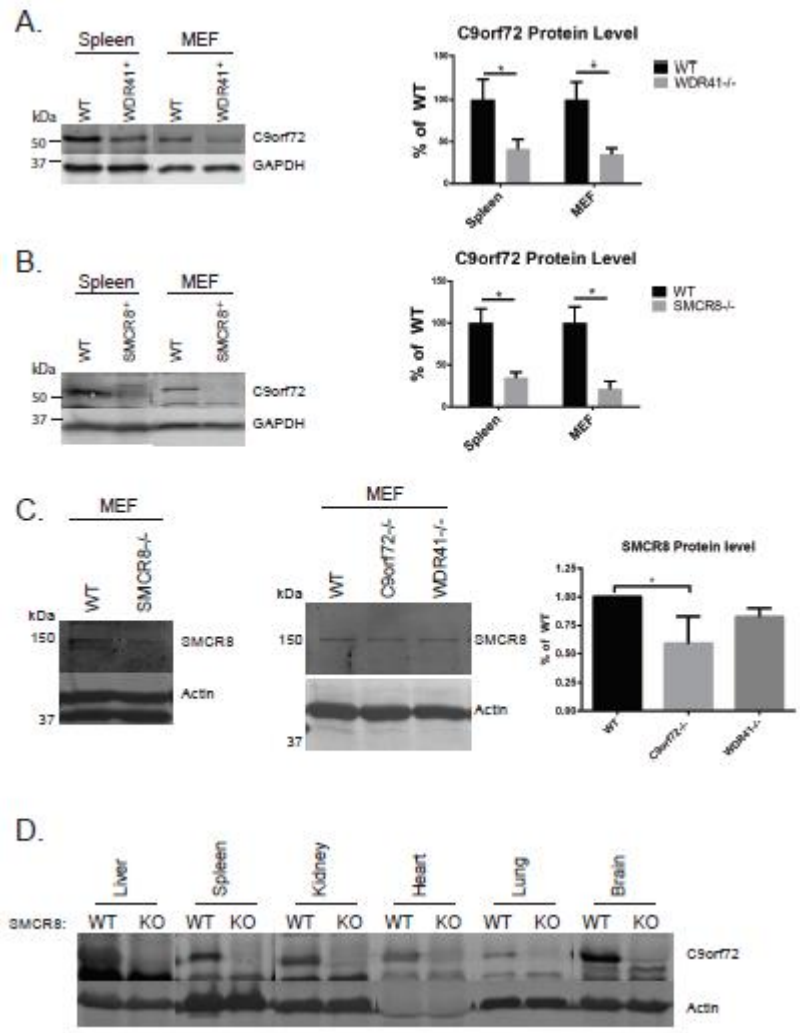

Figure 4-3: Loss of C9orf72 complex components destabilizes the entire complex. **a**. WDR41-/- spleen tissue and MEF cell lysate blotted for C9orf72 and GAPDH. Quantification of C9orf72 levels normalized to GAPDH on right (n=3). **b**. SMCR8-/- spleen tissue and MEF cell lysate blotted for C9orf72 and GAPDH. Quantification of C9orf72 levels normalized to GAPDH on right (n=3). **c**. Verification of SMCR8 antibody and C9orf72-/- and WDR41-/- MEF cell lysate blotted for SMCR8 and actin. Quantification of SMCR8 levels normalized to actin on right (n=3). **d**. Tissue lysates from WT and SMCR8-/- mice blotted for C9orf72 and actin.

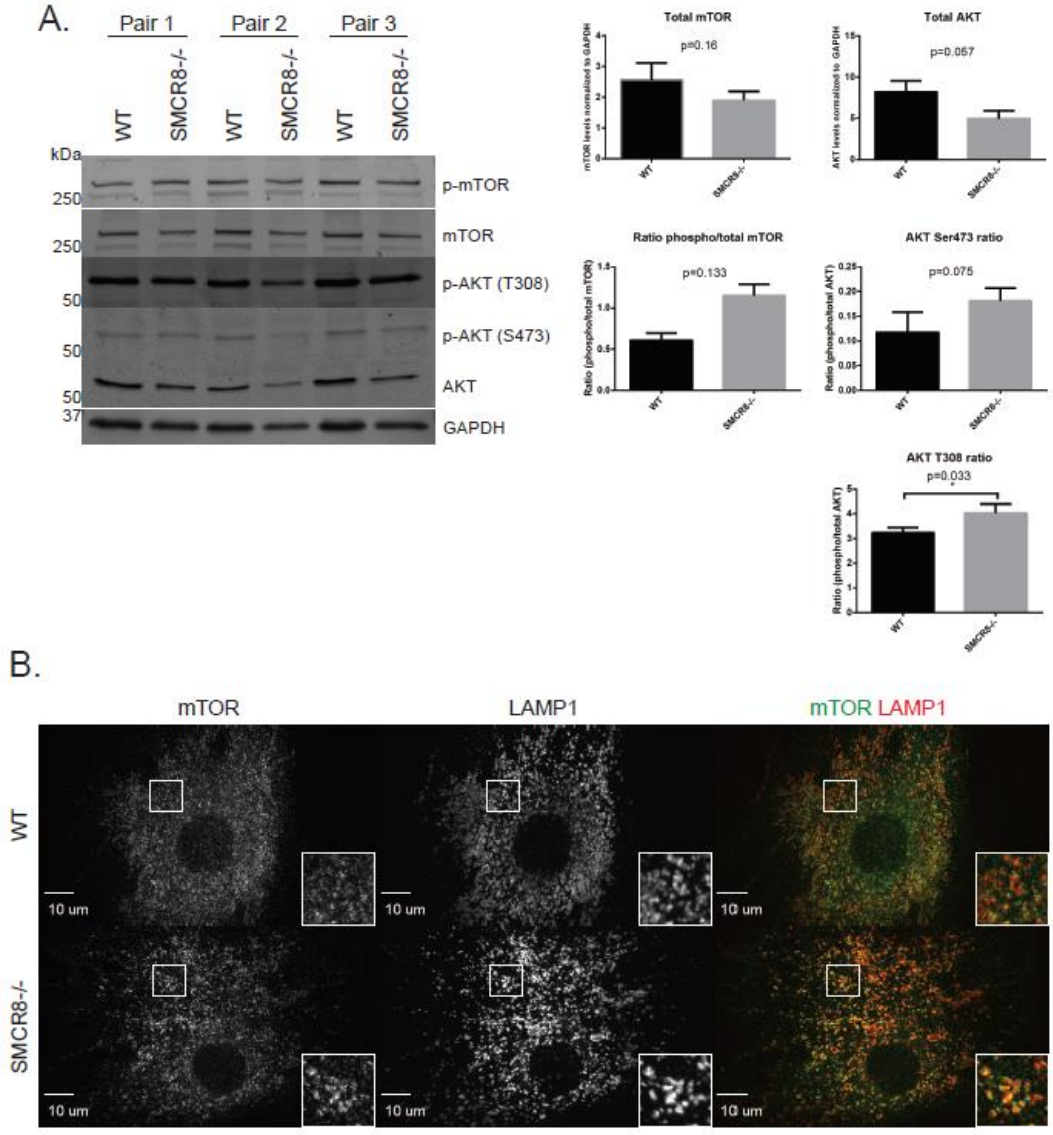

Figure 4-4: Loss of SMCR8 increases AKT and mTOR activity. a. Western blot of WT and SMCR8-/- MEF lysates blotted for phosphor-Ser2448 mTOR (p-mTOR), total mTOR, p-AKT (T308), p-AKT (S473), and total AKT. Quantification on the right (n=3). **b**. WT and SMCR8-/- MEF stained for mTOR and LAMP1.

4.4 Discussion

Despite many recent publications relating to the function of C9orf72 and SMCR8, the physiological role of this complex remains unclear. Many reports suggest that autophagy and mTOR are disrupted by loss of C9orf72 or SMCR8, however they disagree on the precise contribution of C9orf72 and SMCR8 to these pathways. Our data has suggested that C9orf72 and SMCR8 may function upstream of mTOR and AKT, thus affecting downstream signaling events that initiate autophagy and control TFEB localization. However, as our group and others have reported direct interaction with the Ulk1 complex, these data may indicate that C9orf72, SMCR8, and WDR41 play multiple roles in the cell, both directly affecting autophagy through the interaction with Ulk1 and upstream by affecting growth factor signaling through the PI3K/AKT pathway. Interestingly, we see binding of C9orf72 and SMCR8 to Rab35, which has been reported to modulate the activity of AKT through its direct interaction with PI3K [8, 9]. More experiments will be needed to address the hypothesis that C9orf72 and SMCR8 act on Rab35 to modulate the activity of AKT. Additionally, it remains unclear why loss of C9orf72 and SMCR8 produce a similar phenotype in mice while WDR41 does not. This may be due to the relative decreases in C9orf72 and SMCR8 in WDR41 knockout tissues. While C9orf72 is greatly reduced, SMCR8 is not. This would suggest that the level of SMCR8 may be more important than C9orf72. Many of these hypothesis will need to be further addressed through cellular and molecular approached to fully appreciate the function of the C9orf72-SMCR8-WDR41 complex.

4.5 Materials and methods

Mouse strains – SMCR8 and WDR41 knockout mice were produced using CRISPR/Cas9 genome editing with a guide RNA (gRNA) targeting exon 1 of mouse

gene SMCR8 or WDR41. C57BL/6J x FvB/N mouse embryos were injected with gRNA and Cas9 mRNA at the Cornell Transgenic Core Facility. Editing was confirmed by sequencing PCR products from genomic DNA. Offspring from the founder containing 128bp deletion in SMCR8 or 122bp deletion in WDR41 were used for the study. The following primers were used to genotype SMCR8 knockout mice: 5'- GCTGGTGACCTAGCTTCAGG -3' (forward) and 5'- ACCGACATAATCCGCAAAGA -3' (reverse). The following primers were used to genotype WDR41 knockout mice: 5'- CGAGACTTCTGTTTTCCCGCT -3' (forward) and 5'- TGTTGTGTGGCACATGAAGT -3' (reverse).

Antibodies - The following primary antibodies were used in this study: anti-GAPDH from Abcam (ab8245), mTOR (7C10) and p-mTOR (D9C2) from Cell Signaling Technology, anti-Actin from Lifetein, anti-SMCR8 from Bethyl, anti-AKT, anti-phosphoSer473 AKT, and anti-phsophoT308 AKT from Santa Crus Biotechnology, LAMP1 from BD Biosciences, and anti-C9orf72 long was a gift from Dr. Janice Robertson (University of Toronto). The following secondary antibodies were used: donkey anti-mouse 800 and donkey anti-rabbit 800 from LI-COR, AlexaFluor donkey anti-rabbit 680, donkey anti-mouse 680, and donkey anti-rabbit 488 from Invitrogen, donkey anti-rat568 from Jackson ImmunoResearch.

Protein analysis- To quantify protein levels in tissue samples, tissues were homogenized in RIPA buffer (50 mM Tris pH 8.0, 150 mM NaCl, 1% Triton X-100, 0.1% SDS and 0.1% deoxycholic acid) with protease and phosphatase inhibitors on ice and then equal volume of 2X SDS sample buffer was added before sonication. 50µg of each protein sample was loaded onto a 12% poly-acrylamide gel. Blots were analyzed

by LiCor Odyssey system and normalized to GAPDH or actin.

Cell Culture and DNA Transfection - MEF cells were maintained in Dulbecco's Modified Eagle's Medium (Cellgro) supplemented with 10% fetal bovine serum (Gibco) and 1% Penicillin–Streptomycin (Invitrogen) in a humidified incubator at 37ºC and 5% CO_2. Cells were transiently transfected with polyethyleneimine. MEF cells were collected from P0 mouse pups by removing the head and limbs, then dissecting the skin from each pup. The resulting tissue was minced using a razor blade, then suspended in 3 ml trypsin for 30 minutes with pipetting every 10 minutes to mechanically break up the tissues. Trypsin was then quenched with 7 mL of growth media. The total 10 mL volume was then plated in 10cm plates and allowed to grow to 90% confluence before splitting for use.

Immunofluorescence microscopy- MEF cells grown on glass coverslips were fixed in 3.7% paraformaldehyde for 10 minutes, washed 3 times with PBS, and permeabilized and blocked in Odyssey Blocking Buffer with 0.05% saponin. Primary antibodies diluted in blocking buffer with 0.05% saponin were applied to the cells overnight at 4°C. Coverslips were washed 3 times with PBS. Secondary antibodies diluted in blocking buffer with 0.05% saponin were applied to the cells for 2 hours at room temperature. Coverslips were washed and mounted onto slides with Fluoromount G (Southern Biotech). Images were acquired on a CSU-X spinning disc confocal microscope (Intelligent Imaging Innovations) with an HQ2 CCD camera (Photometrics) using a 100x objective.

Statistical analysis -The data were presented as mean ± SEM. Two-group analysis was performed using the Student's t test. P-values <0.05 were considered

statistically significant. Graphpad Prism was used for statistical analysis.

REFERENCES

1. Sellier, C., et al., *Loss of C9ORF72 impairs autophagy and synergizes with polyQ Ataxin-2 to induce motor neuron dysfunction and cell death.* EMBO J, 2016. **35**(12): p. 1276-97.

2. Sullivan, P.M., et al., *The ALS/FTLD associated protein C9orf72 associates with SMCR8 and WDR41 to regulate the autophagy-lysosome pathway.* Acta Neuropathol Commun, 2016. **4**(1): p. 51.

3. Amick, J., A. Roczniak-Ferguson, and S.M. Ferguson, *C9orf72 binds SMCR8, localizes to lysosomes, and regulates mTORC1 signaling.* Mol Biol Cell, 2016. **27**(20): p. 3040-3051.

4. Yang, M., et al., *A C9ORF72/SMCR8-containing complex regulates ULK1 and plays a dual role in autophagy.* Sci Adv, 2016. **2**(9): p. e1601167.

5. Jung, J., et al., *Multiplex image-based autophagy RNAi screening identifies SMCR8 as ULK1 kinase activity and gene expression regulator.* Elife, 2017. **6**.

6. Ugolino, J., et al., *Loss of C9orf72 Enhances Autophagic Activity via Deregulated mTOR and TFEB Signaling.* PLoS Genet, 2016. **12**(11): p. e1006443.

7. Webster, C.P., et al., *The C9orf72 protein interacts with Rab1a and the ULK1 complex to regulate initiation of autophagy.* EMBO J, 2016. **35**(15): p. 1656-76.

8. Klinkert, K. and A. Echard, *Rab35 GTPase: A Central Regulator of Phosphoinositides and F-actin in Endocytic Recycling and Beyond.* Traffic, 2016. **17**(10): p. 1063-77.

9. Wheeler, D.B., et al., *Identification of an oncogenic RAB protein.* Science, 2015. **350**(6257): p. 211-7.

CHAPTER 5

CONCLUDING REMARKS AND FUTURE RESEARCH DIRECTIONS

In early 2012, C9orf72 was reported to be associated with Amyotrophic Lateral Sclerosis (ALS) and FrontoTemporal Labor Degeneration (FTLD) [1-3]. Since these initial reports, many groups have studied the mechanisms that lead from an intronic hexanucleotide repeat expansion to ALS/FTLD. Observing the molecular pathology, groups found that long, repetitive RNA are transcribed in both the sense and anti-sense direction which can sequester RNA-binding proteins and disrupt nucleocytoplasmic translocation[2, 4-8]. Additionally, these repetitive transcripts are translated by Repeat-Associated Non-atg (RAN) translation into multiple dipeptide repeats[9-11]. These dipeptide repeats form persistent aggregates and are also thought to disrupt nucleocytoplasmic transport. Early reports also suggested that translation of the normal protein C9orf72 is suppressed by hypermethylation of the repeat expansion leading to haploinsufficiency of this uncharacterized protein[2, 12-14]. With these three potential mechanisms of disease in mind, we set out to understand the function the protein product of C9orf72 and uncover its contribution to ALS/FTLD.

Over the past five years, multiple groups have found that introducing RNA repeats or dipeptide repeats into cellular, fly, and mouse models is sufficient to cause neurodegeneration[15-19]. However, loss of C9orf72 in mouse models produces only mild impairment of motor and cognitive function[20-24]. These models have led groups to believe that the toxic gain of function from the RNA repeats and dipeptide repeats

are responsible for the onset of disease, though loss of C9orf72 protein may contribute to pathology in conjunction with gain of toxicity.

Yet, the function of C9orf72 remains unclear. Several groups have proposed functions for C9orf72, but few of these reports fully agree with one another. During my studies in Dr. Hu's lab, we have found that C9orf72 binds to two previously uncharacterized proteins, SMCR8 and WDR41. Together, these proteins are able to further interact with the autophagy initiation complex composed of ULK1, FIP200, ATG13, and ATG101. We also reported that loss of C9orf72 in mice leads to splenomegaly and mis-regulation of the immune system, but had no obvious effect on the brain or microglia[24]. How C9orf72 depletion leads to this immune phenotype is still unclear, though several groups have independently reported the phenomenon[22-24]. To further characterize this immune phenotype, I had begun a collaborative project with Dr. Cynthia Leifer's lab to test whether Toll-Like Receptor signaling was impaired in C9orf72 knockout. Our preliminary results suggested that there may be a defect, but follow up experiments were inconsistent.

Additionally, we reported that WDR41 localization is enriched at the Golgi. This is an interesting observation, as we do not see clear evidence that C9orf72 and SMCR8 also are enriched at the Golgi, despite their strong interaction with WDR41. One possibility is that the overexpressed protein does not localize properly, with either C9orf72 and SMCR8's cytoplasmic localization or WDR41's Golgi localization an artifact of overexpression. However, WDR41 overexpression is sufficient to cause vesicle formation and bind to these unidentified vesicles, as I show in appendix II. For future studies, either quality antibodies or endogenous tagging of these proteins using

CRISPR-mediated editing will be useful in determining reliable localization of C9orf72, SMCR8, and WDR41 at physiological conditions. To better understand the WDR41-induced vesicles, overexpressing WDR41 in either C9orf72-/- or SMCR8-/- cells will help discern whether WDR41 acts with the C9orf72 complex or independently to cause this phenomenon. Characterizing this event may suggest potential Rab GTPases as binding partners, as many Rabs are involved in vesicle formation.

In trying to determine the function of C9orf72, we conducted several SILAC experiments to identify binding partners that might place C9orf72 in a specific cellular pathway. I tested several candidates including MMS19, the TRiC complex, tubulin, and many small GTPases. MMS19 contains many HEAT domains, which are usually involved in mediating multiple protein-protein interactions. Since these domains coordinate the multiple interactions, they may be binding nonspecifically to C9orf72 and SMCR8 in the overexpressed conditions. To show that this is a physiological interaction, the binding should be shown at the endogenous level. Furthermore, if C9orf72 is regulating MMS19, rather than being a substrate, loss of C9orf72 should disrupt iron-sulfur (FeS) cluster assembly. Most notably, many DNA repair proteins use FeS clusters to carry out enzymatic functions[25, 26]. If they do not receive an FeS cells will become more susceptible to DNA damage, which may be a good indication of disrupted FeS assembly in C9orf72 or SMCR8 knockout.

I did not observe any binding with another top candidate, the TRiC complex. If there is binding that was too weak to detect by Co-IP, it may be for the proper folding of WDR41, as the TRiC complex is known to help for WD repeat proteins[27]. Nonetheless, I do not think that C9orf72 has any functional role with the TRiC complex.

On the other hand, the interaction between C9orf72 and tubulin is interesting. Originally disregarded as a contaminant, I verified the interaction by Co-IP and found that the interaction was dependent on nutrient status. Furthermore, microtubules in C9orf72-/- macrophages seemed to be more stable, showing stronger signal and possibly longer polymers. Confirming the interaction at the endogenous level, as well as following microtubule dynamics in knockout cells will be an important next step. Discovering what regulates this interaction in a nutrient-dependent manner will also provide insight.

The possible interaction with several small GTPases adds to a continued assumption that C9orf72 and SMCR8 actually do contain a DENN domain and act as a guanine exchange factor to activate a small GTPase. With only structural predictions of a DENN domain and no consensus on which GTPase is the target of C9orf72 and SMCR8, the field needs compelling data that includes GEF activity assays and connection to demonstrated phenotypes, such as changes in mTOR signaling and autophagy induction. Along these lines, our results show that Rab35 binds C9orf72 and SMCR8. Rab35 has been reported to affect AKT signaling through direct interaction with PI3K[28] and constitutively active Rab35 increased AKT phosphorylation and activity[29]. As I show in Chapter 4, our data suggests that AKT phosphorylation is increased. If C9orf72 and SMCR8 act as a GTPase Activating Protein (GAP), then loss of SMCR8 would increase the active, GTP-bound Rab35 and mimic the constitutively active results. Although DENN domains usually act as GEFs, the DENN domain-containing protein Folliculin acts as a GAP[30]. Since Folliculin was used to predict the DENN domain in C9orf72 and SMCR8, there is a possibility that these proteins act as GAPs rather than the canonical GEFs. Folliculin was also shown to have GEF activity

towards Rab35 in vitro[31]. These data together support the hypothesis that C9orf72 and SMCR8 act on Rab35. Future studies of this interaction should include binding affinity to the constitutively active (Q67L) and dominant negative (S22N) mutants of Rab35, colocalization of Rab35 with the C9orf72 complex, and GTPase activity assays using purified proteins.

In chapter 4, I provide evidence that loss of SMCR8, but not WDR41, results in a similar immune phenotype as C9orf72-/- mice. Furthermore, loss of any component of the C9orf72 complex decreased the stability of the remaining proteins, reinforcing the hypothesis that these proteins function as a complex. The stability of WDR41 in C9orf72-/- and SMCR8-/- still needs to be assessed when a quality antibody is available. Finally, loss of SMCR8 results in altered mTOR activity, seen by increased phosphorylation and increased localization of mTOR to lysosomes under basal conditions. We found that upstream of mTOR, AKT phosphorylation is also increased, indicating that AKT also has higher activity. How the C9orf72 complex is able to regulate AKT is still unclear, though Rab35 activity is a potential candidate as mentioned earlier (Figure 5-1).

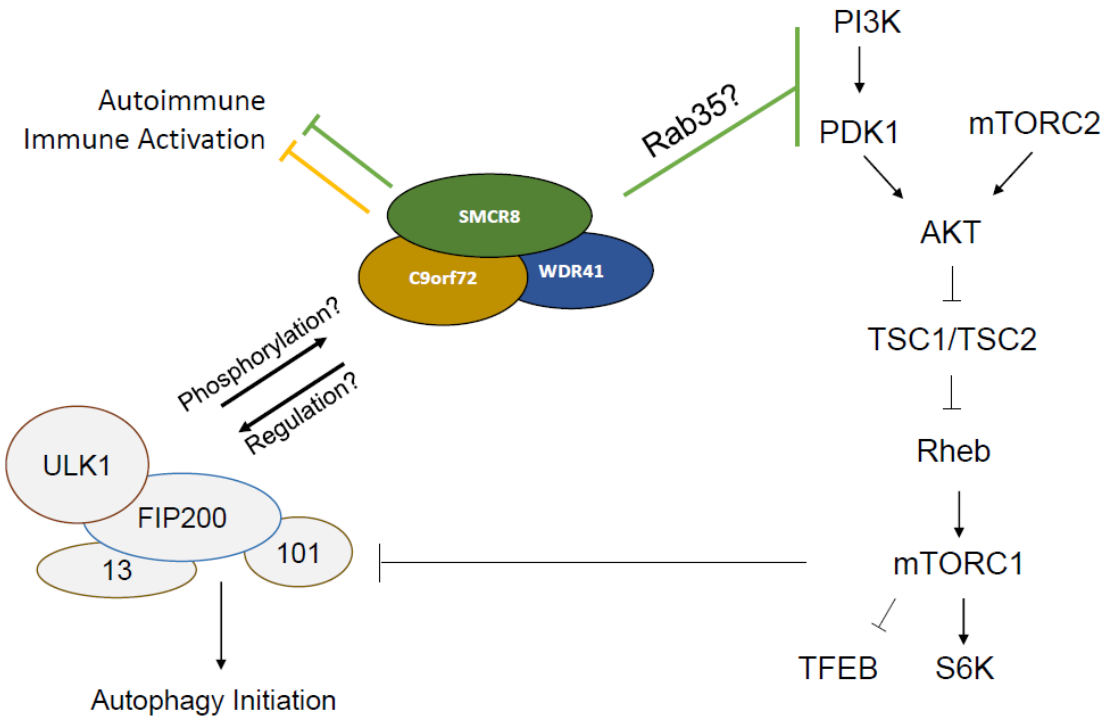

Figure 5-1: Summary of C9orf72/SMCR8/WDR41 functions. The C9orf72 complex directly interacts with the Ulk1 complex as well as several Rab GTPases. Loss of SMCR8 results in mis-regulated autophagy/lysosomal signaling. Loss of either C9orf72 or SMCR8 results in immune activation *in vivo*.

Here, I have presented data that begins to elucidate the function of C9orf72 at a cellular and organismal level. My data has found that C9orf72 binds SMCR8 and WDR41 to form a protein complex. Each component of this complex is important for the stability of the entire complex, as loss of any one of these three protein causes a decrease of other complex components. SMCR8 protein is almost completely lost in the C9orf72-/- cells and tissues, but has little change in the WDR41-/-, whereas C9orf72 levels are decreased by loss of either SMCR8 or WDR41. I have also shown that the C9orf72 complex interacts with the Ulk1-FIP200 complex, as well as the cytoskeletal component tubulin, and several Rab GTPases. Furthermore, I provide evidence that mTOR phosphorylation and localization is mis-regulated and that AKT phosphorylation is also altered in SMCR8-/- cells. Finally, I have created knockout mice for C9orf72, SMCR8, and WDR41 using CRISPR-Cas9 and preliminarily characterized the phenotypes that these mice exhibit. Altogether, my data support a role for the C9orf72-SMCR8-WDR41 complex in regulating the AKT-mTOR signaling pathway and maintaining proper immune regulation.

REFERENCES

1. DeJesus-Hernandez, M., et al., *Expanded GGGGCC hexanucleotide repeat in noncoding region of C9ORF72 causes chromosome 9p-linked FTD and ALS.* Neuron, 2011. **72**(2): p. 245-56.

2. Gijselinck, I., et al., *A C9orf72 promoter repeat expansion in a Flanders-Belgian cohort with disorders of the frontotemporal lobar degeneration-amyotrophic lateral sclerosis spectrum: a gene identification study.* Lancet Neurol, 2012. **11**(1): p. 54-65.

3. Renton, A.E., et al., *A hexanucleotide repeat expansion in C9ORF72 is the cause of chromosome 9p21-linked ALS-FTD.* Neuron, 2011. **72**(2): p. 257-68.

4. Lagier-Tourenne, C., et al., *Targeted degradation of sense and antisense C9orf72 RNA foci as therapy for ALS and frontotemporal degeneration.* Proc Natl Acad Sci U S A, 2013. **110**(47): p. E4530-9.

5. Mizielinska, S., et al., *C9orf72 frontotemporal lobar degeneration is characterised by frequent neuronal sense and antisense RNA foci.* Acta Neuropathol, 2013. **126**(6): p. 845-57.

6. Gendron, T.F., et al., *Antisense transcripts of the expanded C9ORF72 hexanucleotide repeat form nuclear RNA foci and undergo repeat-associated non-ATG translation in c9FTD/ALS.* Acta Neuropathol, 2013. **126**(6): p. 829-44.

7. Freibaum, B.D., et al., *GGGGCC repeat expansion in C9orf72 compromises nucleocytoplasmic transport.* Nature, 2015. **525**(7567): p. 129-33.

8. Gendron, T.F. and L. Petrucelli, *Disease Mechanisms of C9ORF72 Repeat Expansions.* Cold Spring Harb Perspect Med, 2017.

9. Khosravi, B., et al., *Cytoplasmic poly-GA aggregates impair nuclear import of TDP-43 in C9orf72 ALS/FTLD.* Hum Mol Genet, 2017. **26**(4): p. 790-800.

10. Zhang, Y.J., et al., *C9ORF72 poly(GA) aggregates sequester and impair HR23 and nucleocytoplasmic transport proteins.* Nat Neurosci, 2016. **19**(5): p. 668-77.

11. Lee, K.H., et al., *C9orf72 Dipeptide Repeats Impair the Assembly, Dynamics, and Function of Membrane-Less Organelles.* Cell, 2016. **167**(3): p. 774-788 e17.

12. Fratta, P., et al., *Homozygosity for the C9orf72 GGGGCC repeat expansion in frontotemporal dementia.* Acta Neuropathol, 2013. **126**(3): p. 401-9.

13. van Blitterswijk, M., et al., *Novel clinical associations with specific C9ORF72 transcripts in patients with repeat expansions in C9ORF72.* Acta Neuropathol, 2015. **130**(6): p. 863-76.

14. Waite, A.J., et al., *Reduced C9orf72 protein levels in frontal cortex of amyotrophic lateral sclerosis and frontotemporal degeneration brain with the C9ORF72 hexanucleotide repeat expansion.* Neurobiol Aging, 2014. **35**(7): p. 1779 e5-1779 e13.

15. O'Rourke, J.G., et al., *C9orf72 BAC Transgenic Mice Display Typical Pathologic Features of ALS/FTD.* Neuron, 2015. **88**(5): p. 892-901.

16. Peters, O.M., et al., *Human C9ORF72 Hexanucleotide Expansion Reproduces RNA Foci and Dipeptide Repeat Proteins but Not Neurodegeneration in BAC Transgenic Mice.* Neuron, 2015. **88**(5): p. 902-9.

17. Tran, H., et al., *Differential Toxicity of Nuclear RNA Foci versus Dipeptide Repeat Proteins in a Drosophila Model of C9ORF72 FTD/ALS.* Neuron, 2015. **87**(6): p. 1207-14.

18. Liu, Y., et al., *C9orf72 BAC Mouse Model with Motor Deficits and Neurodegenerative Features of ALS/FTD.* Neuron, 2016. **90**(3): p. 521-34.

19. Jiang, J., et al., *Gain of Toxicity from ALS/FTD-Linked Repeat Expansions in C9ORF72 Is Alleviated by Antisense Oligonucleotides Targeting GGGGCC-Containing RNAs.* Neuron, 2016. **90**(3): p. 535-50.

20. Sudria-Lopez, E., et al., *Full ablation of C9orf72 in mice causes immune system-related pathology and neoplastic events but no motor neuron defects.* Acta Neuropathol, 2016. **132**(1): p. 145-7.

21. Koppers, M., et al., *C9orf72 ablation in mice does not cause motor neuron degeneration or motor deficits.* Ann Neurol, 2015. **78**(3): p. 426-38.

22. Atanasio, A., et al., *C9orf72 ablation causes immune dysregulation characterized by leukocyte expansion, autoantibody production, and glomerulonephropathy in mice.* Sci Rep, 2016. **6**: p. 23204.

23. O'Rourke, J.G., et al., *C9orf72 is required for proper macrophage and microglial function in mice.* Science, 2016. **351**(6279): p. 1324-9.

24. Sullivan, P.M., et al., *The ALS/FTLD associated protein C9orf72 associates with SMCR8 and WDR41 to regulate the autophagy-lysosome pathway.* Acta Neuropathol Commun, 2016. **4**(1): p. 51.

25. Gari, K., et al., *MMS19 links cytoplasmic iron-sulfur cluster assembly to DNA metabolism.* Science, 2012. **337**(6091): p. 243-5.

26. Hatfield, M.D., et al., *Identification of MMS19 domains with distinct functions in NER and transcription.* DNA Repair (Amst), 2006. **5**(8): p. 914-24.

27. Miyata, Y., et al., *The molecular chaperone TRiC/CCT binds to the Trp-Asp 40 (WD40) repeat protein WDR68 and promotes its folding, protein kinase DYRK1A binding, and nuclear accumulation.* J Biol Chem, 2014. **289**(48): p. 33320-32.

28. Wheeler, D.B., et al., *Identification of an oncogenic RAB protein.* Science, 2015. **350**(6257): p. 211-7.

29. Klinkert, K. and A. Echard, *Rab35 GTPase: A Central Regulator of Phosphoinositides and F-actin in Endocytic Recycling and Beyond.* Traffic, 2016. **17**(10): p. 1063-77.

30. Tsun, Z.Y., et al., *The folliculin tumor suppressor is a GAP for the RagC/D GTPases that signal amino acid levels to mTORC1.* Mol Cell, 2013. **52**(4): p. 495-505.

31. Nookala, R.K., et al., *Crystal structure of folliculin reveals a hidDENN function in genetically inherited renal cancer.* Open Biol, 2012. **2**(8): p. 120071.

APPENDIX I

THE INTERACTION BETWEEN PROGRANULIN AND PROSAPOSIN IS MEDIATED BY GRANULINS AND THE LINKER REGION BETWEEN SAPOSIN B AND C

This work was accepted for publication in the Journal of Neurochemistry on 22 June 2017. The manuscript has not yet been published and is currently cited as: Zhou X*, Sullivan PM*, Sun L, and Hu F. (2017), The interaction between progranulin and prosaposin is mediated by granulins and the linker region between saposin B and C. J. Neurochem.. Accepted Author Manuscript. doi:10.1111/jnc.14110. Author contributions to each figure are listed in the figure legends. *Denotes co-first authors

A1.1 Abstract

The frontotemporal lobar degeneration (FTLD) protein progranulin (PGRN) is essential for proper lysosomal function. PGRN localizes in the lysosomal compartment within the cell. Prosaposin (PSAP), the precursor of lysosomal saposin activators (saposin A, B, C, D), physically interacts with PGRN. Previously we have shown that PGRN and PSAP facilitate each other's lysosomal trafficking. Here we report that the interaction between PSAP and PGRN requires the linker region of saposin B and C (BC linker). PSAP protein with the BC linker mutated fails to interact with PGRN and target PGRN to lysosomes in the biosynthetic and endocytic pathways. On the other hand, PGRN interacts with PSAP through multiple granulin motifs. Granulin D and E bind to PSAP with similar affinity as full length PGRN. In summary, our data shows that the BC linker of PSAP interacts with multiple granulin motifs in PGRN.

A1.2 Introduction

Frontotemporal lobar degeneration (FTLD) is the most prevalent early onset dementia after Alzheimer's disease (AD) and accounts for 20-25% of pre-senile dementias [1]. A large subset of FTLD cases has characteristic ubiquitin-positive inclusions comprised of the protein TDP-43 (FTLD-TDP) [2, 3]. Haploinsufficiency of progranulin (PGRN) due to mutations in the granulin (GRN) gene is one of the major causes of FTLD-TDP [4-6]. PGRN is an evolutionarily conserved glycoprotein of 7.5 granulin repeats with multiple functions in the nervous system, including neuronal survival and regulating microglia mediated inflammation [7-9]. Recent studies, however, have supported a surprising role of PGRN in the lysosome. While PGRN haploinsufficiency causes FTLD, total loss of PGRN in humans results in neuronal ceroid lipofuscinosis (NCL) [10, 11], a lysosomal storage disease [12, 13]. Furthermore, PGRN is transcriptionally co-regulated with a number of essential lysosomal genes by the transcriptional factor TFEB [14]. Finally, within the cell, PGRN localizes to the lysosomal compartment. The VPS10 family trafficking receptor sortilin is highly expressed in neurons and interacts with the C-terminus of PGRN to mediate PGRN lysosomal targeting [15, 16]. More recently, PGRN was also shown to directly bind another lysosomal protein, prosaposin (PSAP), and get a "piggyback" ride to lysosomes through the PSAP receptors M6PR and LRP1 [17]. In fibroblasts which do not express sortilin, PGRN lysosomal trafficking is totally dependent on PSAP [17]. The interaction between PGRN and PSAP was further confirmed by a large family-based genome-wide association study (GWAS) study, in which polymorphisms in PSAP were shown to affect plasma PGRN levels [18].

PSAP is the precursor of lysosomal saposin activators (saposin A, B, C and D) essential for glycosphingolipid degradation, and mutations in the saposin motifs are known to cause several distinct lysosomal storage diseases [19-21]. The physical interaction of PGRN and PSAP not only facilitates PGRN lysosomal trafficking but also PSAP trafficking, as we have recently shown that PGRN bridges the interaction between PSAP and sortilin to facilitate PSAP uptake and lysosomal delivery in neurons [22]. Furthermore, PGRN haploinsufficiency in FTLD patients impairs PSAP lysosomal trafficking and decreases neuronal saposin level [22]. Thus PGRN and PSAP facilitate each other's lysosomal trafficking, and PGRN-PSAP interaction is important for maintaining proper lysosomal function in the aged brain. In addition, both PGRN and PSAP are also secreted and both have been reported to have neurotrophic functions [7-9, 19-21, 23]. The interaction of PGRN and PSAP in the extracellular space might also regulate their neurotrophic properties. Thus given the importance of PGRN-PSAP interaction and relevance to FTLD, we decided to map domains involved in PGRN-PSAP binding. Here we report that PSAP interacts with PGRN through granulin motifs in PGRN and the linker region between saposin B and C (BC linker) in PSAP.

A1.3 Results

PSAP interacts with granulin motifs in PGRN

To determine the binding site for PSAP in PGRN, we made a series of deletion constructs of individual granulin (Grn) motifs (Fig. AI-1A). While deletion of both Grn D and Grn E motifs results in a great decrease of the interaction between PGRN and PSAP, further deletion of other granulin motifs only slightly weaken the interaction,

suggesting that Grn D and Grn E are the main binding site for PSAP in PGRN (Fig. 1B). To further confirm that PSAP interacts with granulins, we tested the interaction between PSAP and individual granulins tagged with alkaline phosphatase (AP) or GFP. Among the AP-tagged granulins with decent expression, granulin A, B, D and E coimmunoprecipitate with PSAP, but Grn D and E exhibited the strongest binding towards PSAP (Fig. AI-1C). Grn G, on the other hand, does not show any detectable binding to PSAP (Fig. AI-1C). Similarly, with GFP-tagged granulins, granulins D and E showed the strongest interaction followed by granulin B (Fig. AI-1D). Taken together, these results suggest that PGRN binds to PSAP through multiple granulin motifs with highest affinity to Grn D and E.

To determine the relative affinity for the PSAP and PGRN/Grn binding, we anchored PSAP to the cell surface by fusing it to the transmembrane domain of PDGF receptor and measured the binding affinity using an alkaline phosphatase (AP) based cell surface binding assay (Hu et al., 2010). AP-Grn D and AP-Grn-E bind to PDGFR fused PSAP on the cell surface with a Kd around 20nM, similar to that of full length PGRN (Fig. A1-2), confirming that these two granulin motifs are the main binding sites for PSAP in PGRN.

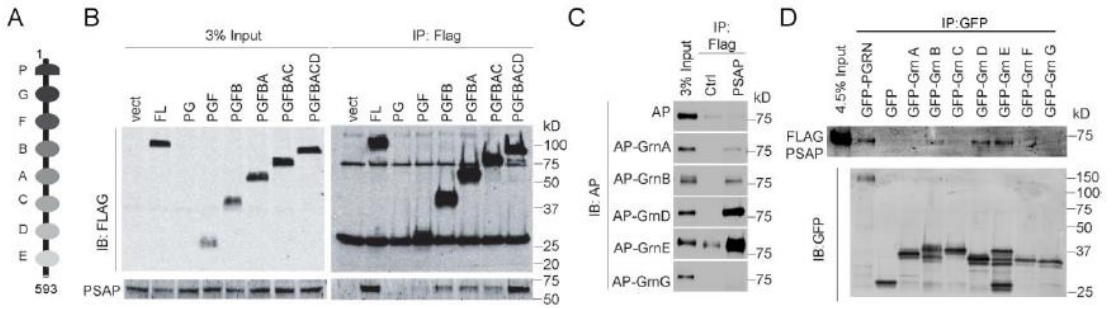

Figure AI-1: Domain structure of human PGRN (aa 1-593). (**B**) HEK293T cells were co-transfected with FLAG tagged PGRN truncation constructs and untagged human PSAP as indicated. Cells were lysed two days after transfection and the lysates were immunoprecipitated with anti-FLAG antibodies. The IP products were analyzed by Western blot using anti-FLAG and anti-PSAP antibodies (RRID:AB_2172462). (**C**) Conditioned medium from HEK293T expressing different AP-fusion proteins were incubated with FLAG beads only or FLAG beads with FLAG-PSAP recombinant proteins. The amount of AP proteins co-immunoprecipitated with FLAG-PSAP was analyzed by Western blot. (**D**) Conditioned medium from HEK293T expressing different GFP-fusion proteins were mixed with 1μg purified recombinant FLAG-PSAP. Immunoprecipitations were then performed with anti-GFP antibodies and the IP products were analyzed by Western blot. (Conducted by FH and PS)

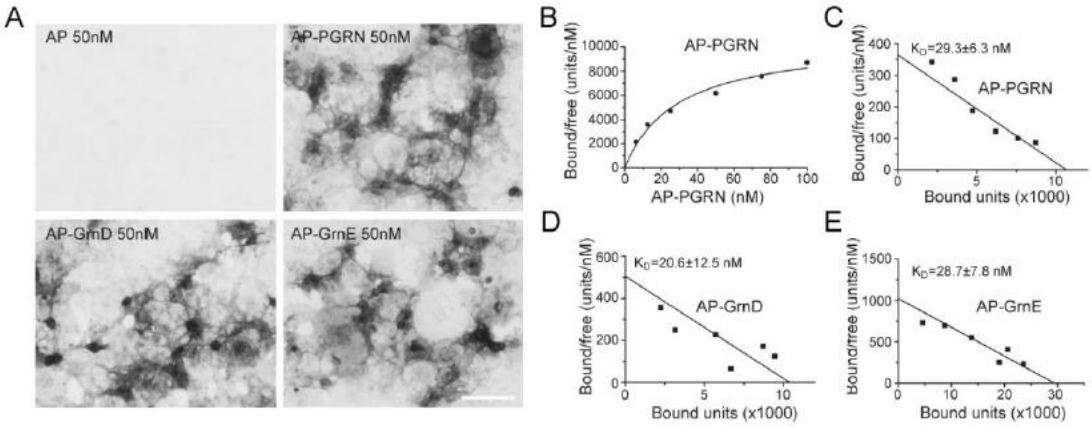

Figure AI-2: Granulin D and E bind to PSAP with similar affinity as full length PGRN. (**A**) Conditioned medium containing AP, AP-PGRN, AP-Grn D, or AP-Grn E were incubated with COS-7 cells transfected with PSAP fused to PDGFR. Cells were fixed and AP binding was visualized with AP substrates. Scale bar=100μm. (**B**) AP–PGRN binding to PSAP-PDGFR expressing COS-7 cells measured as a function of AP–PGRN concentration. (**C-E**) Scatchard plot of AP-PGRN (C), AP-GRN D (D) or AP-GRN E (E) binding to PSAP-PDGFR expressing COS-7 cells. KD, mean ± sem, n = 4. (Conducted by XZ)

PSAP interacts with PGRN through the linker region between saposin B and C

To map the binding site for PGRN in PSAP, we created a series of PSAP deletion constructs and tested their interaction with PGRN. While deletion of saposin D (ABC) has no effect on the PSAP-PGRN interaction, further deletion of saposin C and the linker region between saposin B and C (AB) results in loss of the PGRN-PSAP interaction (Fig. AI-3A). The construct containing saposin B, the BC linker, and saposin C (BC), binds to PGRN as strong as full-length PSAP (Fig. AI-3B). This suggests that PGRN interacts with saposin C or the linker region between B and C. However, saposin C itself is not sufficient to interact with PGRN (Fig. AI-3B). Addition of the BC linker region to saposin C (L+C) allows full binding to PGRN despite very weak expression, suggesting that the BC linker region is the binding site for PGRN in PSAP (Fig. AI-3B). This is further supported with purified recombinant saposin proteins from bacteria. None of the recombinant saposin domains interact with PGRN, but fusion of the BC linker region with saposin C allows strong binding to PGRN (Fig. AI-3C). To determine if the BC linker alone is able to bind with PGRN, we fused either saposin B plus BC linker or BC linker alone with the transmembrane and cytoplasmic domains of LAMP1 (TcLAMP1). The co-immunoprecipitation result shows that FLAG-tagged BC linker-TcLAMP1 was able to co-immunoprecipitate PGRN as efficiently as FLAG tagged saposin B plus BC linker and FLAG tagged full-length PSAP (Fig. AI-3D), suggesting that the BC linker alone is sufficient for PGRN binding.

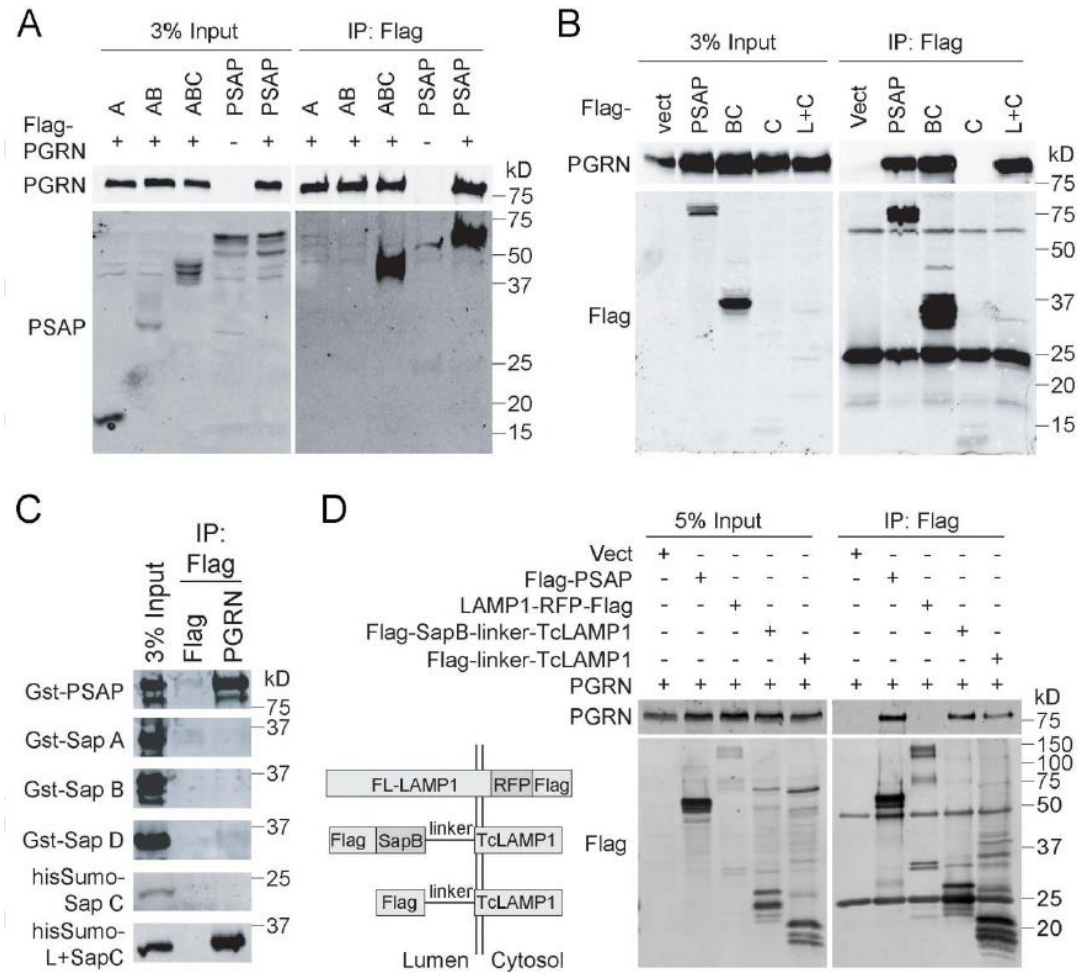

Figure AI-3: PSAP interacts with PGRN through the BC linker. (**A**) HEK293T cells were co-transfected with FLAG tagged PGRN and full length his-PSAP or PSAP truncation mutants as indicated. Cells were lysed two days after transfection and the lysates were immunoprecipitated with anti-FLAG antibodies. The IP products were analyzed by Western blot using anti-FLAG and anti-PSAP antibodies (RRID:AB_2172462). (**B**) HEK293T cells were co-transfected with untagged PGRN and FLAG tagged PSAP fragments as indicated. Cells were lysed two days after transfection and the lysates were immunoprecipitated with anti-FLAG antibodies. (**C**) Recombinant Gst- or his-sumo tagged saposins purified from bacteria were incubated with FLAG beads only or FLAG beads with FLAG-PGRN recombinant proteins. The amount of saposin co-immunoprecipitated with FLAG-PGRN was analyzed by Western blot. (**D**) HEK293T cells were co-transfected with untagged PGRN and FLAG tagged full-length PSAP, full-length LAMP1, saposin B with BC linker fused with transmembrane and cytoplasmic domain of LAMP1 (Tc-LAMP1) and BC linker fused with Tc-LAMP1 as indicated. Cells were lysed two days after transfection and the lysates were immunoprecipitated with anti-FLAG antibodies and immunoblotted with anti-PGRN and anti-FLAG antibodies. (Conducted by PS and XZ).

To further prove that the BC linker is the binding site for PGRN in PSAP, we generated a PSAP mutant construct in which the BC linker is replaced by the linker between saposin C and D (CD linker) (Fig. AI-4A). This replacement totally abolished the binding between PSAP and PGRN in the co-immunoprecipitation (Fig. AI-4A) and cell surface binding assays (Fig. AI-4B), further supporting that the BC linker is required for binding between PSAP and PGRN.

PSAP mutant that fails to bind to PGRN cannot deliver PGRN to lysosomes

Previously, we showed that PSAP mediates sortilin-independent delivery of PGRN into lysosomes (Zhou et al., 2015). In fact, since sortilin is not expressed in fibroblasts, lysosomal trafficking of PGRN is totally abolished in PSAP deficient fibroblasts (Zhou et al., 2015). We predicted that the PSAP mutant with its PGRN binding site mutated cannot facilitate PGRN lysosomal trafficking. Indeed, the PSAP mutant with the BC linker replaced by the CD linker fails to rescue the PGRN trafficking defect in PSAP deficient fibroblasts, although lysosomal trafficking of the PSAP mutant itself is not impaired (Fig. AI-5A, AI-5B). PSAP also facilitates lysosomal delivery of PGRN from the extracellular space. However, this is also abolished by mutation of the BC linker region of PSAP. While recombinant wild type PSAP facilitates neuronal uptake and lysosomal delivery of recombinant PGRN protein lacking the sortilin binding site (Zheng et al., 2011), the PSAP mutant with the BC linker replaced fails to do so (Fig. AI-5C, AI-5D, AI-5E).

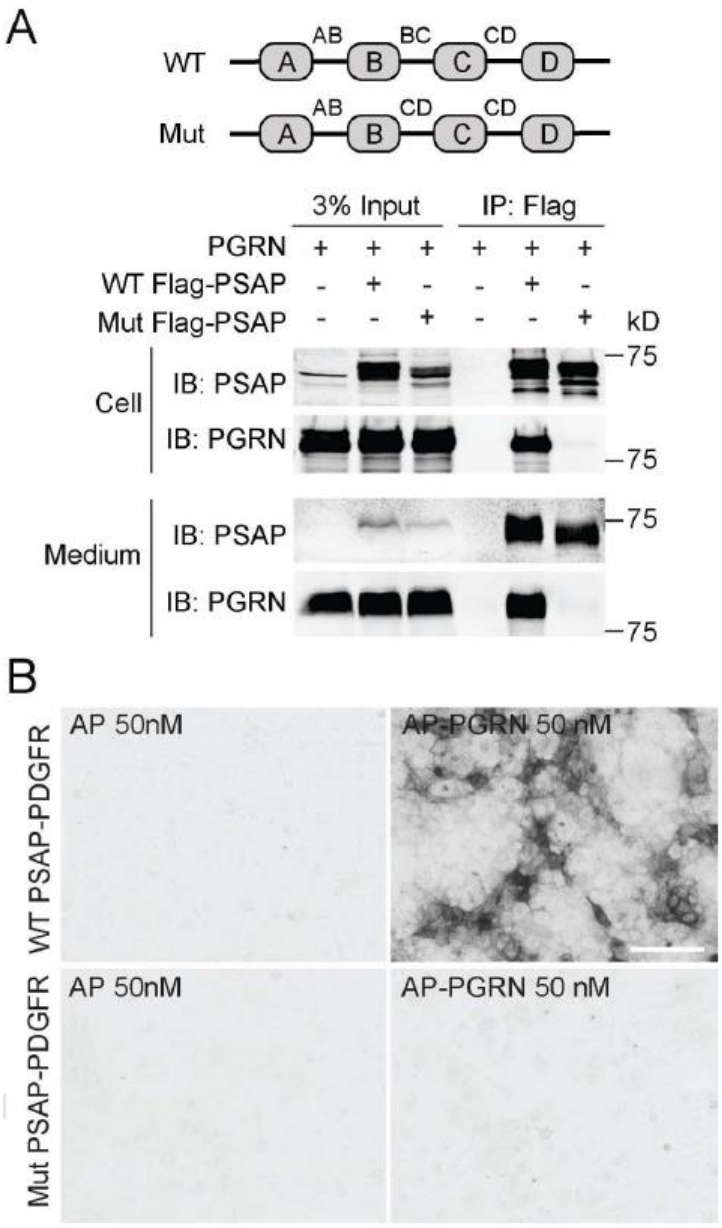

Figure AI-4: PSAP mutant with the BC linker replaced failed to interact with PGRN. (A) HEK293T cells were co-transfected with FLAG tagged wild type (WT) or mutant (mut) PSAP and untagged human PGRN as indicated. Media was collected and cells were lysed three days after transfection. The lysates and media were separately immunoprecipitated with anti-FLAG antibodies. (B) Conditioned medium containing AP or AP-PGRN were incubated with COS-7 cells transfected with WT or mutant PSAP fused to PDGFR. Cells were fixed and AP binding were visualized with AP substrates. Scale bar=100μm (Conducted by XZ and LS)

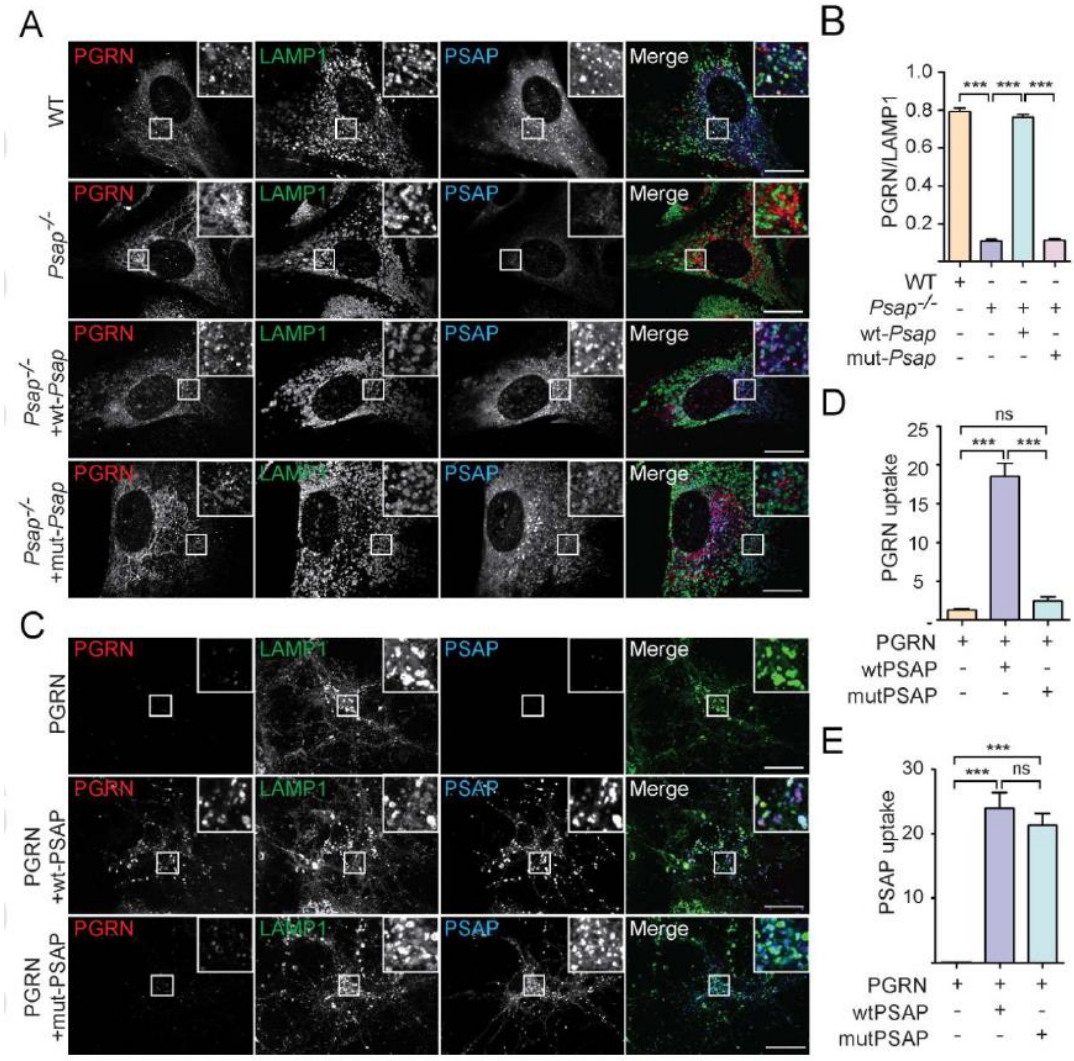

Figure AI-5: PSAP mutants fail to deliver PGRN to lysosomes. (**A**) PSAP-/- mouse fibroblasts were infected with lentivirus expressing WT or mutant PSAP with the BC linker replaced by CD linker. Cells were fixed and stained with rabbit anti-human saposin B, sheep anti-mouse PGRN and rat anti-LAMP1 antibodies. Scale bar=10 μm. (B) The colocalization of PGRN with lysosomal marker LAMP1 in (A) were quantified using Image J. n=3, ***, p<0.001. (**C**) *Grn-/-* cortical neurons were incubated with C-terminally FLAG his tagged human PGRN which does not bind to sortilin (5ug/ml) together with recombinant WT PSAP or mutant PSAP with the BC linker replaced by CD linker (5ug/ml). 12 hours later, cells were fixed and stained with rabbit anti-human saposin B, goat anti-human PGRN and rat anti- LAMP1 antibodies. Scale bar=10 μm. (**D, E**) The endocytosed PGRN (D) and PSAP (E) for the experiment in (C) were quantified by using Image J. n=3; ns, no significance; ***, p<0.001. One way ANOVA. (Conducted by XZ).

A1.4 Discussion

Our previous studies have shown that PGRN and PSAP form a complex both intracellularly and extracellularly and facilitate each other's lysosomal delivery (Zhou et al., 2015; Zhou et al., 2017b). Since both PGRN and PSAP are essential for proper lysosomal function and loss of function in either gene causes lysosomal storage diseases, more studies on the interaction of PGRN and PSAP will help us develop strategies to enhance the function of PGRN and PSAP. This will be of therapeutic interest for FTLD, since haploinsufficiency of PGRN is a leading cause of FTLD and impaired PSAP lysosomal trafficking is observed in FTLD patients with GRN mutations (Zhou et al., 2017b). Future studies to design or screen small molecules to enhance the binding affinity between these two proteins might be therapeutic interest. Thus it is important for us to understand the molecular mechanisms involved in the physical interaction between PGRN and PSAP.

In agreement with our previous finding that saposins do not bind to PGRN (Zhou et al., 2015), here we show that PGRN interacts with the linker between saposin B and C domain through multiple granulin motifs. Granulin D and E bind to PSAP with similar affinity as full length PGRN. How the BC linker region interacts with granulin motifs is still unclear and structural studies will be useful to further understand this interaction. We have failed to further narrow down the binding site in the 37 amino acid BC linker to a shorter peptide (data not shown). But most likely PSAP-PGRN binding involves an interaction between a peptide (BC linker) and a folded domain (granulins).

PSAP is known to undergo processing into saposins during its trafficking to lysosomes (Matsuda et al., 2007; O'Brien and Kishimoto, 1991; Qi and Grabowski,

2001). Additionally, PGRN is hypothesized to be processed into granulin peptides in the lysosome (Cenik et al., 2012). Both PGRN and PSAP have been shown to interact with cathepsin D (Beel et al., 2017; Gopalakrishnan et al., 2004; Laurent-Matha et al., 2002; Zhou et al., 2017a) and cathepsin D is known to cleave PSAP during trafficking (Gopalakrishnan et al., 2004). Thus it is possible that binding of PGRN to the BC linker region of PSAP will affect the kinetics of PSAP, and maybe also PGRN processing. Since granulin peptides, especially granulin D and E, bind to PSAP with the similar affinity as full length PGRN, granulins might interact with full length PSAP or its processing intermediates with BC linker still attached. The relative rates of PGRN and PSAP processing during trafficking and in the lysosome might determine the interaction modes between the final products and processing intermediates of these two proteins. Further studies on these aspects of PGRN-PSAP biology will allow a better understanding on how these two proteins interact and regulate each other's functions and help develop therapeutic means to enhance their activities.

A1.5 Materials ad Methods

Antibodies- The following antibodies were used in this study: mouse anti-FLAG (M2) from Sigma (RRID:AB_439685), rabbit anti-human PSAP antibodies from Proteintech Group (RRID:AB_2172462), goat anti-human PGRN (RRID:AB_2114489), and sheep anti-mouse PGRN (RRID:AB_2114504) from R&D systems, rat anti-mouse LAMP1 (1D4B) from BD Biosciences (RRID:AB_2134499). Rabbit anti-human saposin B antibodies (Leonova et al., 1996) is a gift from Dr. Xiaoyang Qi (University of Cincinnati School of Medicine, Cincinnati, OH).

DNA and Plasmids **-** Full length human PSAP and PGRN expression constructs were previously described (Zhou et al., 2015). FLAG tagged PGRN and PSAP truncation constructs were generated by cloning the PGRN and PSAP fragments into the pSectag2B vector (Invitrogen) with an N-terminal FLAG tag. GST-saposin constructs and his Sumo saposin constructs were generated by cloning saposin and linker regions into pGEX6p-1 and pET his Sumo vector, respectively. AP-granulin constructs were generated by cloning granulins into pAP5 vector (Genhunter). GFP-granulins were generated by inserting GFP and granulin sequences into pSectag2B vector after the signal sequence. PSAP mutant with the BC linker (amino acid sequence: VKEMPMQTLVPAKVASKNVIPALELVEPIKKHEVPAK) replaced by CD linker was generated from hPSAP construct by PCR using following primers (hSap B 3: 5PhosCTCATCACAGAACCCAACC and CD linker hSap C 5: 5Phos ACGCGGCTGCCTGCACTGACCGTTCACGTGACTCAGCCAAAGGACGGTTCT GATGTTTACTGTGAGGTG). His tagged and lentiviral human WT PSAP, human mutant PSAP with the BC linker replaced by CD linker, and human PGRN constructs were generated by cloning corresponding genes into pSectag2B vector (Invitrogen) and into pCDH-puro vector (System bio), respectively. To generate fusion construct of PSAP with the platelet derived growth factor receptor (PDGFR) transmembrane domain, full-length WT and mutant PSAP with the BC linker replaced by CD linker were cloned into the pDisplay vector (Invitrogen). Rat FLAG-RFP-LAMP1 was obtained from Addgene. FLAG tagged SapB-BC linker-TcLAMP1 or BC linker-TcLAMP1 were generated by clone rat transmembrane and cytosolic domains of LAMP1 (Tc) into FLAG-SapB-BC linker and FLAG-BC linker constructs (with stop

codon removed) using XhoI and PmeI sites.

Cell Culture- HEK293T (RRID:CVCL_0063, from ATCC), COS-7 (RRID:CVCL_0224, from ATCC) and WT and PSAP-/- fibroblast cells (derived from Psap-/- mice (RRID:IMSR_JAX:002792)) were maintained in Dulbecco's Modified Eagle's medium (Cellgro) supplemented with 10% fetal bovine serum (Gibco) and 1% Penicillin–Streptomycin (Invitrogen) in a humidified incubator at 37ºC and 5% CO2. Cells were transiently transfected with polyethyleneimine (PEI) as described (Vancha et al., 2004). Psap-/- fibroblasts were infected with lentivirus expressing WT or mutant PSAP.

Primary cortical neurons were isolated from P0-P1 pups from Grn-/- mice (Jackson laboratories, RRID:IMSR_JAX:013175) using a modified protocol (Beaudoin et al., 2012). Briefly, cortices were rapidly dissected from the brain in 2 mL HBSS supplemented with B27 (ThermoFisher Scientific catalog#17504044) and 0.5 mM L-glutamine (ThermoFisher Scientific catalog#25030024) at 4°C. Meninges were removed before digestion with papain (Worthington LS003119, 2mg/ml in HBSS) and DNaseI (1mg/ml in HBSS, Sigma) for 12 minutes at 37°C. Tissues were then dissociated using fire polished glass pipettes. Cells were spun down and resuspended in Neuroplex medium (Gemini) plus B27 and plated onto poly-lysine (Sigma) coated dishes.

Protein preparation and Western blot analysis- Purification of recombinant his-human WT PSAP, mutant PSAP with BC linker replaced with CD linker, and his-human PGRN proteins, co-immunoprecipitation (IP) assays and Western blots were performed as previously described (Zhou et al., 2015). Gst and his-sumo saposin fusion proteins were

purified using Gst or cobalt beads, respectively, from Origami™ B(DE3) strain (Novagen) after IPTG induction.

Cell surface binding assay and binding- AP binding assays were done as previously described (Hu et al., 2010). Briefly, conditioned medium with AP or AP-PGRN/Granulins generated from HEK293T cells were incubated with pDisplay-PSAP-transfected COS-7 cells or for 2 h at room temperature before fixation and heat inactivation of endogenous AP at 65°C overnight. Bound AP to the primary cortical neurons was measured using NIH image software. Followed by measuring the intensity of bound AP signal, the saturation binding curves and scatchard plots were generated, and binding KD were calculated by using GraphPad Prism 5.0 software.

Immunofluorescence staining- Immunofluorescence staining was performed as previously described (Zhou et al., 2015). Briefly the cells were fixed with 4% paraformaldehyde and permeabilized and blocked with blocking buffer (0.05% saponin, 3% BSA in PBS). The cells were incubated with primary antibodies in blocking buffer overnight at 4 °C and CF488A, CF568, or CF660C (Biotum) conjugated secondary antibodies. Images were acquired on a CSU-X spinning disc confocal microscope (Intelligent Imaging Innovations) with an HQ2 CCD camera (Photometrics) using a 100× objective.

Quantitative analysis of lysosomal PGRN and endocytosed PGRN and PSAP- Images were processed and analyzed by ImageJ program as previously described (Zhou et al., 2015). Briefly, the colocalization between PGRN and lysosomal markers, LAMP1, was quantified by using JACoP plugin. To quantify the endocytosed PGRN and PSAP, the entire cell was selected and the fluorescence intensity was measured directly by ImageJ.

Ethical Approval and Consent to participate- All applicable international, national, and/or institutional guidelines for recombinant DNA and cell lines were followed. The work under protocol (MUA#: 15965) were approved by the Cornell University Institutional Biosafety Committee (IBC).

REFERENCES

1. Neary, D., et al., *Frontotemporal lobar degeneration: a consensus on clinical diagnostic criteria.* Neurology, 1998. **51**(6): p. 1546-54.

2. Neumann, M., et al., *Ubiquitinated TDP-43 in frontotemporal lobar degeneration and amyotrophic lateral sclerosis.* Science, 2006. **314**(5796): p. 130-3.

3. Arai, T., et al., *TDP-43 is a component of ubiquitin-positive tau-negative inclusions in frontotemporal lobar degeneration and amyotrophic lateral sclerosis.* Biochem Biophys Res Commun, 2006. **351**(3): p. 602-11.

4. Baker, M., et al., *Mutations in progranulin cause tau-negative frontotemporal dementia linked to chromosome 17.* Nature, 2006. **442**(7105): p. 916-9.

5. Cruts, M., et al., *Null mutations in progranulin cause ubiquitin-positive frontotemporal dementia linked to chromosome 17q21.* Nature, 2006. **442**(7105): p. 920-4.

6. Gass, J., et al., *Mutations in progranulin are a major cause of ubiquitin-positive frontotemporal lobar degeneration.* Hum Mol Genet, 2006. **15**(20): p. 2988-3001.

7. Bateman, A. and H.P. Bennett, *The granulin gene family: from cancer to dementia.* Bioessays, 2009. **31**(11): p. 1245-54.

8. Cenik, B., et al., *Progranulin: a proteolytically processed protein at the crossroads of inflammation and neurodegeneration.* J Biol Chem, 2012. **287**(39): p. 32298-306.

9. Nicholson, A.M., et al., *Progranulin axis and recent developments in frontotemporal lobar degeneration.* Alzheimers Res Ther, 2012. **4**(1): p. 4.

10. Smith, K.R., et al., *Strikingly Different Clinicopathological Phenotypes Determined by Progranulin-Mutation Dosage.* Am J Hum Genet, 2012. **90**(6): p. 1102-7.

11. Almeida, M.R., et al., *Portuguese family with the co-occurrence of frontotemporal lobar degeneration and neuronal ceroid lipofuscinosis phenotypes due to progranulin gene mutation.* Neurobiol Aging, 2016.

12. Cotman, S.L., et al., *Neuronal ceroid lipofuscinosis: impact of recent genetic advances and expansion of the clinicopathologic spectrum.* Curr Neurol Neurosci Rep, 2013. **13**(8): p. 366.

13. Kousi, M., A.E. Lehesjoki, and S.E. Mole, *Update of the mutation spectrum and clinical correlations of over 360 mutations in eight genes that underlie the neuronal ceroid lipofuscinoses.* Hum Mutat, 2012. **33**(1): p. 42-63.

14. Belcastro, V., et al., *Transcriptional gene network inference from a massive dataset elucidates transcriptome organization and gene function.* Nucleic Acids Res, 2011. **39**(20): p. 8677-88.

15. Hu, F., et al., *Sortilin-mediated endocytosis determines levels of the frontotemporal dementia protein, progranulin.* Neuron, 2010. **68**(4): p. 654-67.

16. Zheng, Y., et al., *C-terminus of progranulin interacts with the beta-propeller region of sortilin to regulate progranulin trafficking.* PLoS ONE, 2011. **6**(6): p. e21023.

17. Zhou, X., et al., *Prosaposin facilitates sortilin-independent lysosomal trafficking of progranulin.* J Cell Biol, 2015. **210**(6): p. 991-1002.

18. Nicholson, A.M., et al., *Prosaposin is a regulator of progranulin levels and oligomerization.* Nat Commun, 2016. **7**: p. 11992.

19. O'Brien, J.S. and Y. Kishimoto, *Saposin proteins: structure, function, and role in human lysosomal storage disorders.* FASEB J, 1991. **5**(3): p. 301-8.

20. Qi, X. and G.A. Grabowski, *Molecular and cell biology of acid beta-glucosidase and prosaposin.* Prog Nucleic Acid Res Mol Biol, 2001. **66**: p. 203-39.

21. Matsuda, J., A. Yoneshige, and K. Suzuki, *The function of sphingolipids in the nervous system: lessons learnt from mouse models of specific sphingolipid activator protein deficiencies.* J Neurochem, 2007. **103 Suppl 1**: p. 32-8.

22. Zhou, X., et al., *Impaired prosaposin lysosomal trafficking in frontotemporal lobar degeneration due to progranulin mutations.* Nat Commun, 2017. **8**: p. 15277.

23. Ahmed, Z., et al., *Progranulin in frontotemporal lobar degeneration and neuroinflammation.* J Neuroinflammation, 2007. **4**: p. 7.

APPENDIX II

WDR41 LOCALIZES TO THE GOLGI AND ENDOPLASMIC RETICULUM AND OVEREXPRESSION OF WDR41 INDUCES VESICLE FORMATION

Summary

WDR41 is an approximately 50 kDa protein comprised almost entirely of WD-repeat and binds to the SMCR8-C9orf72 dimer. While knockout of WDR41 in a mouse model does not replicate the immune phenotype observed in SMCR8 and C9orf72 knockout mice, it is the only component of this complex to show clear localization to membrane structure in the cell. We previously reported that WDR41 is enriched at the Golgi, but C9orf72 and SMCR8 appear mostly cytosolic. Here, I present evidence that WDR41 also resides at the endoplasmic reticulum (ER) and that strong overexpression of WDR41 is sufficient to produce WDR41-positive vesicles of unknown identity.

Figure AII-1 shows the localization of WDR41-GFP expressed in HeLa cells for 20 hours. As shown in Chapter 2, fixed HeLa cells with WDR41 overexpressed show clear WDR41 enrichment at the Golgi, stained by GPP130 here. However, viewing WDR41-GFP in live cells allows more structural detail to be discerned. In live images, WDR41 colocalizes with Sec61-β, a marker of the ER. This suggests that WDR41 may traffic between the Golgi and ER and that ER localization is lost during the fixation process (Figure AII-1).

In addition to this Golgi and ER localization, the overexpression of WDR41 occasionally (5% of cell population) seems to induce the formation of novel vesicles of

unknown identity (Figure AII-2). The presence of these vesicles appears to correlate with the expression level of WDR41. This data confirms that WDR41 is indeed interacting with membranes in the cell, though it is unclear how WDR41 is recruited and what role WDR41 plays there. Whether vesicular phenomena is dependent on C9orf72 and SMCR8 is also uncertain. Overexpression of WDR41 in C9orf72-/- or SMCR8-/- cells may help to answer whether this effect is due to the C0orf72-SMCR8-WDR41 complex or a separate function of WDR41. So far, I have not been able to identify any common organelle markers on these WDR41-positive vesicles.

While WDR41 likely acts as a scaffolding protein, as many other WD-repeat proteins do, for SMCR8 and C9orf72, the presence of a cellular localization and phenotype may provide an alternative route to understanding the function of this protein complex. Better characterization of these WDR41-positive vesicles may suggest additional binding partners that are needed to carry out vesicle formation, such as Rab GTPases. Additionally, whether or not WDR41 is able to recruit C9orf72 and SMCR8 to the Golgi or ER is still unclear, but will provide insight into the dynamics of the C9orf72-SMCR8-WDR41 complex.

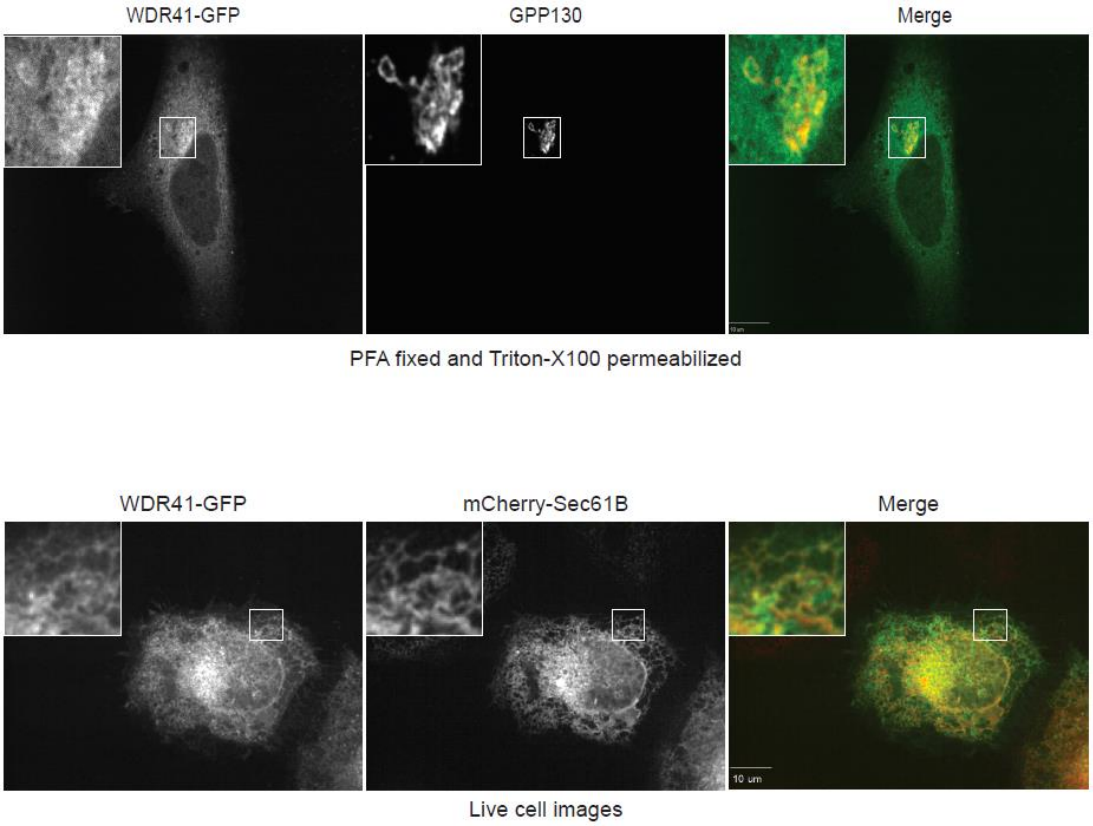

Figure AII-1: WDR41 localizes to the Golgi and ER. (Top panel) WDR41-GFP overexpressed in HeLa cells. These cells were fixed in PFA and stained for a Golgi marker, GPP130. (Bottom panel) WDR41-GFP co-expressed in HeLa cells with mCherry-Sec61β to label the ER. These images are taken with live cells.

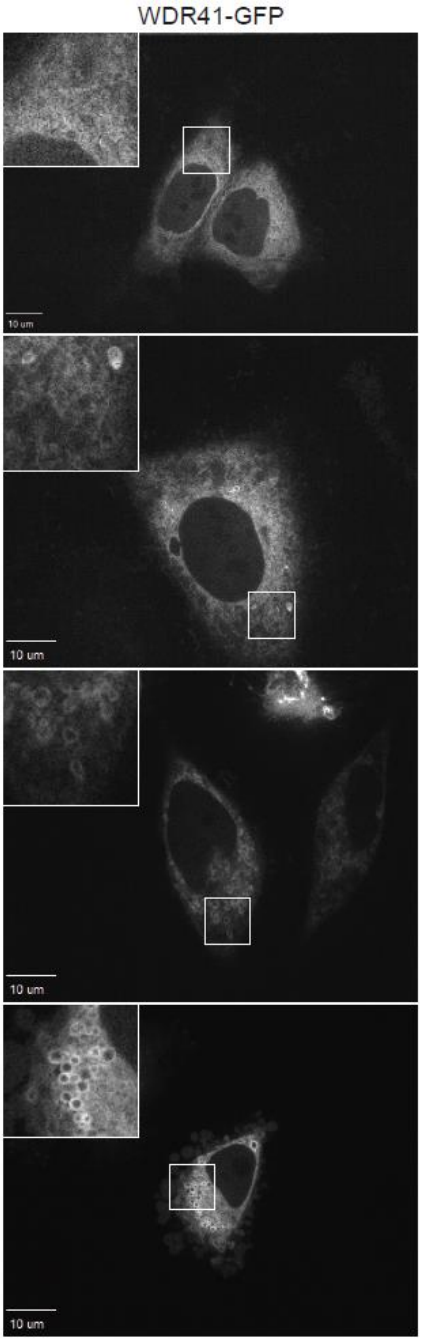

Figure AII-2: Overexpression of WDR41 results in the appearance of WDR41-positive vesicles. Top: WDR41 most commonly localizes with a cytosolic/ER appearance. Bottom: Examples of cells with WDR41-postive vesicles.